Dynamics of Complex Systems

Water, Biopolymers and Their Coupling

Marco Lagi

Department of Chemistry and CSGI

University of Florence

Candidate	:	Marco Lagi	.....
Advisor	:	Prof. Piero Baglioni	.....
PhD Coordinator	:	Prof. Gianni Cardini	.....

A thesis submitted for the degree of

PhilosophiæDoctor in sector CHIM02 - CHIMICA FISICA

December 2009

Abstract

We investigate the rich dynamics of two complex systems, *water* and *proteins*, and the effects of their coupling. The importance of this study is implicit in the fundamental biological role of proteins: their function depends on their ability to sample the energy landscape, and if their dynamics is inhibited they are not able to work. Understanding their relaxations is therefore necessary to relate structure to function. Moreover, the strong coupling proteins have with the environment makes the biomolecules extremely sensitive to the dynamics of their biological solvent, water.

We approach this problem studying first the slow dynamics of supercooled water. While this task is easy with computer simulations, from an experimental point of view it requires the confinement of water, to prevent crystallization. Our results show the presence of a dynamic transition at $T_L = 225 \pm 5$K in all the systems studied (bulk water and 1D, 2D, 3D confined water).

We then examine the dynamics of hydrated proteins in the temperature range of their biological activity, i.e. below their denaturation temperature, T_d, and above their glass transition temperature, T_l. They show an exotic fast logarithmic relaxation, followed by a more common slow exponential relaxation. The former agrees with the predictions of the most popular liquid theory, the mode-coupling theory, for particular glass transitions.

Finally, we studied the coupled dynamics of water and proteins. It turns out that both the low temperature limit (*glass transition*) and

the high temperature limit (*denaturation*) of protein functionality coincide with dynamic transitions in the hydration water. On the low temperature side, T_l coincides with the above mentioned T_L in hydration water, while at high temperature the protein denaturation at T_d coincides with an analogous transition in hydration water at $T_D = 340 \pm 5$K.

Acknowledgements

First and foremost, I feel very privileged to have worked with my supervisors, Prof. Piero Baglioni and Prof. Sow-Hsin Chen. Supplying me with different skills and motivations, they both pushed me through these three years in a productive and satisfying way. Lucky PhD students have a great supervisor, but I got two of them! Also, I owe a great debt to Prof. Francesco Sciortino for showing me the simulation techniques and their effective (at times coarse-grained) potential, and to Emiliano for assistance in every way and in all kinds of field.

I would also like to thank my fellow students, at the University of Florence (Nicola), at MIT (Yang, Xiangqiang, Dazhi) and at the University of Rome I (John, Piggí, Emanuela): the interaction with them has always been stimulating, and it helped me in each and every single task that this thesis brought about.

Thanks also to my family who have been extremely understanding, and who supported my studies at home and abroad. This allowed me to spend a long period in Boston, that has been rich of every kind of joy, novelty, opportunity and excitement. And these four are combined in Rebecca, the biggest gift the US had to offer.

Glossary

1. Acronyms

MD	Molecular Dynamics	Experimental/Simulation Techniques
QENS	Quasi-Elastic Neutron Scattering	
DSC	Differential Scanning Calorimetry	
NIR	Near Infra-Red	
IXS	Inelastic X-ray Scattering	
iMCT	ideal Mode-Coupling Theory	Theoretical Models
eMCT	extended Mode-Coupling Theory	
DHO	Damped-Harmonic Oscillator	
JCM	Jennings Colloidal Model	
RCM	Relaxing-Cage Model	
LYZ	Lysozyme	Proteins
BSA	Bovine Serum Albumin	
RNAse	RiboNucleAse	
CS	Conformational Substates	
APS	Argonne Photon Source	Facilities
SNS	Spallation Neutron Source	
DCS	Disc Chopper Spectrometer	
BASIS	BAck Scattering Spectrometer	
LLCP	Liquid-Liquid Critical Point	Transitions
FSC	Fragile-to-Strong Crossover	
SFC	Strong-to-Fragile Crossover	
CM	Center of Mass	Physical Quantities
DH	Dynamic Heterogeneity	
ISF	Intermediate Scattering Function	

2. Symbols

$\langle\tau\rangle$	Structural Relaxation Time	Transport Properties
η	Viscosity	
D	Self-Diffusion Constant	
q	Scattering Vector Modulus (Å^{-1})	Scales
E	Energy (meV)	
ω	Frequency (Hz)	
T	Temperature (K)	
t	Time (ps)	
$\phi_q(t)$	Density Correlation Function	Dynamics of Liquids
$S_q(E)$	Dynamic Structure Factor	
S_q	Static Structure Factor	
ρ	Numerical Density	
$\langle x^2\rangle$	Mean Square Displacement	
$\chi_T(t)$	Dynamic Response Function	
$\chi_4(t)$	Four-point Correlation Function	
T_l	Dynamic Transition of Proteins	Relevant Temperatures
T_d	Reversible Denaturation of Proteins	
T_L	Dynamic Crossover of Water (low-T)	
T_D	Dynamic Crossover of Water (high-T)	
T_g	Glass Transition Temperature	
T_H	Homogeneous Nucleation	
T_c	Mode-Coupling Critical Temperature	
f_q	Debye-Waller Factor	Physical Quantities
C_p	Specific Heat	
k_B	Boltzmann Constant	
E_A	Activation Energy	

Contents

List of Figures v

1 Introduction to the Dynamics of Liquids 1

1.1 The concept of *relaxation* 1

1.2 Density correlation functions, $\phi_q(t)$ 3

1.3 Relaxations in liquids 5

1.3.1 Transport Properties 5

1.3.2 Relaxations in supercooled liquids 7

1.3.3 Dynamic transitions 12

1.3.4 Dynamic heterogeneity 15

2 Water Dynamics 19

2.1 Overview of water dynamics 19

2.2 Supercooled and confined water dynamics 25

2.2.1 1-D Confined water dynamics: Silica nanopores 25

2.2.2 2-D Confined water dynamics: Biomacromolecules 27

2.2.3 3-D Confined water dynamics: Cement paste 28

2.3 Bulk water dynamics: computer simulations 34

2.4 Summary 36

3 Protein Dynamics 39

3.1 Overview of protein dynamics 39

3.2 Short-time dynamics: Phonons 43

3.2.1 An introduction to collective motions 43
3.2.2 Phonon detection 44
3.2.3 Temperature dependence of the phonon dispersion 47
3.3 Mid-time dynamics: Log decay 49
3.3.1 An introduction to the logarithmic decay 49
3.3.2 β relaxation: logarithmic decay 50
3.3.3 Temperature dependence of β relaxation 52
3.4 Long-time dynamics: Diffusion 57
3.4.1 An introduction to the protein-glass analogy 57
3.4.2 α relaxation: exponential decay 59
3.4.3 Temperature dependence of α relaxation 60
3.5 Summary 62

4 Water-Protein coupling **65**
4.1 Overview of protein hydration water dynamics 65
4.2 The low temperature dynamic crossover 68
4.2.1 An introduction to protein dynamic transition 68
4.2.2 Theoretical framework 70
4.2.3 The crossover from experiments and simulations 71
4.3 The high temperature dynamic crossover 78
4.3.1 An introduction to protein denaturation 78
4.3.2 Theoretical framework 81
4.3.3 The crossover from experiments and simulations 84
4.4 Summary 88

5 Conclusion **91**

A Liquid Theories **95**
A.1 The ideal mode-coupling approach 95
A.2 MCT higher-order singularities 99
A.3 Extended mode-coupling theory 101

A.4 The Adam-Gibbs theory 103

B Computer Experiments **107**

B.1 Simulations in physics and chemistry 107

B.2 Molecular dynamics simulations 109

B.3 Details of the computer experiments 111

C Published Papers **115**

C.1 Specific Anion Effects on the Optical Rotation of α-Amino Acids . 116

C.2 Organogels from a Vitamin C-based Surfactant 117

C.3 The Low-Temperature Dynamic Crossover Phenomenon in Protein Hydration Water: Simulations vs Experiments 118

C.4 Collective headgroup conformational transition in twisted micellar superstructures 119

C.5 DNA Closed Nanostructures: a Structural and Monte Carlo Simulation Study 120

C.6 Interconnected Networks: Structural and Dynamic Characterization of Aqueous Dispersions of diC_8PC 121

C.7 Studies of phononlike low energy excitations of protein molecules by inelastic x-ray scattering 122

C.8 Observation of dynamic crossover and dynamic heterogeneity in hydration water confined in aged cement paste 123

C.9 Observation of high-temperature dynamic crossover in protein hydration water and its relation to reversible denaturation of lysozyme 124

C.10 Dynamic Susceptibility of Supercooled Water and its relation to the Dynamic Crossover Phenomenon 125

C.11 Absence of the Density Minimum of Supercooled Water in Hydrophobic Confinement 126

C.12 Neutron Scattering Studies of Dynamic Crossover Phenomena in a Coupled System of Biopolymer and Its Hydration Water 127

C.13 Logarithmic decay in single-particle relaxation of hydrated lysozyme powder 128
C.14 Evidence of dynamic crossover phenomena in water and other glass-forming liquids: experiments, MD simulations and theory . . 129

References **131**

List of Figures

1.1 How to extract the relaxation time of a system 7
1.2 Typical $\phi_q(t)$ for a Supercooled Liquid 8
1.3 Stretching of the relaxation 10
1.4 Typical C_p of a glass former 11
1.5 Temperature dependence of $\phi_q(t)$ 12
1.6 The Arrhenius Plot 13
1.7 Different methods to extract the dynamic transition temperature . 15
1.8 Dynamic Heterogeneities 16

2.1 Specific heat of supercooled confined water 20
2.2 Comparison between water and argon dynamics 22
2.3 Water molecule inside its cage 23
2.4 MCM-41 structure 25
2.5 1D-confined water dynamic transition 26
2.6 1D-confined water χ_T 27
2.7 Chemistry and physics of cement 29
2.8 Cement hydration water does not crystallize 30
2.9 QENS spectra of cement hydration water 31
2.10 3D-confined water dynamic transition 33
2.11 3D-confined water χ_T 34
2.12 Bulk water dynamics 35
2.13 Bulk water dynamic transition 36
2.14 Bulk water χ_T and χ_4 37

2.15 Relaxation time of confined water: a timeline 38

3.1 Protein Energy Landscape 40
3.2 Traffic model for the conformational space 41
3.3 Complete time-dependence of protein $\phi_q(t)$ 42
3.4 Typical phonons 43
3.5 Structure of BSA and LYZ 44
3.6 Protein S_q 46
3.7 DHO model fitting of the measured IXS spectra of BSA 47
3.8 Phonon-like excitation in BSA and LYZ 48
3.9 Examples of logarithmic dynamics 49
3.10 Protein $\phi_q(t)$: a comparison with hydration water 51
3.11 Protein $\phi_q(t)$: different protein states 52
3.12 Protein $\phi_q(t)$: a comparison between backbone and side chains . . 53
3.13 Protein $\phi_q(t)$: different proteins 54
3.14 Protein $\phi_q(t)$: different temperatures 55
3.15 MCT parameters: f_q, H'_q, H''_q 56
3.16 MCT parameters: τ^β 57
3.17 The protein-glass analogy 59
3.18 Long-time behavior of protein $\phi_q(t)$ 60
3.19 q-dependence of τ_q^α 61
3.20 Arrhenius plot of the inverse diffusion constant 62

4.1 Perspective view of the simulation box 67
4.2 Protein and water $\langle x^2 \rangle$ 72
4.3 Protein hydration water QENS 73
4.4 Protein hydration water $\phi_q(t)$ 74
4.5 Protein hydration water $\langle \tau \rangle$: experiments 75
4.6 Coincidence of T_l and T_L 76
4.7 Protein hydration water $\langle \tau \rangle$: simulations 77
4.8 Numerical results for $h = 0.3$ 78
4.9 Hydration level dependence of $\langle \tau \rangle$ 79

4.10 Adam-Gibbs theory for protein hydration water 81
4.11 QENS spectrum of protein hydration water at high T 84
4.12 Fitting parameters 85
4.13 Transport property of hydration water 86
4.14 Migration distance 87
4.15 Backbone RMSD for different temperatures. 88
4.16 Arrhenius plot of the inverse diffusion constant at high T 89
4.17 Water-Protein coupling 90

A.1 Ergodic to Nonergodic transition 100
A.2 Comparison between A_2 and A_3 correlators close to the transition 101
A.3 Comparison between iMCT and eMCT: $\phi_q(t)$ 102
A.4 Comparison between iMCT and eMCT: τ 103
A.5 Adam-Gibbs theory and water dynamic crossover 105

B.1 Simulation techniques in physical chemistry 108
B.2 Simulation boxes 113

1

Introduction to the Dynamics of Liquids

Time *is the measure of movement*
Aristotle

1.1 The concept of *relaxation*

The term *dynamics* refers to phenomena that produce time-changing properties $X(t)$, with values at one time being correlated with those at other times ($corr(X(t), X(t + \Delta t) > 0$). It refers to the unfolding of events in a continuing evolutionary process. Nearly all observed phenomena in our daily lives or in scientific investigation have important dynamic aspects, such as in (a) a *physical system*, like a fluid; (b) a *social system*, like the movement within hierarchy; or (c) a *life system*, like a population growth. Many dynamic systems can be understood and analyzed intuitively, but in order to approach unfamiliar situations efficiently, it is necessary to proceed systematically. From now on we will focus our attention on the dynamics of a particular complex system: the liquid state of matter.

The *H theorem*, first proved by the unfortunate Professor Boltzmann, guarantees that

"an isolated many particle system will eventually reach equilibrium, irrespective of its initial state."

The typical time-scale for this process is called the *relaxation time*, τ, and it depends in detail on the interaction between particles[1].

When an external perturbation is applied to a system, the disturbance is damped by the relaxation processes in the system (20). The simplest rate of disappearance of a small perturbation $\delta X(t) = X(t) - X_0$ from the equilibrium value X_0 of the relaxing property $X(t)$ is approximately proportional to the magnitude of the displacement. This relationship is given by the differential equation

$$-\frac{d}{dt}(\delta X) = \frac{\delta X}{\tau} \tag{1.1}$$

Solution of this equation is the exponential relaxation ($\delta X(t) \sim e^{-t/\tau}$ or *Debye law*), characteristic of gases and simple liquids (10). The word *relaxation* was originally applied to a molecular process by the Scottish physicist James Clerk Maxwell (97). He referred to the *relaxation time* of a force as the time required for it to decay to $1/e$ times its initial value. In fact when $t = \tau$, $\delta X(t) = 1/e$.

In the absence of external perturbations, $\delta X(t)$ can be considered a spontaneous microscopic fluctuation, that always occurs in a system at finite temperature. These are dissipated in the medium in the same way as the external disturbances[2], so by observing them one can study transport properties in a system at thermodynamic equilibrium and obtain the basic information concerning the *dynamics of a fluid*.

[1] The Milky Way is an isolated dynamical system that can be thought of as a self-gravitating gas of stars, which interact via occasional *near miss* events in which they exchange energy and momentum. The best estimate for the relaxation time of our galaxy is about 10^{13} years, while its age is about 10^{10} years. So the Milky Way has not been around long enough to reach an equilibrium state.

[2] Onsager's *regression hypothesis* states that spontaneous fluctuations in equilibrium regress back to equilibrium according to the same relaxation equation that describes the macroscopic relaxation due to a weak external perturbation

1.2 Density correlation functions, $\phi_q(t)$

In order to study the dynamics of a system, we need to introduce the concept of *time correlation function* (66). This is the thermodynamic average of the product of two dynamical variables, each of which expresses the instantaneous deviation $\delta X(t)$ (fluctuations) of a fluid property $X(t)$ from its equilibrium value at particular points in space and time. A time correlation function is therefore a function of space and time, and it describes the thermal fluctuations which occur spontaneously in the equilibrium system. It basically tells how long a given property persists until it is averaged out by microscopic motions of system, i.e. how and when a statistical relationship has vanished (151). The dynamical variable of greatest interest in this thesis is the number density of molecules, ρ. The correlation function formed from the average of two density variables will be called the *density correlation function* or *intermediate scattering function*, $\phi_q(t)$[1].

Consider N particles that have coordinates $\{\mathbf{r}^N\} = \{\mathbf{r}_1, \mathbf{r}_2, ..., \mathbf{r}_N\}$. The local density is defined as

$$\rho_r = \sum_{j=1}^{N} \delta(\mathbf{r} - \mathbf{r}_j) \tag{1.2}$$

and gives the number density $n = \langle \rho(\mathbf{r}) \rangle$. Its spatial Fourier transform with wavevector q is

$$\rho_q = \int_V e^{i\mathbf{q}\cdot\mathbf{r}} \rho(\mathbf{r})\, d\mathbf{r} = \sum_{j=1}^{N} e^{i\mathbf{q}\cdot\mathbf{r}} \tag{1.3}$$

The normalized time-dependent density correlators of the Fourier components of the density $\rho_q(t)$ is

$$\phi_q(t) = \frac{\langle \rho_q(t)\rho_{-q}(0) \rangle}{\langle |\rho_q|^2 \rangle} \tag{1.4}$$

[1]These functions are called *intermediate* since one of their variables is in the direct space (t) and one in the Fourier-transformed space (q). They are therefore intermediate between the *dynamic structure factor*, $S_q(\omega)$, and the *van Hove correlation function*, $G_r(t)$, i.e. $S_q(\omega) \xleftarrow{TimeFT} \phi_q(t) \xleftarrow{SpaceFT} G_r(t)$

$\phi_q(t)$ is the most important function in any study of nonequilibrium properties of fluids because it essentially contains all the relevant information on the dynamics of the system (20). When the appropriate theory is available, a knowledge of the density correlation function will enable one to extract thermodynamic, structural, and transport properties of the fluid. For instance, all transport coefficients can be expressed in terms of time correlation functions so that the set of these functions plays the same fundamental role in transport phenomena as the partition function in thermodynamics, as a link between microscopic and macroscopic descriptions. Unlike the partition function though, the density correlation function can be measured directly, or calculated from a simulation trajectory with the formula $\phi_q(t) = \langle \exp[i\mathbf{q} \cdot (\mathbf{r}_i(t) - \mathbf{r}_j(0)] \rangle$, where i and j are particle indexes. This set of functions is sufficient to examine all the essential aspects of the dynamics of fluids. Its single-particle counterpart is the *single-particle density correlation function* or *self-intermediate scattering function*, i.e. the auto-correlation function of density fluctuations, $\phi_q^S(t) = \langle \exp[i\mathbf{q} \cdot (\mathbf{r}_i(t) - \mathbf{r}_i(0)] \rangle$. Since it is directly comparable with neutron scattering experiments of hydrogen atom based systems (like water and proteins), we are going to focus on this latter function throughout the thesis and, even though they are basically different quantities, for the sake of simplicity we will refer to it with the same symbol used for the density correlation function, $\phi_q(t)$.

Time correlation functions also allow a more rigorous and general definition of τ, the *relaxation time*, as the area under the curve:

$$\tau = \int_0^\infty dt \phi_q(t) \tag{1.5}$$

This definition includes Maxwell's one: if $\phi_q(t) = e^{-t/\tau_{exp}}$, $\tau = \tau_{exp}$.

The theoretical problem of studying time correlation functions has been analyzed using different formalisms, that differ in the manner of calculating the *memory function*, a time-dependent phase-space function. Let us consider a typical equation that relates a time correlation function $\phi_q(t)$ to its memory function $m_q(t)$

$$\frac{\partial}{\partial t}\phi_q(t) = -\int_0^t m_q(t')\phi_q(t-t')\,dt' \tag{1.6}$$

Given $m_q(t)$, this equation can be used to calculate $\phi_q(t)$. The reason why $m_q(t)$ is called the memory function can be seen from Equation 1.6. Since time correlation functions describe the decay of spontaneous thermal fluctuations, $\phi_q(t)$ is a function with its maximum value at $t = 0$ which decreases with time. Equation 1.6 shows that the decay rate of $\phi_q(t)$ at time t depends on its values at earlier times, and how much it remembers its past history is expressed by the memory $m_q(t)$. Suppose $m_q(t)$ is a sharply peaked function about $t = 0$, the right-hand side of Equation 1.6 then gives a decay rate that is proportional to $\phi_q(t)$. In this case the decay depends only on the instantaneous value of $\phi_q(t)$ so one can say that there is no memory. On the other hand, if $m_q(t)$ is itself a slowly decaying function in time, then the values of $\phi_q(t)$ at different times will be closely correlated, a behavior which one can describe as *memory effects*, i.e. $corr(\phi_q(t), \phi_q(t + \Delta t)) > 0$.

Besides modeling $m_q(t)$ by postulating a time-dependent function, one can also determine the memory function by expressing its decay in terms of coupling to higher-order (quadratic) time correlation functions which involve more than two dynamical variables. This approach is the most successful in liquid theory and is called *mode coupling* (A.1). It derives equations for $\phi_q(t)$ starting only from the number density n and the *static structure factor* $S_q = \langle|\delta\rho_q|^2\rangle/N = \phi_q(0)$[1].

1.3 Relaxations in liquids

1.3.1 Transport Properties

The physics of systems without translational invariance, such as liquids, dense fluids and glasses, has been fascinating scientists for many years with the liquid-to-glass transition, thermal anomalies and divergence of transport properties (3;

[1]From their definition, it is obvious that $\phi_q(0) \neq 1$ and $\phi_q^S(0) = 1$. This means that initially the atoms are precisely localized. As time evolves, the atoms move away from their initial position and the correlators decrease.

6). In contrast to the crystalline case, in disordered systems the comprehension of dynamics is complicated both by the absence of translational invariance and by the presence of other degrees of freedom, such as the following relaxation processes.

When an external perturbation is applied to a fluid, the disturbance is damped by dissipation phenomena as *diffusion* (D), *viscous flows* (η) and *thermal conduction* (κ). These are the processes that determine the *transport properties* of a fluid. Fluctuations δX in a fluid are characterized by a length scale (their wavelength, λ) and a time scale (their period, T), more commonly expressed in their Fourier transformed space (wave vector $q \sim 1/\lambda$ and frequency $\omega \sim 1/T$). For long-wavelength ($q \to 0$) and long-period ($\omega \to 0$) fluctuations, the fluid behaves like a continuum: the response can be described by the equations of *hydrodynamics*. But at wavelengths comparable to the intermolecular distances, the local structure of the fluid becomes important: the continuum picture is no longer valid and one must describe the system as an assembly of interacting particles. This is the domain of *molecular dynamics*. Molecular dynamics provides the framework for extending hydrodynamic calculations to the region of finite (q, ω) where spatial and time variations are comparable to the collision mean free path and mean time between collisions. Our study will be limited in this latter space-time range.

Therefore, a large amount of information can be experimentally deduced by determining $\phi_q(t)$. Equivalently, one can determine its time Fourier transform, the *dynamic structure factor* or *power spectrum*,

$$S_q(\omega) = \frac{1}{2\pi} \int_{-\infty}^{+\infty} e^{-i\omega t} \phi_q(t)\, dt. \tag{1.7}$$

$S_q(\omega)$ can be measured by means of scattering experiments (neutrons or x-ray) or calculated by molecular dynamics simulations. The physical processes which give rise to nuclear scattering of neutrons are in fact density fluctuations, so scattering experiments directly measure density correlation functions and their

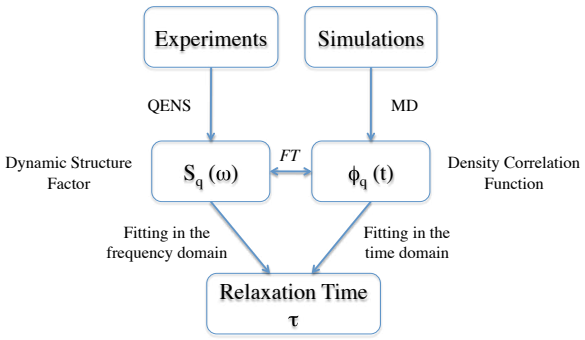

Figure 1.1: How to extract the relaxation time of a system - Scheme employed in this thesis to extract the relaxation time of a liquid system, either from experiments (quasi-elastic neutron scattering, in the frequency domain) or from simulations (molecular dynamics, in the time domain). The two are related by the Fourier transform.

Fourier transforms[1]. The decay rate of $\phi_q(t)$ increases with q, an indication that the shorter wavelength fluctuations die out more rapidly, or equivalently, the atom can move out of a smaller spatial region faster. It follows that the $S_q(\omega)$ central peak will become broader with increasing q.

In this thesis, we will employ both techniques to study the (q, ω)-dependence of the dynamics of complex systems, according to the scheme sketched in Figure 1.1. In particular, we are going to focus on the dynamics of water and protein, two of the most interesting and relevant complex liquid systems, whose coupling and interaction allowed life (as we know it) to develop.

1.3.2 Relaxations in supercooled liquids

The presence of these relaxations in a liquid automatically introduces different time-scales when the system is supercooled (i.e. cooled below its crystallization temperature): the slowest dynamics is called α relaxation (τ^α), collective and coupled to η, while the fastest dynamics is called β relaxation (τ^β), characterizing the vibrational dynamics of particles around their quasi-equilibrium positions[2].

[1] For isotropic fluids, $\phi_q(t)$ depends on the magnitude of q and not its direction. When treated classically, these functions are real and even in t. Their Fourier transforms, $S_q(\omega)$ are therefore even functions of ω.

[2] This process is allowed by the formation of a cage around the tagged particle by its nearest neighbors, as we shall see later in more details.

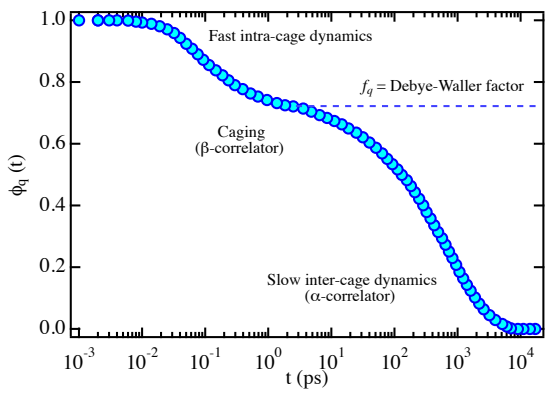

Figure 1.2: Typical $\phi_q(t)$ for a Supercooled Liquid - Sketch of the typical shape of a density correlation function of a supercooled liquid. The initial microscopic intra-cage relaxation is followed by the caging dynamics (β dynamics), and then by the cage-restructuring decay (α dynamics).

This is of the order of the inverse *Debye frequency*, i.e. that of a crystal with similar density and sound velocity (96). Moreover, one has to consider that the topological disorder introduces a second length scale, ξ, beside the interparticle distance, γ, that is typical for crystals. The rich phenomenology observed in the dynamics of disordered systems can be ascribed to the interplay between these different structural (ξ, γ) and dynamical (τ^α, τ^β) scales. An exhaustive understanding of dynamics in disordered systems in the so-called *mesoscopic region* (defined by length and time scales comparable to ξ and τ^α) is still not available and it represents a real challenge to modern physics. A typical density correlator, $\phi_q(t)$ for a supercooled liquid is sketched in Figure 1.2. The two different time-scales (τ^α, τ^β) are evident as two steps in the decay of the correlator to zero. The two steps are separated by a plateau, often referred to as the *Debye-Waller factor* or *nonergodic parameter*, for reasons that will be clear later on.

Liquids are dense systems, which do not contain channels or holes. Long-range diffusion thus requires a collective rearrangement of many particles. The relevant spatial scale is set by the intermolecular distance γ, since each particle is constrained by a cage of nearest neighbors and the α relaxation requires the escape out of this cage as an essential initial step. This inter-cage transfer is a plausible picture of the α-process, which restores the ergodicity on the respective α-time scale. As the liquid is further cooled down, the cage becomes a trap and macroscopic structural arrest results.

Naturally, in order to study the appropriate dynamics, special attention should be paid to the portion of the (q, ω)-plane corresponding to the characteristic length-scales (ξ, γ) and time-scales (τ^α, τ^β) of the system. In most liquids ξ and γ are $\sim$ 10 and 0.1 nm, respectively, while τ^β is usually $<$ 1 ps. On the other hand, τ^α can assume rather disparate values, since it strongly depends both on the specific nature of the relaxation process under consideration and on the thermodynamic conditions[1]. For studying the physics of disordered systems, the most important (q, ω)-range is therefore 0.2 - 5 Å^{-1} and 0.001 - 10 meV.

When a liquid is supercooled, instead of the exponential relaxation described above, the α-relaxation becomes *stretched* (see Figure 1.3), according to the following equation:

$$\phi_q(t) = e^{-(t/\tau_q^\alpha)^\beta} \tag{1.8}$$

where $0 < \beta < 1$[2]. The symbol β of the stretched exponent is not to be confused with the β relaxation seen before. The origin of the stretching of the relaxation can be understood as a linear superposition of simple exponential decays,

$$e^{-(t/\tau_q)^\beta} = \int_0^\infty du \rho(u) e^{-t/u} \tag{1.9}$$

where $\rho(u)$ is a nontrivial distribution of relaxation times. This is evident in the frequency domain, where peaks appear corresponding approximately to the main relaxation times. In order to define an average relaxation time, we consider the area under the curve (see Equation 1.5):

$$\langle \tau \rangle = \int_0^\infty dt e^{-(t/\tau)^\beta} = \frac{\tau}{\beta} \Gamma \left(\frac{1}{\beta} \right) \tag{1.10}$$

[1] The α-relaxation time is connected with the shear viscosity of the liquid, η, by the Maxwell equation: $\tau = G\eta$, where G denotes the shear modulus of the liquid.

[2] It was first introduced by Kohlrausch in 1854 to describe the discharge of a capacitor (81), and in 1970 Williams and Watts used the Fourier transform of the stretched exponential to describe dielectric spectra of polymers (142): in this context, the stretched exponential is also called the Kohlrausch-Williams-Watts (KWW) function. Outside condensed matter physics, it is used, for example, to describe the removal rates of small bodies in the solar system.

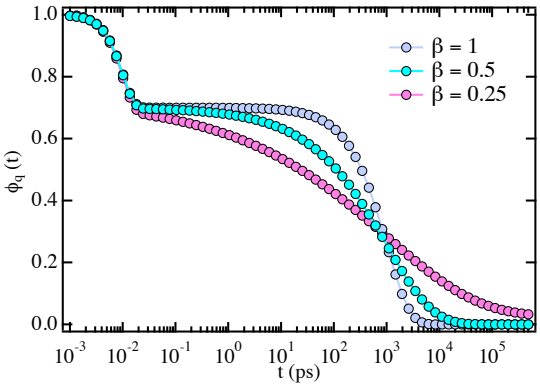

Figure 1.3: Stretching of the relaxation - Sketch of the typical shape of the density correlators in a liquid as a function of the stretch exponent β. The three curves intersect at the α-relaxation time, that does not depend on the value of β.

where Γ is the gamma function[1]. For the exponential decay, $\beta = 1$ and $\langle\tau\rangle = \tau$.

A supercooled liquid is not in thermodynamic equilibrium, which would be the crystalline state, but is still in dynamic equilibrium since density fluctuations can relax (i.e. $\phi_q(t)$ decays to zero, η is finite and the material can flow). But at low enough temperature, the correlation functions decay to a non-zero plateau value and the system falls out of dynamic equilibrium (crossover from ergodic to nonergodic behavior)[2]. When a fluid is supercooled so deeply that an amorphous solid form of matter results, it becomes a *glass*. By convention, the glass transition temperature T_g is where the viscosity η reaches a value of 10^{12} Pa s or the structural relaxation time τ reaches an order of 100 s. This definition on a scale of seconds is technologically relevant to the glassblower, but it has no deep physical meaning and it is actually non-consistent with the calorimetric definition of T_g (98). The microscopic structure, expressed by the structure factor S_q, changes smoothly across T_g.

[1]These degrees of freedom contribute independently to $\phi_q(t)$ with its own relaxation time, thus *parallel* relaxation. A different point of view was proposed by Palmer et al. (111), who suggested that the path to equilibrium is governed by many sequential correlated steps, thus a *series* interpretation in which there are strong correlations between different degrees of freedom. This model (*hierarchically constrained dynamics*) also leads to the Kohlrausch law.

[2]This is strictly true only considering the finite time window of the experiment: if one could wait long enough, ergodicity will be eventually restored. See the discussion on the Deborah number in the next page

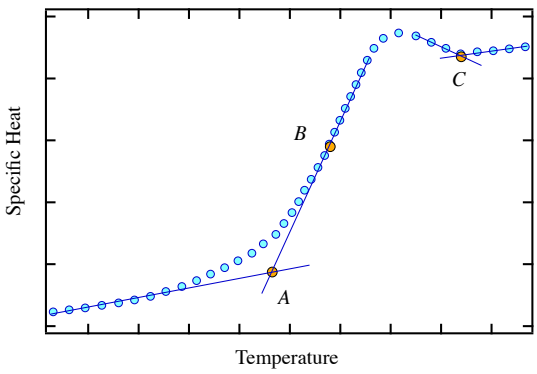

Figure 1.4: Typical C_p of a glass former - Typical temperature dependence of the specific heat of a supercooled liquid undergoing a glass transition. A, B and C are different options for the definition of the glass transition temperature. Redrawn from Statistical Calculation of Glass Properties.

A glass (*dynamic*) transition is different from a structural (*thermodynamic*) transition (e.g. crystallization). The latter exhibits a sharp transition temperature, which is a thermodynamic time-independent property. The glass transition, in contrast, has a finite width and the effective glass temperature varies with the cooling rate and more generally with the experimental time scale, according to the *Deborah number*. This is a dimensionless number to characterize how fluid a material is, and it is defined as $D_e = \tau/t_0$ where τ is the relaxation time and t_0 is the characteristic time scale of an experiment. The smaller the Deborah number, the more fluid the material appears[1]. The time scale of the experiment is thus an essential ingredient of the transition and cannot be ignored.

Experimentally, a small peak followed by a step-like decrease in the specific heat is observed around T_g. In Figure 1.4 we show a typical profile of the C_p of a substance undergoing a glass transition. There is no agreement in literature on the definition of T_g: out of 300 papers published during the period 2005-2006 on this subject, 16% of them chose point A, 5% B and 2% C, while 77% of them did not even bother to specify it (98). This step in the specific heat ΔC_p is proportional to the plateau value of $\phi_q(t)$, $\Delta C_p \sim f_q$, expressing the degree of nonergodicity of the system (see Figure 1.2). The glass transition is always linked to the increasing α-relaxation time of the system, and this explains why the T_g

[1]The origin of the name is the line "The mountains flowed before the Lord" in a song by prophetess Deborah recorded in the Bible (Judges 5:5)

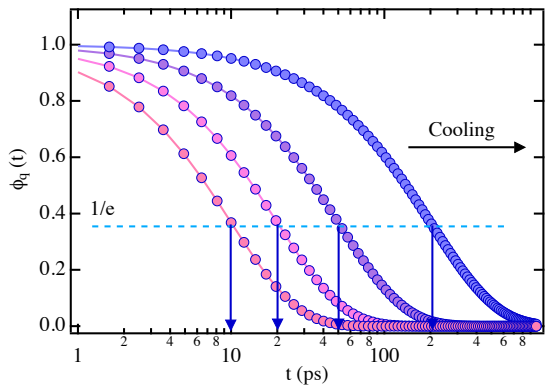

Figure 1.5: Temperature dependence of $\phi_q(t)$ - Typical temperature dependence of $\phi_q(t)$ for a supercooled liquid. Assuming an exponential relaxation, the $1/e$ value of $\phi_q(t)$ is the relaxation time of the system. As temperature is decreased, τ increases dramatically.

depends on the experimental time scale.

So T_g has a conventional definition both from a dynamic (η, τ) and a thermodynamic (C_p) point of view. A more meaningful parameter to characterize the slow dynamics of a supercooled liquid is the *dynamic transition* temperature.

1.3.3 Dynamic transitions

Glasses are, in the estimate of a Nobel laureate (4),

> "the deepest and most interesting unsolved problem in condensed matter physics"

In this respect, one of the most confusing aspects is the slowing down of the dynamics on decreasing the temperature of the liquid, as shown in Figure 1.5. The rate at which transport properties change by lowering temperature is called their *fragility* (5). The approach to large values of η (or τ) upon supercooling differs from one liquid to another. When displayed in an Arrhenius plot of $\log \eta$ (or $\log \tau$) versus inverse temperature $1/T$, some liquids (such as silica) show a steady, linear increase, while others display a much steeper dependence on $1/T$ (such as o-terphenyl). The former are called *strong* liquids, and the latter *fragile* liquids. Thus, the glassy liquid is called *fragile* when its viscosity (or relaxation time) varies according to super-Arrhenius law, such as the Vogel-Fulcher-Tammann (VFT) law:

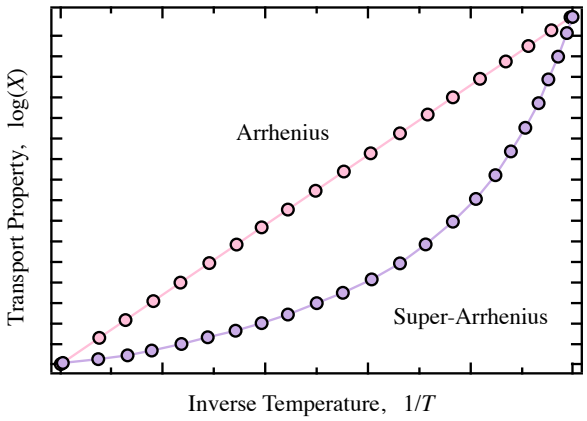

Figure 1.6: The Arrhenius Plot - Sketch of the Arrhenius plot of a typical transport property X of a fluid, i.e. $\log(X)$ vs $1/T$. Two different behaviors are common: Arrhenius behavior (straight line) and Super-Arrhenius behavior (divergent curve at T_0, see Equation 1.11).

$$\tau = \tau_0 \exp\left(\frac{BT_0}{T - T_0}\right) \tag{1.11}$$

where T_0 is the temperature of apparent divergence of the relaxation time (or sometime called Kauzmann temperature[1]); the magnitude of B gives the degree of fragility; τ_0 is a prefactor related to microscopic vibrational relaxation time inside the cage forming by neighbors in the liquid state. The liquid is called *strong* when the viscosity or relaxation time obeys Arrhenius law:

$$\tau = \tau_0 \exp\left(\frac{E_A}{k_B T}\right) \tag{1.12}$$

where E_A is the energy barrier for the relaxation process. These terms derive from their ability to reorganize through fluctuations: if thermal excitation do not offer much resistance to the reorganization, the liquid is said to be fragile. It is said to be strong if it resists structural changes

When the transport properties of a liquid change qualitatively their dynamic behavior as a function of temperature (from super-Arrhenius to Arrhenius or vice versa), the liquid is said to undergo a *dynamic transition*. This kind of transition is particularly evident in the Arrhenius plot, since an Arrhenius behavior appears

[1]This refers to the *Kauzmann paradox*, the decrease of entropy of a supercooled liquid that, if extrapolated, would cross the entropy of the crystal at T_0, the ideal glass transition.

as a straight line, while a Super-Arrhenius behavior as a diverging curve (see Figure 1.6).

During the past years, we realized that there are at least 4 ways to define and extract the dynamic transition temperature (148):

1. Fitting the low-temperature and the high-temperature part of the mean square displacement $\langle x^2 \rangle$ vs T plot separately with a straight line, and taking the intersection of the two (onset of the non-harmonicity).

2. Fitting the Arrhenius plot with two curves (VFT law in the diverging part and Arrhenius law in the linear part) and taking the intersection. This way is probably the most popular, even though it may lead to the conclusion that the dynamic transition is cusp-like, when it could actually be smoother.

3. Plotting the derivative of the Arrhenius plot, i.e. $d\log(X)/d(1/T)$ vs $1/T$, and taking the temperature at which the plot has a maximum (or a minimum).

4. Calculating the derivative of the density correlators as a function of T, $\chi_T(t) = d\phi_q(t)/dT$, and taking the temperature at which $\chi_T(t)$ is maximum (or minimum).

These four criteria agree (within the experimental error bars) in the definition of the dynamic transition temperature. We exemplified them in Figure 1.7. Throughout this thesis, we will use either the Method 3 or 4: they are preferable over the others since they are fitting-independent, and they do not require any assumption (see next section for an explanation of Method 4).

In the following chapters, we are going to explore these kind of transitions in bulk water, proteins and protein hydration water. This demonstrates how rich the dynamics of these two complex systems is, and how their coupling produces non-trivial dynamic phenomena, possibly responsible for protein biological function.

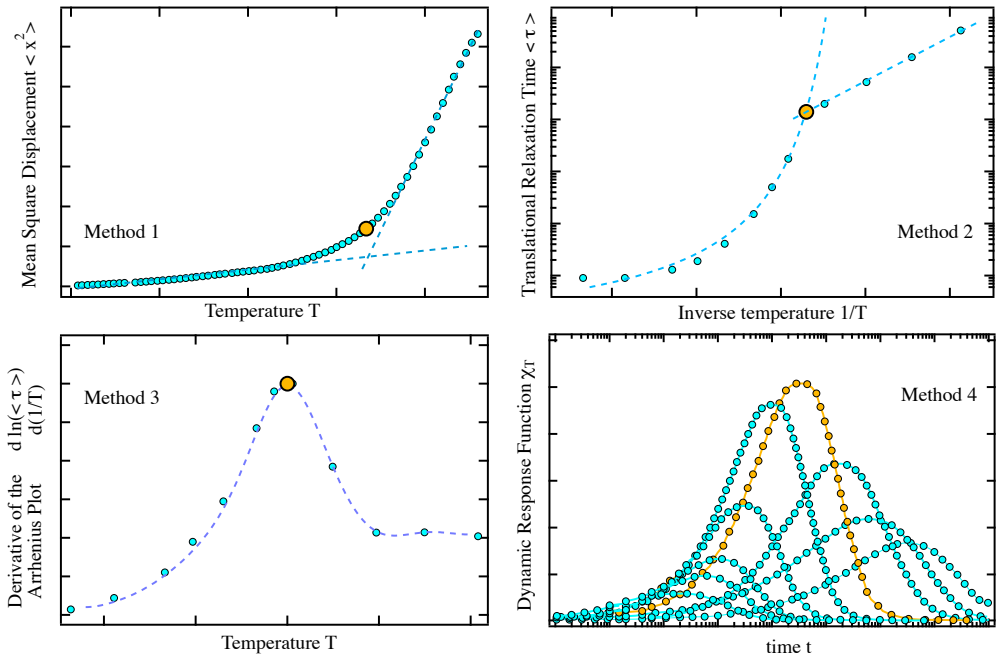

Figure 1.7: Different methods to extract the dynamic transition temperature - The orange dots indicate the transition temperature. *Method 1*: Mean square displacement, $\langle x^2 \rangle$; *Method 2*: Arrhenius plot of the translational relaxation time, $\langle \tau \rangle$; *Method 3*: Derivative of the Arrhenius plot, $d \log\langle \tau \rangle / d(1/T)$; *Method 4*: Dynamic response function $\chi_T(t)$, the transition temperature corresponds to the curve with the highest maximum (orange dots).

1.3.4 Dynamic heterogeneity

A clear explanation of the dramatical increase of the viscosity of glass-forming liquids approaching the glass transition is not yet available (17). The conundrum is that the static structure of a glass is indistinguishable from that of the corresponding liquid, with no sign of increasing *static* correlation length scales accompanying the glass transition. Numerical simulations reveal instead the existence of a growing *dynamic* length scale associated with dynamic heterogeneities (48), while experiments have suggested a characteristic length scale of about 5 to 20 molecular diameters at T_g (41). We have therefore to introduce multi-point dynamic susceptibilities that quantify the correlated nature of the dynamics in

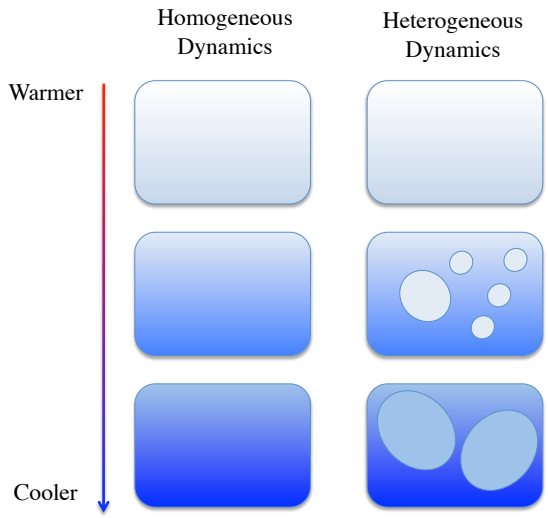

Figure 1.8: Dynamic Heterogeneities - Two possible scenarios are proposed to describe diffusion in cold liquids. In the spatially *homogeneous dynamics* scenario molecules relax in the same way, while in the spatially *heterogeneous dynamics* scenario, sets of more mobile molecules (in comparison to the average motion of the molecules in the system) form patches or clusters. The size of these clusters increases upon cooling.

glass formers (18).

In the spatially heterogeneous dynamics scenario (58), correlation functions for different molecules decay exponentially, but with a very broad distribution of relaxation times (see Equation 1.9). The superposition of these individual exponential contributions produces a nonexponential decay of the ensemble-averaged time correlation function, and the exponent β is a measure of the width of the distribution of relaxation times. In the heterogeneous scenario, the locally averaged molecular displacements are different depending on the part of the system we are looking at and when we look at it[1]. One finds groups of molecules that are more mobile and groups that are less mobile than the average molecule in the system. As the temperature is lowered, patches formed by mobile molecules increase in size, as shown in Figure 1.8. These patches have a short lifetime; they appear and disappear constantly in different parts of the system. In Section 2.3, we will show that the heterogeneous scenario can describe the dynamics of supercooled water.

[1]The idea that dynamic heterogeneity might play an important role near the glass transition can be traced back to Adam and Gibbs (2). They provided a theoretical argument of the existence of cooperatively rearranging regions in glassy liquids (see section A.4)

This heterogeneity implies the existence of significant fluctuations of the dynamics, because the number of independently relaxing regions is reduced. Numerical simulations have focused on a four-point dynamic susceptibility $\chi_4(t)$, which quantifies the amplitude of spontaneous fluctuations around the average dynamics. The latter is usually measured through ensemble-averaged correlators, $\phi_q(t)$. Dynamic correlation leads to large fluctuations measured by

$$\chi_4(t) = N\langle(\delta\phi_q(t))^2\rangle \tag{1.13}$$

where N is the total number of particles and $\delta X(t)$ stands for the fluctuation $\delta X(t) = X(t) - \langle X\rangle$. By definition, $\chi_4(t)$ quantifies the expectation of the square of the fluctuations of the density correlator. If we do not take the square in Equation 1.13, its ensemble average would go to zero in the long-time limit. $\chi_4(t)$ typically presents a non-monotonic time dependence with a peak centered at the liquid's relaxation time τ^α: the height of this peak is proportional to the volume within which correlated motion takes place (139). Unfortunately, numerical findings are limited to short time scales ($\sim$ 100 ns) and $T \gg T_g$.

We now introduce another quantity, $\chi_T(t)$. As we saw in Section 1.3.3, this is the derivative of the self-density correlation function $\phi_q(t)$ with respect to the temperature T, namely

$$\chi_T(t) = -\left(\frac{\partial\phi_q(t)}{\partial T}\right)_P \tag{1.14}$$

It is defined in analogy with the thermodynamic response functions (such as the specific heat, C_p) which are temperature derivative of the thermodynamic state functions (such as enthalpy) and describe the response of a system to an external perturbation field (in this case, temperature). This function shows a peak, located at the relaxation time of the system τ_q, the height of which (χ_T^*) is related to some sort of dynamic correlation length. χ_T^* grows as T is lowered and reaches a maximum, but this growth is interrupted when the dynamic crossover sets in. The reason for this behavior is clear if one considers that, combining Equations 1.14 and 1.8,

$$\chi_T(t) = \phi_q(t)\beta \left(\frac{t}{\tau_q(T)}\right)^{\beta} \frac{\partial \ln \tau_q(T)}{\partial(1/T)} T^{-2} \tag{1.15}$$

The only parameter of $\phi_q(t)$ that has to be differentiated with respect to T is, in our case, $\tau_q(T)$ since β remains almost constant and close to 0.5 ± 0.1 as T of confined water is lowered (31). χ_T^* is therefore directly proportional to the change in slope of the Arrhenius plot of $\langle\tau\rangle$, hence Method 4 in Section 1.3.3.

Experimentally, detecting spontaneous fluctuations of dynamic correlators (χ_4) remains an open challenge, because dynamic measurements have to be resolved in both space and time. Induced fluctuations (χ_T) are more easily accessible experimentally than spontaneous ones and can be related to one another by fluctuation-dissipation theorems. Thus, $\chi_T(t)$ is an experimentally accessible multipoint dynamic susceptibility that directly quantifies dynamic heterogeneity in glass formers.

In our experiments, the total number of particles N, pressure P and temperature T are constant, so we can apply the fluctuation-dissipation theorem in the NPT ensemble to relate the induced fluctuations to the spontaneous fluctuations,

$$\chi_T(t) = \frac{N}{k_B T^2} \langle \delta\phi_q(t) \delta H(0) \rangle \tag{1.16}$$

where $H(t)$ is the fluctuating enthalpy per particle. Therefore, $\chi_T(t)$ directly probes the correlations between the fluctuations of the single-particle density and the enthalpy ones. Transforming from the NPT to the NPH ensemble we have

$$\chi_4(t) = \chi_4^{NPH}(t) + \frac{k_B T^2}{C_p} \chi_T^2(t) \geq \frac{k_B T^2}{C_p} \chi_T^2(t) \tag{1.17}$$

This inequality can be considered an equality at low temperatures.

2

Water Dynamics

Nothing is more flexible and fragile than water.
Yet when it attacks the adamant and the strong, none can withstand it.
So the flexible overcomes the adamant, the fragile overcomes the strong.
Lao Tzu

2.1 Overview of water dynamics

Water has always occupied a unique role in the physics of liquids. Its numerous peculiar properties depict an intriguing scenario[1], and one of its most peculiar dynamic characteristics is an anomalous increase in thermodynamic response functions (such as the specific heat (150) and the thermal expansion coefficient (90), see Figure 2.1) and an apparent divergent behavior of transport properties (such as viscosity), on approaching an apparent singular temperature $T_L = 225 \pm 5$ K (135). Different models have been proposed to explain this anomalous behavior: i) the existence of two liquid phases that originate a liquid-liquid critical point in the *no man's land* temperature region (113); ii) the retracting spinodal hypothesis, where thermodynamic anomalies are ascribed to the vicinity of the spinodal line (131); iii) a singularity-free scenario where thermodynamic anomalies can be

[1] As of December 2009, around 67 anomalies of water are listed at Martin Chaplin's Water Website

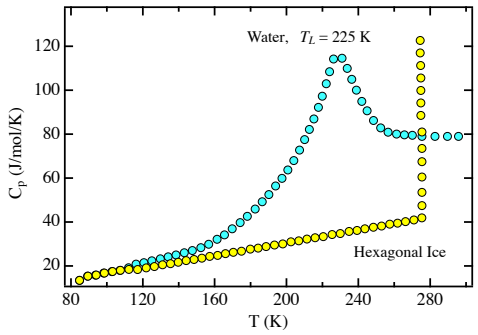

Figure 2.1: Specific heat of supercooled confined water - The total heat capacity of nanoconfined water, according to the measurements of Maruyama et al. [as plotted in (6)]. Note the absence of any normal glass transition between 100 and 200 K visible on the scale of this figure.

ascribed to structural heterogeneities (114), and iv) the mode-coupling theory (MCT, A.1) which describes water features without resorting to an underlying thermodynamic singularity (59). Let us revise the fast and slow relaxations of liquid water, in order to provide a suitable theoretical framework to study its dynamics by experiments and simulations.

What makes a water molecule so special is, as everybody knows, its capacity of forming strong hydrogen bonds with other water molecules. A time line of the short-time diffusion of water, and a comparison with a simple liquid like argon, is shown in Figure 2.2. For a water molecule, between the initial free particle relaxation and the final free diffusion, there is a lengthy period of *cage effect* during which the molecule moves very little, rattling inside the cage. In contrast, for an argon atom, the initial free flight and the final free diffusion are interrupted by only a brief period: its cage relaxes more easily, since it is not held together by hydrogen bonds.

For water, which is a fragile liquid at room temperature and at moderately supercooled temperatures, Angell and co-workers (74) proposed that a fragile-to-strong transition would occur at around 228 K at ambient pressure, based on a thermodynamic argument. This dynamic transition would avoid the structural arrest at T_L. But supercooled water nucleates into hexagonal ice at and below the *homogeneous nucleation temperature* $T_H = 235$ K, so this transition lies in an inaccessible region (*no man's land*) of temperatures and it cannot been observed directly. This limitation has been overcome over the years using different kinds

of confinement that prevent crystallization into hexagonal ice[1]. The interest of the scientific community in the properties of confined water is also that, in many real life systems, water is not in its bulk form but is located near surfaces or contained in small cavities. This is the case, for example, for water in rocks, in polymer gels, and in biological systems.

Due to the facts mentioned above, both the structure and dynamics of supercooled and confined water have been widely studied using molecular dynamics (MD) simulations (123; 124). The interaction between the hydrophilic surface and the water molecules has noticeable effects on the structure of the first and second layer of water near the pore surface (86). As far as the dynamics is concerned, when confined near hydrophilic surfaces, water molecules are in a sort of supercooled state even at room temperature. Generally speaking, confined water shows the dynamics similar to that of supercooled water at a lower equivalent temperature of around 30 degrees (147). Experimentally, the structural properties of water at supercooled temperatures and in confinement have been studied extensively using x-ray and neutron diffraction (15; 21), dielectric spectroscopy (16) and nuclear magnetic resonance (42). But is quasi-elastic neutron scattering (QENS) that offers the best advantage for the study of the single particle dynamics of water, since the neutron scattering of hydrogen atoms is mostly incoherent and with a huge cross-section. Using this technique, Chen et al. were able to study the self-dynamics of water in a wide range of time scales (1 ps $< t <$ 10^4 ps) and length scales (0.2 Å^{-1} $< q <$ 2.0 Å^{-1}) in the past few years. The experimentally determined dynamic structure factor, $S_q(\omega)$, is the Fourier transform of the self-intermediate scattering function, $\phi_q(t)$, of the hydrogen atom in a water

[1]Nucleation occurs with more difficulty in the interior of a uniform substance, by a process called *homogeneous nucleation*. The creation of a nucleus implies the formation of an interface: if its radius is smaller than a critical radius, the energy that would be released by forming its volume is not enough to create its surface, and nucleation does not proceed. The greater the supercooling, the smaller the critical radius and the less energy needed to form it. The spontaneous nucleation rate in water changes very rapidly with temperature, so T_H can be quite well defined. The Gibbs-Thompson equation states that the melting temperature of crystals of radius r decreases as r decreases, according to $T_m(r)/T_m(\infty) = 1 - C/r$, where C is a constant.

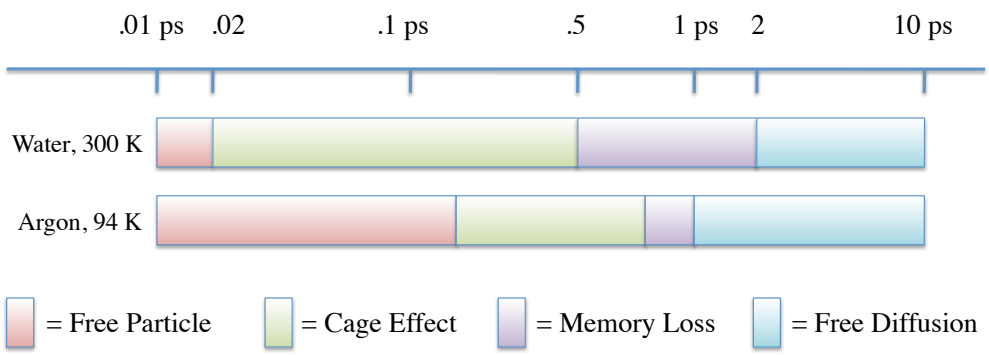

Figure 2.2: Comparison between water and argon dynamics - Comparison of the short-time diffusion between water (a hydrogen bonded liquid) and argon (a simple liquid). The particular feature to be noted is that for a water molecule, between the initial free flight and the final free diffusion there is a lengthy period of cage effect during which the molecule moves very little. In contrast, for an argon atom, the initial free flight and the final free diffusion are interrupted by only a brief period (27).

molecule. This connection facilitates the interpretation of the scattering data and allows a direct comparison with theory and with the data from MD simulations.

In order to fit the experimental $S_q(\omega)$ of water, Chen and collaborators have developed the *relaxing-cage* model (RCM) for the description of translational and rotational dynamics of water at supercooled temperatures (91; 147), deriving an analytical form for $\phi_q(t)$. These models have been tested with MD simulations of SPC/E water, and have been used to analyze QENS data (31; 50; 150). Given the fact that in the process of QENS data analysis, we only focus our attention on the $\phi_q(t)$ with $q < 1.1$ Å^{-1} , we can safely neglect the contribution of rotational motion to the total dynamics, which means that $\phi_q(t) \sim \phi_q^{transl}(t)$.

On lowering the temperature below the freezing point, around a given water molecule there is a tendency to form a hydrogen-bonded, tetrahedrally coordinated first and second neighbor shell (the so-called *cage*, see Figure 2.3). At short times, less than 0.05 ps, the center of mass of a water molecule performs vibrations inside the cage. At long times, longer than 1.0 ps, the cage eventually relaxes and the trapped particle can migrate through the rearrangement of

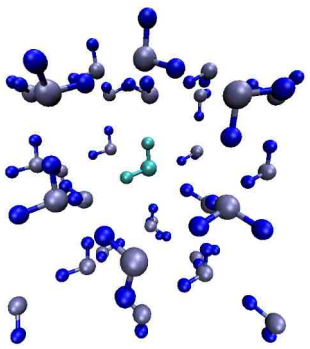

Figure 2.3: Water molecule inside its cage - A water molecule (light blue) is trapped inside the cage formed by its neighbors (dark blue) in the supercooled liquid. The rattling of the molecule in the cage produces the first step in the decay of $\phi_q(t)$, the β relaxation. But in order to escape the cage and diffuse, a collective motion (*hopping*) must take place and open the cage (last step of the decay, α relaxation).

a large number of particles surrounding it. Therefore, there is a strong coupling between the single particle motion and the density fluctuations of the fluid. With water, the cage involves not only van der Waals interactions but also hydrogen bonds. Intra-cage fluctuations are thus associated with opening and closing hydrogen bonds. The fluctuations between open and closed can be modeled with two states of different energy. The down-barrier to closing the bond is quite small and thus rate-limiting, implying a large and nearly temperature-independent β-relaxation rate. The population of open bonds, however, increases exponentially with the temperature.

The RCM assumes that the translational short-time dynamics of the trapped water molecule can be treated approximately as the motion of the center of mass in an isotropic harmonic potential well, provided by the mean field of its neighbors. We can, then, write the short-time part of the translational $\phi_q(t)$ in a Gaussian approximation, connecting it to the velocity auto-correlation function $\langle \mathbf{v}_{CM}(t) \cdot \mathbf{v}_{CM}(0) \rangle$, in the following way:

$$\phi_q^{short}(t) = \exp\left\{-q^2 \frac{\langle \mathbf{r}_{CM}^2(t) \rangle}{2}\right\} = \exp\left\{-q^2 \left[\int_0^t (t-\tau) \langle \mathbf{v}_{CM}(\tau) \cdot \mathbf{v}_{CM}(0) \rangle \, d\tau\right]\right\} \tag{2.1}$$

Since the translational density of states, $Z_T(\omega)$, is the Fourier transform of the normalized center of mass velocity auto-correlation function, one can express the mean squared deviation, $\langle \mathbf{r}_{CM}^2(t) \rangle$, as follows:

$$\langle \mathbf{r}_{CM}^2(t) \rangle = \frac{2}{3} \langle v_{CM}^2 \rangle \int_0^\infty \frac{Z_T(\omega)}{\omega^2} (1 - \cos \omega t)\, d\omega \tag{2.2}$$

where $\langle v_{CM}^2 \rangle = \langle v_x^2 \rangle + \langle v_y^2 \rangle + \langle v_z^2 \rangle = 3v_0^2 = 3k_BT/M$ is the average center of mass square velocity, and M is the mass of a water molecule. Experiments and MD results show that the translational harmonic motion of a water molecule in the cage gives rise to two peaks in $Z_T(\omega)$ at about 10 and 30 meV, respectively (14). Thus, the following Gaussian functional form is used to represent approximately the translational part of the density of states:

$$Z_T(\omega) = (1 - C) \frac{\omega^2}{\omega_1^2 \sqrt{2\pi\omega_1^2}} \exp\left[-\frac{\omega^2}{2\omega_1^2} \right] + C \frac{\omega^2}{\omega_2^2 \sqrt{2\pi\omega_2^2}} \exp\left[-\frac{\omega^2}{2\omega_2^2} \right] \tag{2.3}$$

Moreover, the fit of MD results using Equation 2.3 gives $C = 0.44$, $\omega_1 = 10.8$ THz, and $\omega_2 = 42.0$ THz (30). Using the above equations, we finally get an explicit expression for $\phi_q(t)^{short}$:

$$\phi_q^{short}(t) = \exp\left\{ -q^2 v_0^2 \left[\frac{1 - C}{\omega_1^2} (1 - e^{-\omega_1^2 t^2/2}) + \frac{C}{\omega_2^2} (1 - e^{-\omega_2^2 t^2/2}) \right] \right\} \tag{2.4}$$

Equation 2.4 is the short-time behavior of the translational $\phi_q(t)$. It starts from unity at $t = 0$ and decays rapidly to a flat plateau determined by an incoherent Debye-Waller factor f_q, given by

$$f_q = \exp\left\{ -q^2 v_0^2 \left[\frac{1 - C}{\omega_1^2} + \frac{C}{\omega_2^2} \right] \right\} = \exp\left[-\frac{q^2 a^2}{3} \right] \tag{2.5}$$

where a is the root mean square vibrational amplitude of the water molecules in the cage, in which the particle is constrained during its short-time movements (Figure 2.3).

According to MD simulations, $a \sim 0.5$ Å is fairly temperature independent (56). On the other hand, the cage relaxation at long times can be described with a stretched exponential. Therefore $\phi_q(t)$, valid for the entire time range, can be written as a product of the short-time part and a long-time part:

$$\phi_q(t) = \phi_q^{short}(t) \exp[-(t/\tau_q)^\beta] \tag{2.6}$$

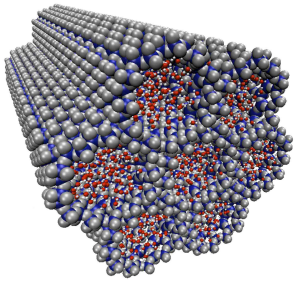

Figure 2.4: MCM-41 structure - 3-dimensional representation of MCM-41. When this mesoporous silica material is fully hydrated ($h = 0.5$ grams of water per gram of dry MCM), water fills the nanopores of its hexagonal lattice. The cylindrical pores have a diameter ranging from 10 to 20 Å. Colors: water molecules are displayed with O = red and H = white, while silica material has Si = blue and O = gray.

The fit of the MD generated $\phi_q(t)$ using Equation 2.6 shows that τ_q obeys the power law $\tau_q = \tau_0(aq)^{-\gamma}$, where $\gamma \leq 2$ and $\beta \leq 1$. In the $q \to 0$ limit, one should approach the diffusion limit, where $\gamma \to 2$ and $\beta \to 1$. Thus, $\phi_q(t) = \exp[-Dq^2t]$, D being the self-diffusion coefficient. In QENS experiments, this low-q limit is not reached, and both β and γ can be considered q-independent in the range $0 < q < 1$ Å (50). The average translational relaxation time can finally be obtained as $\langle\tau\rangle = (\tau_0/\beta)\Gamma(1/\beta)$, where Γ is the gamma function (see Equation 1.10).

2.2 Supercooled and confined water dynamics

2.2.1 1-D Confined water dynamics: Silica nanopores

By containing water in the small cylindrical pores (pore size $\sim$ 18 Å) of MCM-41 (Figure 2.4), Faraone et al. (50) were able to circumvent the homogenous nucleation process and supercool water down to 160 K. High-resolution QENS experiments were used to measure the average translational relaxation time, $\langle\tau\rangle$, of water molecules in the temperature range from 325 K down to deeply supercooled temperature. Two QENS spectrometers in NIST Center for Neutron Research (NIST-NCNR) were used: a disc-chopper time-of-flight spectrometer (DCS) and a high-flux backscattering spectrometer (HFBS). Combination of results from the above two spectrometers enabled them to cover the relaxation time range from 1 ps at high temperatures to 10 ns at the lowest temperature.

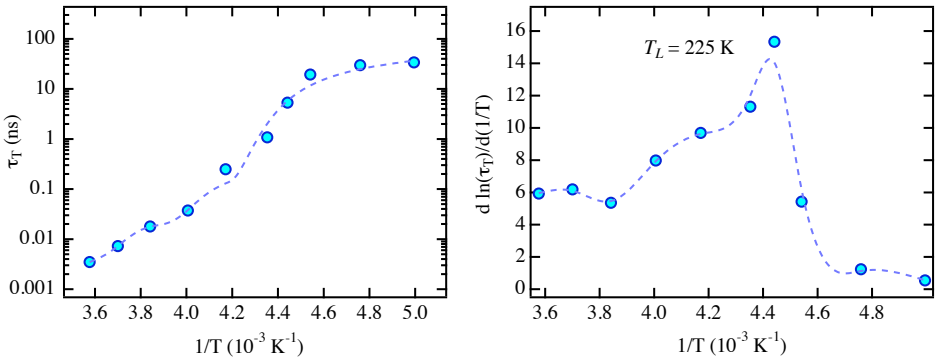

Figure 2.5: 1D-confined water dynamic transition - *Left*: Arrhenius plot of the relaxation time τ_T of water confined in MCM-41 at ambient pressure. *Right*: Derivative of the Arrhenius plot, the peak corresponds to the transition.

Figure 2.5 shows the temperature dependence of $\langle\tau\rangle$ and the derivative of its Arrhenius plot. The critical law predicted by mode-coupling theory, which is usually used for bulk supercooled water, would fit the data above 240 K, but deviates from the data below 240 K (50). At $T \sim 225$ K, there is a sudden change in the slope of the $1/T$-dependence of $\log(\langle\tau\rangle)$, as displayed in the left panel of Figure 2.5. The rate of dynamic slowing down changes abruptly at a temperature around 225 K, signalling the onset of an avoided structural arrest transition. This was the first experimental evidence of a *dynamic transition* (or *crossover*) in supercooled water. These findings were in agreement with the known properties of water below the melting point and in the supercooled region. In fact, a fragile-to-strong crossover (FSC) in water was proposed (74) on the basis of the determination of the fragility of water near the melting and glass transition temperatures: near T_g water is a very strong liquid, whereas in the supercooled region it is the most fragile one.

Another equivalent method to extract the dynamic transition temperature is shown in Figure 2.6, where we plot the analytical self-density correlators $\phi_q(t)$ extracted from the fitting with the RCM of the experimental structure factor $S_q(E)$, and the dynamic response functions χ_T calculated with finite differences of the $\phi_q(t)$. The big gap between the $\phi_q(t)$ at 240 and 230 K (left panel) is the

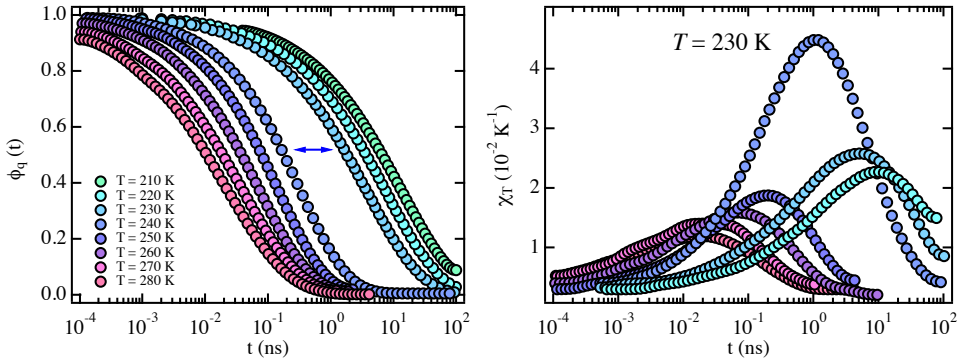

Figure 2.6: 1D-confined water χ_T - *Left*: Correlators $\phi_q(t)$ of confined water in MCM-41, as a function of temperature, extracted from the fitting of the dynamic structure factor $S_q(E)$, measured by QENS. Notice the big gap at the dynamic transition temperature T_L. *Right*: $\chi_T(t)$, calculated with finite differences of $\phi_q(t)$. The highest peak corresponds to T_L.

characteristic signature of the dynamic transition, and it will be seen other times throughout this work. It is also reflected in the highest peak of χ_T at $T_L = 235 \pm 5$ K (right panel).

2.2.2 2-D Confined water dynamics: Biomacromolecules

Water molecules in a protein solution may be classified into three categories: (i) bound internal water; (ii) surface water, i.e., the water molecules that strongly interact with the protein surface; and (iii) bulk water. The bound internal water molecules, which occupy internal cavities and deep clefts, are extensively involved in the protein-solvent H-bonding and play a structural role in the folded protein itself. The surface water, which is usually called the hydration water, is approximately the first layer of water molecules that interacts with the solvent-exposed protein atoms of different chemical character, feels the topology and roughness of the protein surface, and exhibits slow dynamics. Finally, water that is not in direct contact with the protein surface but continuously exchanges with the surface water has properties approaching that of bulk water.

Starting from 2006, Chen and collaborators collected quasi-elastic neutron scattering data of hydrated biopolymer powders, namely lysozyme, DNA and

RNA. The main contribution to the QENS spectra of these systems is the hydration water, which represents the water in category (ii) mentioned above. In all these cases, they found an analogous dynamic transition in water as the one reported in Section 2.2.1. The dynamic crossover temperatures where also in the same range, in spite of the differences in the chemical and topological structures of the biopolymers: $T_L = 225$ K for lysozyme, $T_L = 222$ K for DNA and $T_L = 220$ K for RNA hydration water.

The relation of T_L with the biomolecules functionality (especially for proteins), and its relation with the dynamic transition at T_l in the biomolecules themselves, will be extensively treated in Section 4.2

2.2.3 3-D Confined water dynamics: Cement paste

Cement is a ubiquitous construction material used in buildings, bridges and highways. At a price of roughly \$1 per 20 kg, concrete is one of the lowest cost materials for construction. The annual consumption is approximately 500 million metric tons of concrete. The National Research Council has estimated that improving the durability of roads and bridges by a single percentage point over a 20-year period would yield a saving of $\sim$ \$20 billion. Therefore, the study of cement properties is one of the most cost effective scientific investigations.

Ordinary cement powder (*Portland cement*) consists of calcium silicates, aluminates and alumino-ferrites. When it is combined with water, it forms a plastic paste that sets and eventually hardens to a rock-like consistency. During this curing process a series of chemical hydration reactions take place to form the corresponding hydrated phases, mainly calcium silicate hydrate (CSH), and to develop a 3D interconnected solid random network[1]. Thus, water plays the central role during the overall hydration process, when cement gains the desired hardness and strength. Understanding the dynamic behavior of water confined in the cement paste is therefore crucial for achieving complete control over its mechanical properties. In this section, we study the dynamics of water confined

[1]Cement chemistry notation: C = CaO, H=H_2O, S = SiO_2, A=Al_2O_3. So CSH is calcium silicate hydrate.

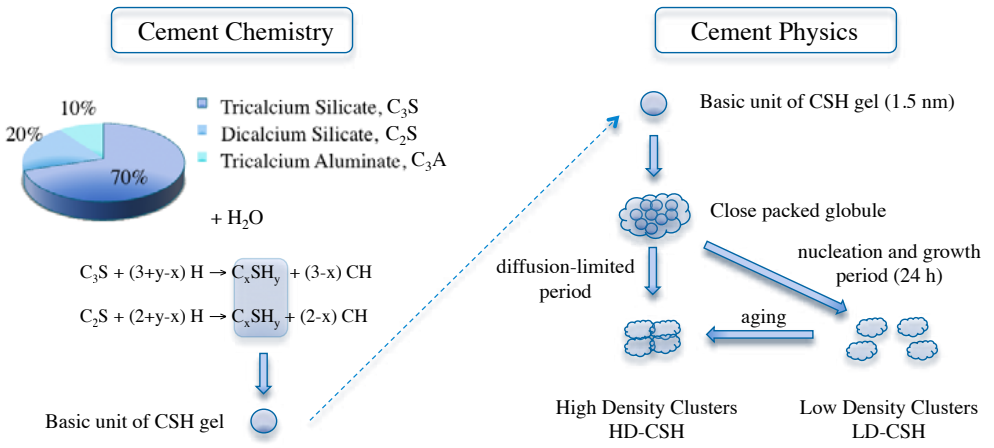

Figure 2.7: Chemistry and physics of cement - *Left*: Chemical composition and reactions that lead to the formation of the CSH colloidal particle. *Right*: Aggregation of CSH basic units to create globules and then two gel phases, a low density (within 24 hours) and a high density one (long-time limit).

in cement ($h = 0.4$), and cured for 8 days, with measurements made for 4 days subsequently using quasi-elastic neutron scattering (QENS) (150).

An example of the 3D confinement of water in cement paste can be pictured through the Jennings colloidal model (76). The calcium silicate hydrate gel (CSH, small spheres in Figure 2.7) is the amorphous gel responsible for the setting and hardening process of cement. It grows between calcium hydroxide particles (CH in the Figure). CSH is composed of colloidal particles with radius ~ 1.5 nm that aggregate to form globules. These globules cluster to form low density (LD) CSH regions within 24 h. The size of these pores inside the LD CSH is estimated to be around 1 nm (77), which corresponds to the interplanar space between the growing CSH lamellae.

Because of the hydration process the LD CSH domains assemble to give a structure with larger pores connected by narrow channels called inter-LD regions. The sizes of these pores are reported to vary over a large range (approximately between 1 and 10 nm (77)). The LD CSH aggregates grow with time, and after one month all the water in the inter-LD CSH is consumed by the hydration re-

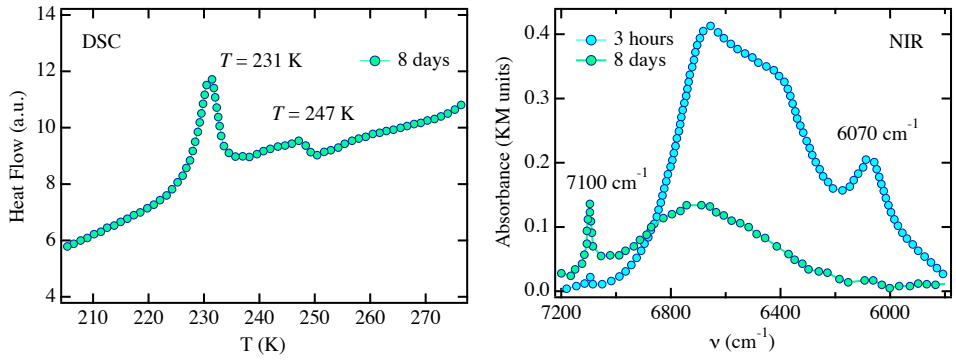

Figure 2.8: Cement hydration water does not crystallize - *Left*: DSC thermogram (cooling scan) of cement paste cured for 11 days. According to the JCM, the peak at 247 K is due to inter-LD pore water and the peak at 231 K to LD pore water. *Right*: NIR spectra acquired at 123 K on cement paste cured for 3 hours and 8 days. The peak at 6070 cm^{-1} is due to hexagonal ice, and disappears after 8 days of curing.

action. The JCM is consistent with the differential scanning calorimetry (DSC) thermogram recorded 11 days after the preparation (Figure 2.8). Two main features (peaks) are present, at 247 and 231 K, of which the second peak represents the main contribution. No peak is detected above 253 K, in the temperature range typical for the freezing of bulk water. Thus, at this hydration time all the unreacted water in the sample is strictly a kind of confined water in the solid matrix. According to the JCM, the two peaks visible in the cooling part of the thermograms are due to water reservoirs, i.e. relatively large pores interconnected through small channels, with nanometric diameter. In particular, the peak in the region between 253 and 238 K is due to water that is only accessible via the inter-LD pores (129). The time evolution of this kind of water is strongly connected to the w/c ratio and in our conditions is totally consumed after 28 days. On the other hand, the peak at 231 K corresponds to pores inside the LD CSH domains. Near infrared (NIR) experiments confirm that after eight days of setting the water in the cement paste is confined. Figure 2.8 reports the NIR spectrum registered at 123 K on a sample cured for 3 h. The absorption at 6070 cm^{-1} is considered as a fingerprint of hexagonal ice (64). The absence of this

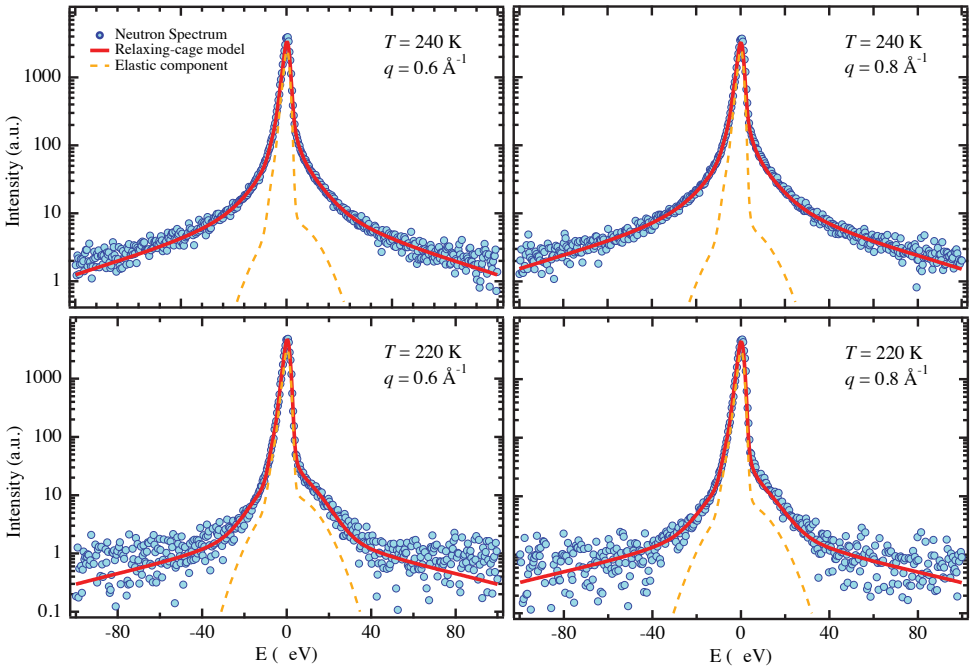

Figure 2.9: QENS spectra of cement hydration water - Illustration of the analysis of QENS spectra at two typical temperatures $T = 240$ K, 220 K and two typical wavevector transfers $q = 0.6$ and 0.8 Å^{-1}, respectively. The circles are the measured neutron intensity as a function of the energy transfer E. The solid line is the fitted curve using the model. The dashed line is the elastic scattering component, whose asymmetric shape derives from the asymmetric q-dependent resolution function.

peak after eight days indicates that, at this hydration time, water is totally 3D confined in the LD CSH domains and cannot crystallize any longer. This is the kind of water that we observed in the neutron scattering experiment. In this experiment, measurements were made on both an eight-day-old H_2O hydrated sample and a dry sample. The scattering from the dry sample was rather small due to the lack of hydrogen atoms, and thus was subtracted out as a background from the wet sample case.

The QENS spectra for each temperature were analyzed for four q values (0.2, 0.4, 0.6 and 0.8 Å^{-1}) simultaneously to extract τ_0 and β, and consequently to

evaluate the average translational relaxation time, according to RCM (see Section 2.1). Examples of data analysis using the model discussed above are shown in Figure 2.9. Two temperatures, one above T_L at 240 K and one below T_L at 220 K, are shown for two typical wavevector transfers $q = 0.6$ and 0.8 Å^{-1}. The figures are plotted on a log scale to show the good agreement between the model and measured spectra over the whole intensity range. The elastic scattering component (shaded area), mainly from scattering of immobile water molecules, ranges from 58% at 300 K to 86% at 180 K, leaving enough scattering coming from the relaxation process of the hydrogen atoms in water molecules. Unlike for the dynamics at room temperature, the line shape of the quasi-elastic peak is non-Lorentzian ($\beta \sim 0.5$)[1], indicating the glassy nature of the confined water. The experimentally extracted $\phi_q(t)$ are shown in Figure 2.11 for a representative $q = 0.6$ Å^{-1}. The big gap between 240 and 220 K is clearly visible, and is a consequence of the dynamic crossover in the translational relaxation time. Unlike ideal glass forming liquids, the $\phi_q(t)$ of this real physical system does not show an infinitely long plateau below T_c as predicted by the idealized mode coupling theory (MCT, Appendix A.1); instead, after struggling in the nanosecond time range, it eventually decays to zero through an α-relaxation process that restores ergodicity. The real structural arrest transition is avoided, as one can also see in the Arrhenius plot of the experimentally extracted $\langle\tau\rangle$ versus $1/T$ (Figure 2.10). It shows clear evidence of a super-Arrhenius (non-linear behavior) to Arrhenius (linear behavior) dynamic crossover as the temperature is cooled down through $T_L = 225 \pm 5$ K.

We calculated the *dynamic susceptibility* $\chi_T(t)$ using finite differencing. $\chi_T(t)$, defined in Section 1.3.3, is a measure of the temperature induced fluctuations. Experimentally, it is a much easier quantity to measure than the four-point dynamic susceptibility $\chi_4(t)$, which quantifies the amplitude of the spontaneous fluctuations; however, they are related to each other by the fluctuation-dissipation theorem (18). Despite the fact that the temperature difference is 20 K (or 10 K), we can clearly see that $\chi_T(t)$ has a peak located at around $T_L = 227$ K

[1]We remind here that the Fourier transform of an exponential function is a Lorentzian function. So if $\phi_q(t)$ is not a simple exponential ($\beta < 1$), $S_q(E)$ will not be a simple Lorentzian.

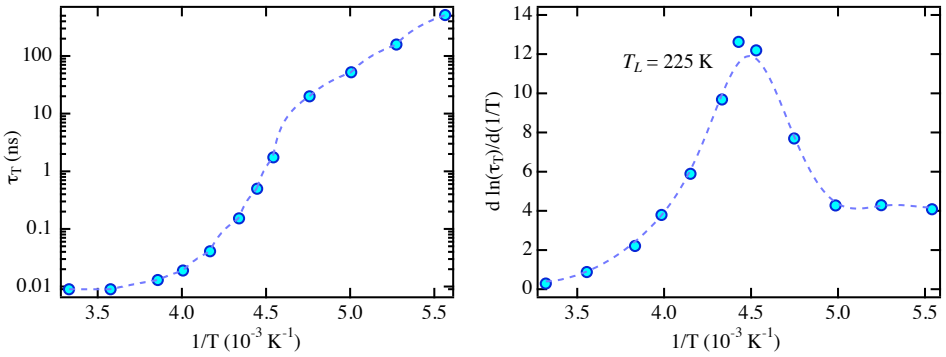

Figure 2.10: 3D-confined water dynamic transition - *Left*: Arrhenius plot of experimentally extracted translational relaxation time versus $1/T$. An evidence of a super-Arrhenius (non-linear behavior) to Arrhenius (linear behavior) dynamic crossover is observed as the temperature is cooled through $T_L = 225 \pm 5$ K. *Right*: Location of the transition temperature through the derivative of the Arrhenius plot.

in Figure 2.11 right panel. The peak height is a measure of the volume within which the correlated motions take place. It grows on approaching T_L and reaches a maximum at T_L, but this growth is interrupted when the dynamic crossover sets in at T_L. This fact indicates that the dynamic fluctuations are enhanced and lead to the maximum of the size of the dynamic heterogeneity in confined water near T_L. Therefore, the three quantities $\langle\tau\rangle$, $\chi_T(t)$, and DSC heat flow all agree in evaluating the crossover temperature as $T_L = 225 \pm 5$ K. The coincidence of the DSC peak and the dynamic crossover temperature at T_L can also be understood with the Adam-Gibbs theory (see Section 4.3.1), where the slope of the Arrhenius plot of the mean α-relaxation time is directly related to the configurational entropy change (see Section 4.1 for details). These experimental findings demonstrate that there are well-defined thermodynamic and dynamic signatures in the response functions of the existence of the crossover temperature T_L. We may predict that below T_L, the structural properties of cement paste become drastically different from those above. Establishing to what extent this would affect the mechanical properties of the concrete at temperatures below T_L awaits future experiments.

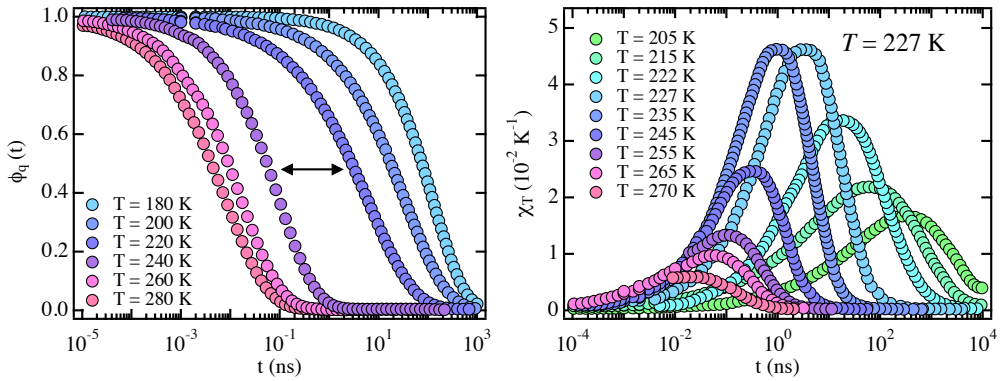

Figure 2.11: 3D-confined water χ_T - *Left Panel*: Self-intermediate scattering function $\phi_q(t)$. Three temperatures each are plotted above and below T_L. *Right Panel*: Dynamic susceptibility $\chi_T(t)$. All the figures are plotted for $q = 0.6$ Å^{-1}

2.3 Bulk water dynamics: computer simulations

To make sure that the dynamic phenomena described in this chapter are inherent properties of water and not due to the confinement, we ran a simulation of a model bulk water, four-point transferable intermolecular potential modified for the Ewald sums (TIP4P-Ew, (72)). The dynamic crossover in the Arrhenius plot of the self-diffusion constant has been previously observed with simulations of bulk water using other water models (144). We calculated long MD trajectories for a box of 512 water molecules of up to 1 μs in the NVT ensemble (148). The systems were considered equilibrated when the mean-square displacement of the water molecules was larger than 0.1 nm^2 (Fig. 2.12). We then calculated the correlators $\phi_q(t)$ for the oxygen atoms for five q values (0.4 , 0.5 , 0.6 , 0.7 , 0.8 Å^{-1}) and fit the data according to the RCM described in Section 2.1(Fig. 2.12). Figures 2.13 show the Arrhenius plots of the transport properties obtained from the trajectories: the translational relaxation time $\langle\tau\rangle$ and the inverse of the self-diffusion constant $1/D$, respectively. Both the plots show a dynamic crossover at $T_L = 215 \pm 5$ K, analogous to the one in Figure 2.10.

As a side note, $\langle\tau(T_L)\rangle$ is between 1 and 10 ns range for both experiments in any kind of confinement and simulations, confirming the general behavior of many glass formers (*magic* relaxation time of the dynamic transition) (107). The

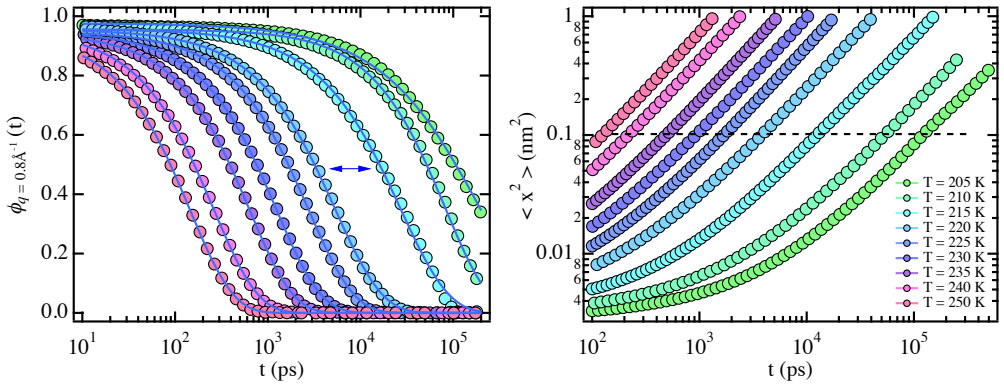

Figure 2.12: Bulk water dynamics - *Left*: Oxygen SISF at $q = 0.8$ Å^{-1} for several temperatures. Continuous lines are the best fittings with RCM. *Right*: Long-time mean-square displacement. $\langle x^2 \rangle \sim 0.1$ is considered to be the equilibration time for a water box at that temperature.

left panel of Figure 2.14 shows the dynamic response function $\chi_T(t)$ extracted from the trajectories. Error bars on $\chi_T(t)$ are on the order of 10^{-2} K^{-1}. As also observed experimentally, $\chi_T(t)$ decreases after the dynamic crossover temperature $T_L = 215$ K. The same phenomenon is not observed for $\chi_4(t)$ calculated from the trajectory (Figure 2.14, right panel). The self-part of this quantity is defined as

$$\chi_4(t) = \langle [\phi_q^l(t) - \langle \phi_q^l(t) \rangle]^2 \rangle \tag{2.7}$$

where the superscript l indicates the function is a sum over all particles. Since $\chi_4(t)$ is related to spontaneous fluctuations, its direct measurement is very difficult. Much easier way is the numerical computation. The general features of $\chi_4(t)$ for bulk water resemble the ones for Lennard-Jones systems (139). The power-law dependences of the short-time regime and the growth of the peak height of $\chi_4(t)$ as one approaches T_L are evident.

Comparing the two panels of Figure 2.14, one notices that while the maximum of $\chi_T(t)$, χ_T^*, has a maximum at $T = T_L$, χ_4^* keeps increasing even below T_L. This phenomenon may be understood by considering that these two quantities are related by the inequality $\chi_4(t) \geq (k_B/c_p)T^2\chi_T^2(t)$. This implies that since the specific heat of confined water has a peak at the dynamic crossover temperature

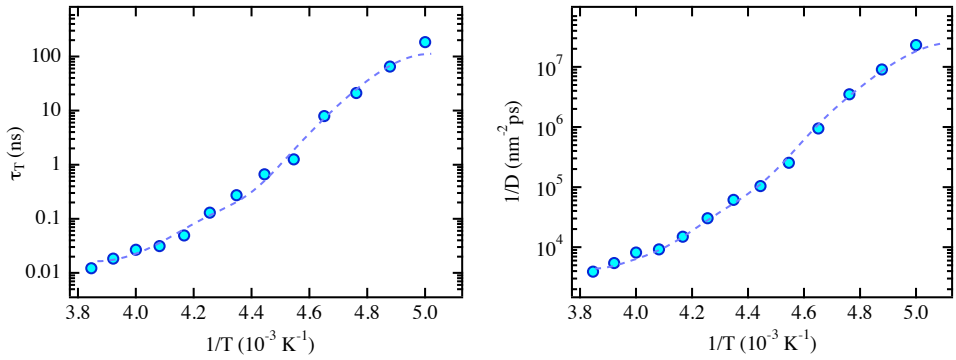

Figure 2.13: Bulk water dynamic transition - *Left*: Arrhenius plot of the translational relaxation time. *Right*: Arrhenius plot of the self-diffusion constant. Both plots show the same sigmoidal behavior, typical of a dynamic transition. The two quantities are in fact both transport properties of the liquid, and are related by the Stokes-Einstein relation.

(150), the dynamic response function $\chi_T(t)$ may decrease after T_L to keep $\chi_4(t)$ growing (only occasionally it is verified that the dynamic heterogeneities drops approaching T_g, (11)). In conclusion, we showed that bulk water simulations are able to reproduce our experimental findings of the three-dimensional confined water. The maximum of $\chi_T^*(t)$ happens at the dynamic crossover temperature T_L and it is not originated from the confinement. On the other hand, the peak height of $\chi_4(t)$, which is a measure of the dynamic heterogeneity, continues to increase below T_L.

2.4 Summary

In this chapter, we observed a dynamic transition in deeply supercooled water, at $T_L = 225 \pm 5$ K. In order to reach this temperature avoiding crystallization, we confined water in a wide variety of systems (1-D confinement in cylindrical nanopores of MCM, 2-D confinement around biomolecules and 3-D confinement in interconnected networks of cured cement pastes). We summarize the results obtained experimentally in the last few years in Figure 2.15. This phenomenon seems to be fairly independent on the dimensionality of the confinement, and is

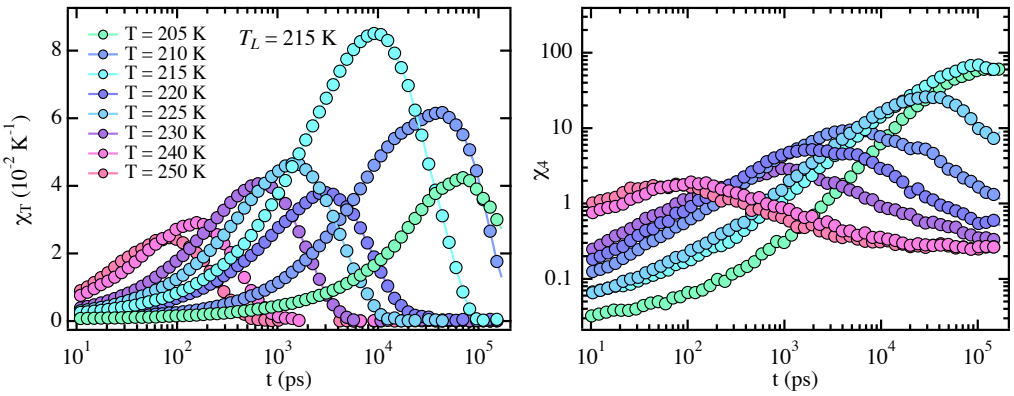

Figure 2.14: Bulk water χ_T and χ_4 - *Left panel*: Dynamic response function $\chi_T(t)$ for TIP4P-Ew water at several temperatures for $q = 1.0$ Å^{-1}. *Right panel*: log-log plot of $\chi_4(t)$ for $q = 1.0$ Å^{-1}. These two quantities are related by the fluctuation dissipation theory.

present in simulations of supercooled bulk water as well[1]. In order to extract the dynamic transition temperature we i) took the derivative of the Arrhenius plot of the translational relaxation time of water molecules, ii) constructed experimentally the dynamic susceptibility $\chi_T(t)$. Both methods agree in evaluating $T_L \sim 225$ K.

The dynamic crossover temperature T_L could be interpreted as a variant of the kinetic glass transition temperature T_c predicted by the idealized MCT (iMCT, Appendix A.1). The structural arrest transition is avoided by activated hopping processes below T_L. iMCT breaks down below T_L. Indeed, by treating hopping as arising from the vibrational fluctuations in a quasi-arrested state, an extended version of the MCT (eMCT, Section A.3) shows that the ergodic to nonergodic transition is replaced by a smooth crossover. Furthermore, the dynamic theory eMCT also demonstrates the growing of the dynamic length scales when approaching T_c. These two predictions were experimentally verified in this chapter.

[1]While the dynamic transition of supercooled water seems to be independent on the confinement, the dimensionality of the confinement turns out to play an important role in the characteristics of the slow dynamics, such as the power law exponent for the fractional Stokes-Einstein relation (33)

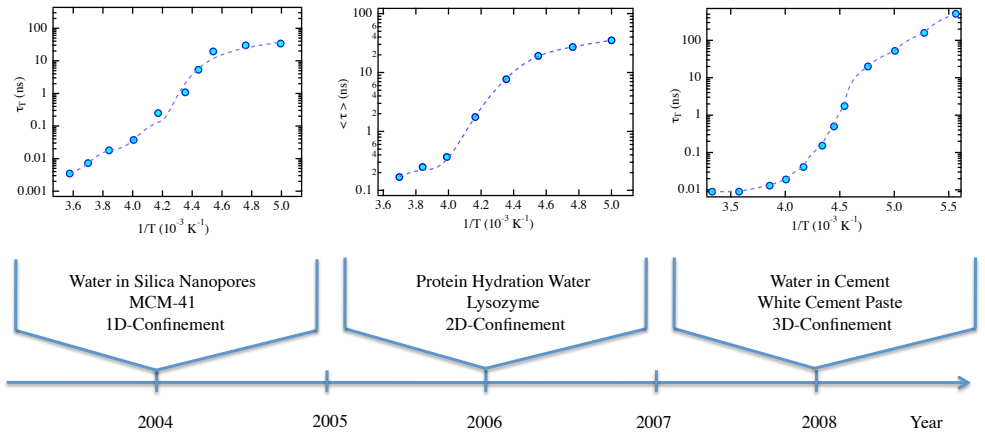

Figure 2.15: Relaxation time of confined water: a timeline - Summary of the temperature dependence of confined water dynamics, in different dimensionalities, as they appeared in literature. See Figures 2.5, 4.5 and 2.10.

Below $T_c \sim T_L$, any structural relaxation requires a cooperative rearrangement of a large cluster of water molecules connected through hydrogen bonds.

In conclusion, while T_g has just a conventional definition (Section 1.3.2) and T_c corresponds to an event that does not happen (Appendix A.1), T_L seems to be a better candidate to describe the slow dynamics of supercooled liquids.

3

Protein Dynamics

Of this many know much,
everybody something, no man enough.
Latin proverb

3.1 Overview of protein dynamics

Crystallographic structures are known for many proteins, but these are not sufficient to predict their behavior. Their biological function is in fact eventually governed by their dynamics, i.e. any time-dependent change in their atomic coordinates (67; 68). Protein dynamics, triggered by thermal energy, allows the biomolecule to sample many conformations around the average structure, the so-called *conformational substates* (CS)[1]. A complete description of proteins requires therefore a multidimensional *energy landscape* (EL, Figure 3.1), a concept proposed for proteins by Frauenfelder and co-workers in the 1970s, that defines the relative probabilities of the CS (minima, thermodynamics) and the energy barriers between them (maxima, dynamics) (8). In particular, the EL of a complex system that contains N atoms is described by the potential energy surface in a space of $3N$ dimensions, where each axis gives one coordinate of a specific atom.

[1]Proteins are never at rest: even at ambient temperature, they fold and unfold all the time

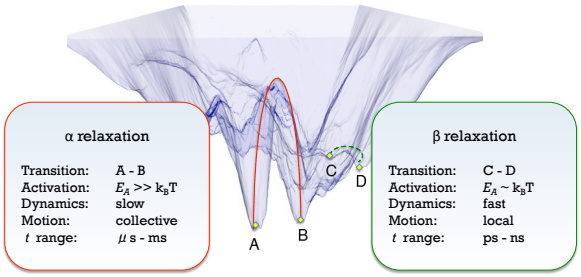

Figure 3.1: Protein Energy Landscape - 3-D cross section of a multidimensional energy landscape. While states A and B are separated by a high energy barrier (α-dynamics), states C and D are separated by a low energy barrier (β-dynamics).

Protein dynamics can be divided into two main groups according to the timescale or, equivalently, to the region of the EL sampled (68): 1) Slow timescale dynamics (μs-ms, or α relaxation) define fluctuations between states separated by energy barriers of $E_A \gg k_BT$, i.e. large-amplitude collective motions. Biological processes like enzyme catalysis and protein-protein interactions occur on this timescale. 2) Fast timescale dynamics (ps-ns, or β relaxation) define fluctuations between structurally similar states that are separated by $E_A \leq k_BT$. They are more local, small-amplitude fluctuations at physiological temperature like loop motions and side-chain rotations.

Slow and fast dynamics are somehow linked to each other. It may be useful at this point to picture the "traffic model for the conformational space" (54). Consider a one-way street with n equally-spaced traffic lights as sketched in Figure 3.2. At any instant of time, some lights will be red, some green. In order to describe an instantaneous conformation, we label the first traffic light 1, the second 2, and so on to n. We observe, for instance, that 1 is red (r), 2 is green (g), and so on to n being red. The entire snapshot then can be characterized by the string '$rg....r$'. Every snapshot at different times is described by a different string. Biomolecules are dynamic systems that change conformations rapidly. We describe the dynamics by imagining a car that drives down the one-way street. The car starts at the first traffic light and the time to move from one traffic light to the next is τ^β. Assume further that the traffic lights fluctuate between r and g and spend on average the time τ^α in either state. Two limiting cases are now easy to understand: (i) the car is very fast and the traffic lights change slowly so

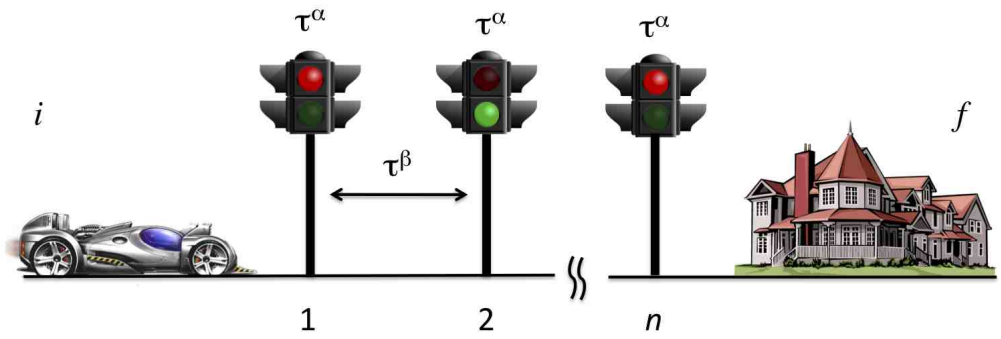

Figure 3.2: Traffic model for the conformational space - A traffic analog to protein dynamics, redrawn from (54). A car drives through a series of equally spaced traffic lights. The traffic lights switch randomly between red and green. The average time in each state is given by τ^{α}. The average time for the car to go from one traffic light to the next is τ^{β}.

that $\tau^{\alpha} \gg \tau^{\beta}$. On average, the car has to wait the long time τ^{α} at every second traffic light, the trip is controlled by the rate at which the traffic lights change, and the time τ_f to reach the goal is approximately given by $\tau_f \sim n\tau^{\alpha}$. (ii) in the other limit, $\tau^{\alpha} \ll \tau^{\beta}$, the car is slow and the traffic lights change rapidly. The wait at the traffic lights is short and the transit is determined by the speed of the car and hence $\tau_f \sim n\tau^{\beta}$.

We now apply the traffic model to proteins. Assume for simplicity that in a hypothetical protein of 50 atoms can be in one of two positions, r and g. Assume in addition that each of 100 water molecules in the hydration shell can alternate between the two positions. The hypoprotein then has 2^{150} or about 10^{45} substates. This number may appear to be excessive, but a real protein is even more complex including, for example, bulk solvent substates. We now return to the traffic analogy and ask if case (i) or case (ii) dominates. In case (i), the actual jump is fast but can only occur if the solvent moves. In case (ii), the solvent fluctuates rapidly compared to the time the protein needs to go from one substate to another. It seems that case (i) applies and that the external gating dominates (54). The question what happens during the time τ^{α} has no experimental answer as yet. Because the β fluctuations can be faster than the α

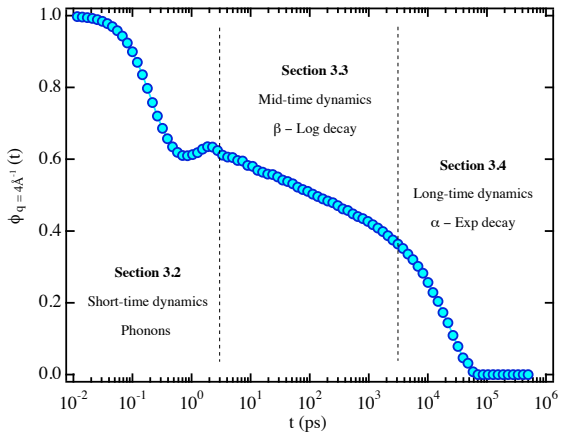

Figure 3.3: Complete time-dependence of protein $\phi_q(t)$ - Results from MD simulations of the hydrated protein powder model at $T = 310$ K. $\phi_q(t)$ was calculated for $q = 4.0$ Å^{-1}, considering the center of mass of each amino acid residue. The 3 sections border at 3 ps and 3 ns.

fluctuations it is conceivable that the protein makes a random walk in the energy landscape during the time τ^{α}.

The correlation between dynamics and biological activity has been demonstrated on the μs-ms timescale, but fluctuations at atomic level are much faster than this, leading to the idea of a *hierarchy of substates*. The EL is organized in a fractal-like hierarchy of a number of tiers; there are valleys within valleys within valleys. Some aspects of protein dynamics are also slaved to solvent fluctuations, with the protein component dictating the relative rates (54).

The complete time-dependence of a typical $\phi_q(t)$ for hydrated protein powder is shown in Figure 3.3. In this chapter we are going to study the whole curve, dividing protein dynamics into 3 sections: short-time dynamics (i.e. phonons in proteins), mid-time dynamics (i.e. the logarithmic dependence of the β relaxation) and the long-time dynamics (i.e. the exponential dependence of the α relaxation). Special attention will be devoted on how lowering the temperature affects protein dynamics.

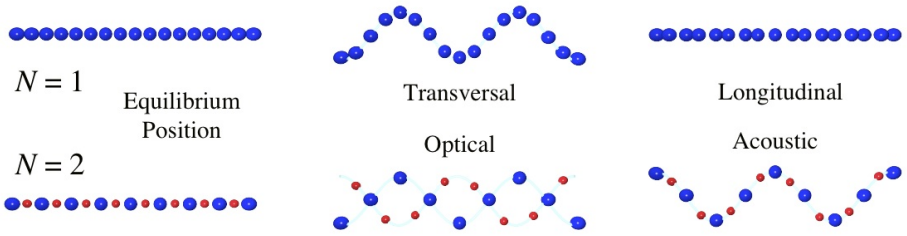

Figure 3.4: Typical phonons - *Up left*: Equilibrium position of a 1D system with one atom per unit cell; *Up middle*: Transverse mode, atoms move perpendicular to the propagation of the wave; *Up right*: Longitudinal, atoms move in the same direction of the propagation of the wave; *Down left*: Equilibrium position of a 1D system with two atoms per unit cell; *Down middle*: Optical branch of the transverse mode, the two atoms are out of phase; *Down right*: Acoustic branch of the transverse mode, the two atoms are in phase

3.2 Short-time dynamics: Phonons

3.2.1 An introduction to collective motions

While *lattice statics* deals with the average positions of atoms in a crystal, *lattice dynamics* extends the concept of crystal lattice to an array of atoms with finite masses that are capable of motion. This motion is not random but is a superposition of vibrations of atoms around their equilibrium sites due to the interaction with neighbor atoms. A collective vibration of atoms in the crystal forms a wave of allowed wavelength and amplitude.

Just as light is a wave motion that is considered as composed of particles called photons, we can think of the normal modes of vibration in a solid as being particle-like. A quantum of lattice vibration is called *phonon*. The problem of lattice dynamics is to find the normal modes of vibration of a crystal. In other words, it seeks to calculate the energies (or frequencies ω) of the phonons as a function of their wave vector q. The relationship between ω and q is called *phonon dispersion*.

There are two possible normal modes of vibrations of atoms in the crystal: *longitudinal* (when the displacement of atoms coincides with the propagation direction of the wave) and *transverse* (when atoms move perpendicular to the

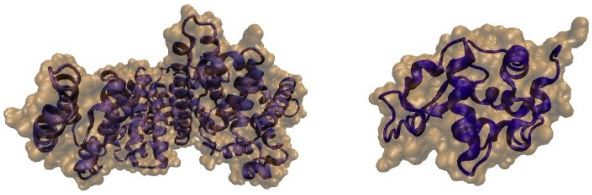

Figure 3.5: Structure of BSA and LYZ - *Left*: Serum albumin (pdb file 1E7I); *Right*: Lysozyme (pdb file 1AKI)

propagation of the wave). The dynamics of the two modes are exemplified in Figure 3.4.

For one atom per unit cell the phonon dispersion curves are represented only by *acoustic branches*. However, if we have more than one atom in the unit cell *optical branches* will appear additionally. The difference between acoustic and optical branches arises because of the more options of vibrations for atoms in the unit cell: it can be found that for optical branch (in the long wavelength limit) the two atoms in the unit cell move opposite to each other and the light mass amplitude is greater. For the acoustic branch (in the long wavelength limit) the displacement of both atoms has the same amplitude, direction and phase. For example, atoms A and B of diatomic cell can move together in phase (acoustic branch) or out of phase (optical branch). Generally, for N atoms per unit cell there will be 3 acoustic branches (1 longitudinal and 2 transverse) and $3N - 3$ optical branches ($N - 1$ longitudinal and $2N - 2$ transverse). The dynamics of the two branches are exemplified in Figure 3.4.

3.2.2 Phonon detection

Recently, some researchers studied the inter-protein phonons in protein crystals by MD simulations (83). However, it is also relevant to study the intra-protein collective atomic motions since it is intimately connected to the biological activities of the macromolecule. IXS is an effective tool to study the collective motions of atoms, such as the *phonon dispersion relation*. We used two structurally different proteins (89), lysozyme (LYZ) and bovine serum albumin (BSA), see Figure 3.5.

LYZ is an enzyme consisting of 129 amino acid residues which folds into a compact globular structure having an ellipsoidal shape with dimensions a x b x b = 2.25 x 1.5 x 1.5 nm^3 and a molecular weight of 14.4 kDa. LYZ has five helical regions and five β-sheet regions consisting of a large amount of random coil and β-turns. BSA is instead a transport protein and the principal carrier of fatty acids that are otherwise insoluble in circulating plasma. It is a prolate ellipsoid with a x b x b = 7 x 2 x 2 nm^3 and a molecular weight of about 66.7 kDa. It consists of 607 amino acid residues that create an all-helix structure. The respective protein powders were hydrated at $h = 0.3$. This hydration level was chosen to have almost a monolayer of water covering the protein surface.

The experiments were performed at the inelastic x-ray scattering beam line, IXS, and the high energy resolution inelastic x-ray scattering (HERIX) beam line, at the Advanced Photon Source (APS), Argonne National Laboratory. Both instruments can measure the dynamic structure factor $S_q(E)$ of the sample, which contains information on collective motions of atoms with an energy resolution of about 2 meV (for IXS) and 1.5 meV (for HERIX). The measured q-range is from 0 to 35 nm^{-1} and an energy window from -20 to 40 meV. A measured IXS spectrum $I_q(E)$ can be expressed as $I_q(E) = S_q(E) \otimes R_q(E)$, where $R_q(E)$ is the resolution function, and $\otimes$ means numerical convolution. In the present analysis we shall use the damped harmonic-oscillator (DHO) model to analyze the normalized dynamic structure factor given by (88):

$$\frac{S_q(E)}{S_q} = \frac{1}{\pi} \frac{\Gamma_q \Omega_q^2}{(E^2 - \Omega_q^2)^2 + (\Gamma_q E)^2} \tag{3.1}$$

where the static structure factor $S_q = \int_{-\infty}^{+\infty} S_q(E)\, dE$, Ω_q is the phonon energy at wave vector transfer q, and Γ_q is the phonon damping. In principle, the DHO model has no central Rayleigh (elastic) peak, only the two Brillouin side peaks. But experimentally we observe the presence of a large resolution limited central peak. Therefore, we phenomenologically added a delta function central peak of a weight fraction g_q. In addition, we also take into account the detailed balance factor, so that the extended DHO model is given as (101)

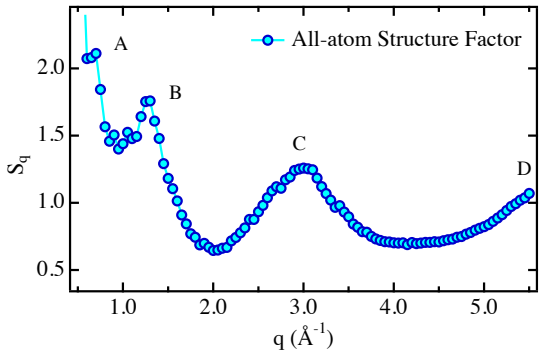

Figure 3.6: Protein S_q - Lysozyme all-atom structure factor S_q calculated from MD. The meaning of the shoulder at 0.5 Å^{-1} is uncertain, while the peak at 1.4 Å^{-1} corresponds to typical distances of the secondary structure, and the one at 3.0 Å^{-1} to some medium range order of residues.

$$S_q(E) = A\frac{E}{k_BT}[n(E)+1]\left[g_q\delta(E) + (1-g_q)\frac{1}{\pi}\frac{\Gamma_q\Omega_q^2}{(E^2-\Omega_q^2)^2+(\Gamma_qE)^2}\right] \quad (3.2)$$

where $n(E)+1$ is the detailed balance factor, $n(E) = (e^{E/k_BT}-1)^{-1}$ the Bose factor and A a normalization constant. We calculated S_q for lysozyme powder from an MD trajectory at $T = 250$ K according to $S_q = \frac{1}{N}|\sum_{j=1}^{N} e^{i\mathbf{q}\cdot\mathbf{r}_j}|^2$, where N is the number of heavy atoms in the protein and $\mathbf{r}_j$ their coordinates. S_q is shown in Figure 3.6: it shows the 4 expected peaks, centered at $q = 7$, 14, 30 and 55 nm^{-1} (49). Peak B, which should be the major peak of the structure factor, arises from the order of the secondary structure (β-sheets average distance and α-helix repeat and width). Peak C is ascribed to the intermediate-range order between amino acidic residues, while peak D is attributed to the covalent bonds between heavy atoms (like C-C, C-N, etc.). Finally, the sharp increase at low-q indicates that, on average, a protein can be regarded as a fluctuating continuum.

We show in Figure 3.7 the analysis of measured IXS spectra $S_q(E)$ of BSA by the DHO model at three different temperatures $T = 170$, 220, and 250 K. For $q = 2.4$, 2.8 and 3.1 Å^{-1}, a clear q dependence of the phonon excitation energy is observed. At a given q value, when the temperature exceeds T_l, we see a substantial decrease in the phonon energy. The softening of the phonons in this q range suggests that the slowing down of motions involving the intermediate-range order in a protein may be the origin of the restoration of its biological activities.

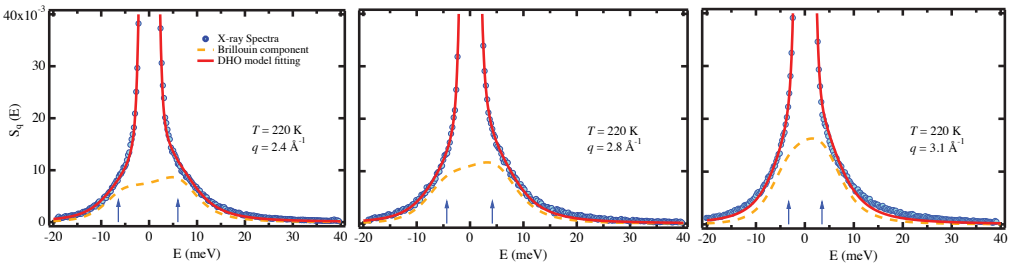

Figure 3.7: DHO model fitting of the measured IXS spectra of BSA - The blue circles, red solid line and orange dashed line represent, respectively, the measured data, DHO model fitted curve and Brillouin component of the DHO model. The arrow signs show the Stokes and the anti-Stokes components of the phonon-like excitation energy at each q. The Figure shows the fitted results at q = 2.4, 2.8 and 3.1 Å^{-1} (from left to right) at T = 220 K.

3.2.3 Temperature dependence of the phonon dispersion

From the results of the DHO analyses of the measured spectra, such as the ones that are illustrated in Figure 3.7, we plotted the phonon dispersion relations in the full q range for BSA and LYZ, respectively, in Figure 3.8. In the high-q range 2 to 3 Å^{-1}, excitation energies have similar dispersion curves to the ones observed in other biosystems (92). This q-range corresponds to the length scale of about 2-3 Å, close to the one of the typical distance of the secondary structure of the proteins ($\sim 4-5$ Å) and reflect the intra-protein collective atomic motions. We can clearly observe the quantitative degree of the softening of phonons for both proteins as temperature exceeds T_l in Figure 3.8. This fact strongly suggests that these temperature dependent intra-protein motions are intimately related to the biological activities of proteins, which are also temperature dependent and strongly decrease below T_l. The presence of the structure factor peak at $q \sim 15$ Å^{-1} leads to a large damping of the phonons, as we can see in the upper panel of Figure 3.8, so we cannot detect the phonons in this region. The phonon damping (Γ_q, middle panel) does not show a temperature dependence and is nearly constant. This fact shows that the temperature dependence of Ω_q is reliable. We calculated the factor $(1-g_q)$ and fit it by a power law. Since the factor g_q is the fraction of the elastic component, which should be proportional to

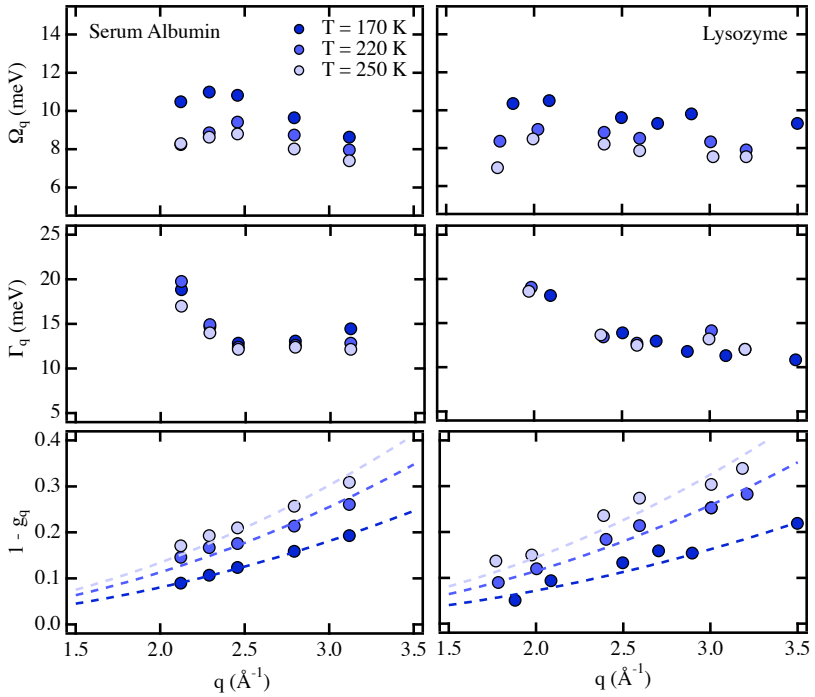

Figure 3.8: Phonon-like excitation in BSA and LYZ - *Upper Panel*: Dispersion of the intraprotein phonon-like energy excitations as a function of q, above peak B of the structure factor (see Figure 3.6). *Middle Panel*: The phonon damping as a function of temperature.*Lower Panel*: Fractional area of the Brillouin peak vs q. The factor $(1 - g_q)$ is found to increase proportionally to q^2

the Debye-Waller factor $f_q = \exp(-q^2\langle x^2\rangle)$, the low-$q$ expansion of g_q should be proportional to q^2. Our data show this q^2 dependence in Figure 3.8, lower panel. The factor $(1 - g_q)$ represents the fractional spectral intensity of the phonon-like excitation in the total intensity. At temperature higher than T_l, $(1 - g_q)$ is larger, which indicates that the phonon population increases as temperature decreases, due to the onset of the conformational flexibility at T_l.

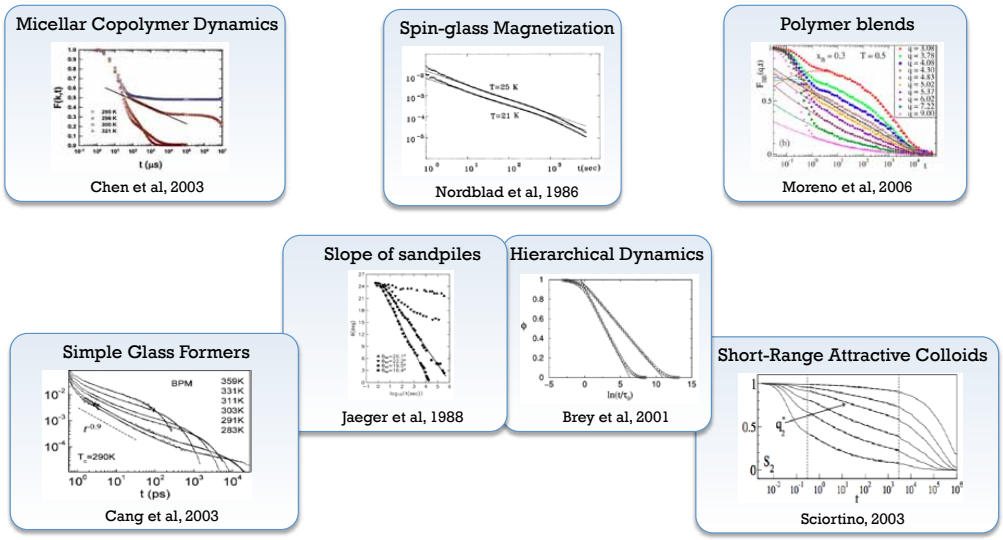

Figure 3.9: Examples of logarithmic dynamics - While this particular relaxation is not very common, we can find it in a wide variety of systems, usually governed by strong interactions.

3.3 Mid-time dynamics: Log decay

3.3.1 An introduction to the logarithmic decay

Among all the relaxations characteristic of complex systems such as exponential, stretched exponential, power law (see Chapter 1), the logarithmic decay is the slowest one and also the least common. In past years, it has been experimentally found in the time evolution of a wide variety of complex strong interacting systems such as spin glasses (106), granular materials (75), simple glass-formers (24; 25), colloidal solutions (28), polymers (9), and protein kinetics (1; 46). To this large number of experimental systems, we can add many numerical simulations on short-ranged attractive colloids (115; 126), polymer blends (102), and kinetically constrained models (22; 103). In Figure 3.9 we show an overview of the systems where the logarithmic decay appears. Nevertheless, no general scenario for its appearance is known.

Starting in 1989, Götze and collaborators have shown that this particular feature is predicted by the idealized mode coupling theory (iMCT) for systems

close to a higher-order glass-transition singularity (see Appendix A.2). In this section, we shall show by means of molecular dynamics (MD) simulations that the protein self-intermediate scattering functions (SISF) display a logarithmic decay in the picosecond to nanosecond time range, that can be fitted according to Equation A.14 (84),

$$\phi_q(t) \sim f_q - H'_q \ln(t/\tau^\beta) + H''_q \ln^2(t/\tau^\beta) \tag{3.3}$$

In a longer time range, instead, the complete time dependence of the function can be fitted with an analytical model as follows:

$$\phi_q(t) \sim [f_q - H'_q \ln(t/\tau^\beta) + H''_q \ln^2(t/\tau^\beta)] \exp(t/\tau_q^\alpha) \tag{3.4}$$

where τ^β and τ_q^α are the characteristic β- and α-relaxation time, respectively.

Molecular dynamics (MD) simulations have the advantage that they can describe protein dynamics completely: the position of each atom can be followed any instant in time, so they are the ideal tool to study ps-ns (fast) protein dynamics. We are also going to show that the presence of this logarithmic decay does not depend on the state of aggregation of the protein (powder, crystal or solution), nor on the globular protein under consideration (lysozyme or ribonuclease). This peculiar relaxation of protein is not shared by its hydration water, as showed in Figure 3.10: while proteins resemble the MCT A_3 scenario, protein hydration water is more similar to a MCT A_2 scenario.

3.3.2 β relaxation: logarithmic decay

We shall start our discussion on protein dynamics proving that globular proteins share, qualitatively, the same exotic relaxation behavior regardless of their environment (a hydrated powder, a hydrated crystal or a solution): an uncommon logarithmic behavior (84). Figure 3.11 compares the dynamics of these 3 forms of protein aggregates for lysozyme: the left panel shows the intermediate scattering functions for several q-values for the center-of-mass of the amino acid residues of lysozyme in its hydrated powder form, while the middle panel shows the same quantity for orthorhombic lysozyme crystal and the right panel for lysozyme in

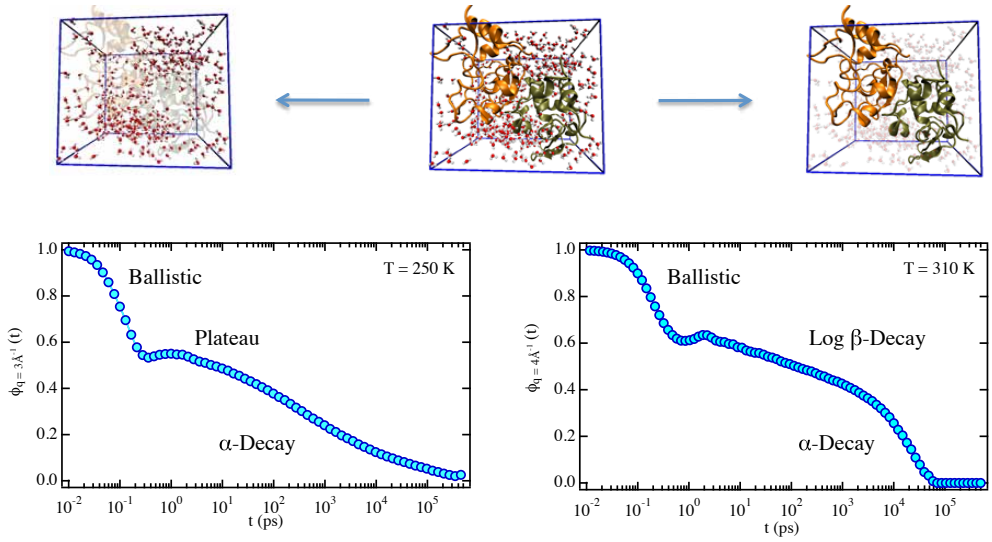

Figure 3.10: Protein $\phi_q(t)$: a comparison with hydration water - *Left*: Single-particle density correlator for protein hydration water showing a plateau followed by a stretched exponential (A_2 scenario of the mode-coupling theory), calculated at $T = 250$ K and $q = 3$ Å^{-1}. *Right*: Single-particle density correlator for protein showing a logarithmic decay followed by a simple exponential (A_3 scenario of the mode-coupling theory), calculated at $T = 310$ K and $q = 4$ Å^{-1}.

solution. In the first two cases, $\phi_q(t)$ shows a logarithmic decay in the intermediate time range 1 ps - 10 ns, followed by the beginning of the slow α-relaxation.

In the solution case, the log decay starts around 100 ps: the initial in-cage gaussian-like ballistic relaxation extends for a larger time range compared to the powder/crystal systems, since the protein has fewer constraints in solution than in a solid form (no protein-protein contacts).

A question arises now: is this peculiar decay localized somewhere in the protein, maybe just in the side chains or only the backbone? As it is clear from Figure 3.12, no qualitative difference can be noticed between the two panels: the logarithmic decay is a general feature of the protein, delocalized over the whole structure. Logarithmic decay was also observed in preliminary spin-echo neutron scattering experiments on deuterated C-phycocyanin (71).

Figure 3.13, instead, compares the dynamics at 300 K of the hydrated powder

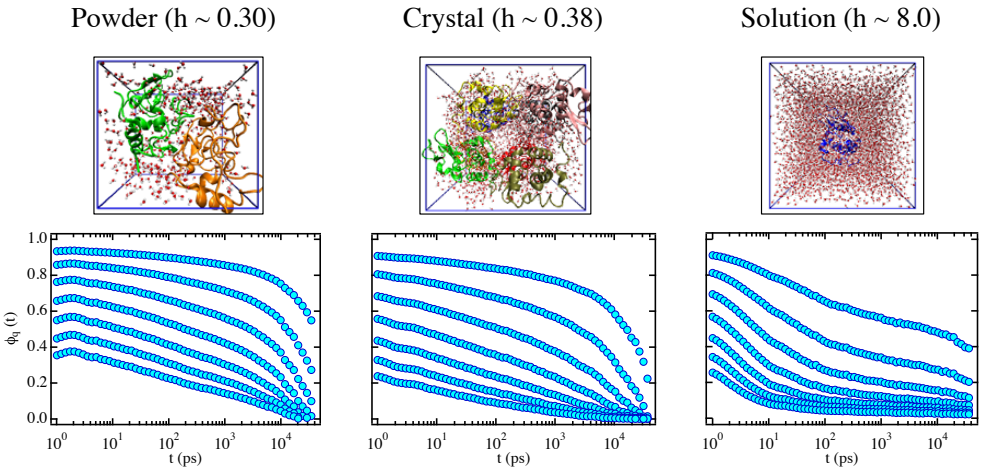

Figure 3.11: Protein $\phi_q(t)$: different protein states - Comparison between $\phi_q(t)$ of amino acid residues of hydrated protein models. *Left*: powder. *Middle*: crystal. *Right*: solution. Seven curves are displayed at different q-values, from 1.6 to 6.4 Å^{-1} (from top to bottom), with a 0.8 Å^{-1} interval.

forms of two different proteins: lysozyme (LYZ) and ribonuclease A (RNAse). Again, the logarithmic behavior is conserved in a similar time range, suggesting that it might be a general feature of globular proteins, a characteristic inherent to their energy landscape profile. Logarithmic decay is in fact often associated with subdiffusion in the mean square displacement, and subdiffusion of protein atoms was recently related to the fractal-like structure of the protein energy landscape (105).

3.3.3 Temperature dependence of β relaxation

We analyze now how temperature affects the logarithmic decay in hydrated protein powder, in the temperature range of its biological activity, roughly from 220 K to 340 K. The lower limit is imposed by the so-called dynamic transition of the protein ((43) and Section 4.2.1), while the higher limit by the reversible denaturation of lysozyme (149).

In Figure 3.14 we plot the intermediate scattering functions $\phi_q(t)$ of the center-of-mass of lysozyme amino acids in the hydrated protein powder model, for 4

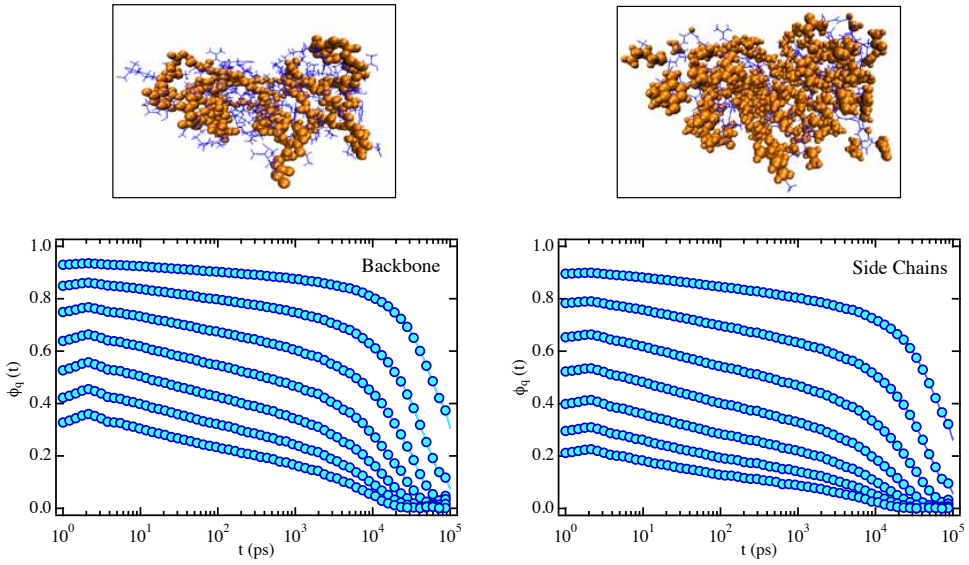

Figure 3.12: Protein $\phi_q(t)$: a comparison between backbone and side chains - *Left*: Density correlators calculated for the atoms belonging to the backbone only, as usual considering only the centers of mass of the backbone atoms of the amino acid residues. *Right*: Same quantity for the side chains. As it appears, no qualitative difference can be noticed between the two plots: the logarithmic decay is a general feature of the protein, delocalized over the whole structure.

different temperatures and a representative set of 7 wave vectors q, in the time range 1 ps to 10 ns. It is evident that the relaxation is far from being the classic two-step decay of a liquid-glass transition, and it is not possible to fit the curves with the stretched exponential form we used for protein hydration water ((85) and Section 4.2). Instead, fitting the correlators with Equation 3.3 produces a very good agreement. We would like to point out here that the logarithmic decay is a feature displayed by the $\phi_q(t)$ of any kind of atom belonging to the protein (H, C, O, etc.), but considering only the c.m. of each amino acid residue is the most convenient choice if one wants to exclude the effect of rotations on the correlators. We show instead in Figure 3.15 the q and temperature dependence of the fitting parameters of Equation 3.3: the intermediate scattering functions were fitted approximately in the same time range, from 2 ps to 6 ns.

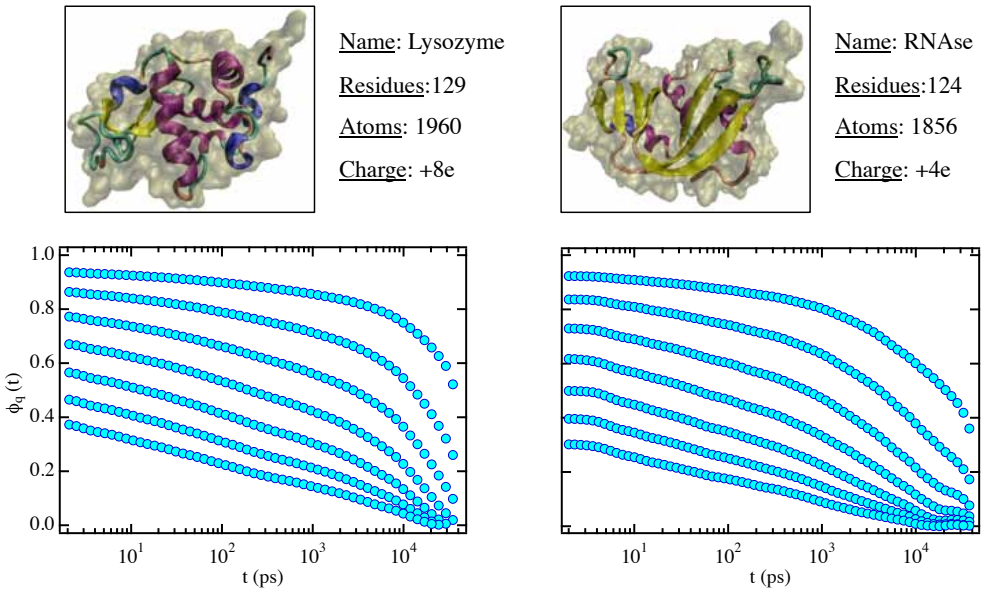

Figure 3.13: Protein $\phi_q(t)$: different proteins - Comparison between ISF of hydrated protein powders for two different protein molecules. *Left*: lysozyme. *Right*: ribonuclease. Seven curves are displayed at different q-values, from 1.6 to 6.4 Å^{-1} (from top to bottom), with a 0.8 Å^{-1} interval.

Several predictions of mode-coupling theory (MCT) for higher order singularities (Appendix A.2) are verified in the temperature interval 280 - 340 K (102; 126):

- the Debye-Waller factor f_q (Figure 3.15, upper panel) does not depend on the state point, as expected if the system is close to the singularity (correction of the order $\sqrt{\epsilon}$ cannot be detected).

- H'_q can be factorized as $H'_q(x) = h_q B'(x)$ where h_q only depends on q and $B'(x)$ only depends on the control parameter x. In fact, the q-dependence of H'_q is the same for all the temperatures.

- H''_q does not display the same behavior as H'_q, since B is also a function of q. Moreover, $|H'_q| < |H''_q|$ since the first is of order ϵ and the second of order $\sqrt{\epsilon}$.

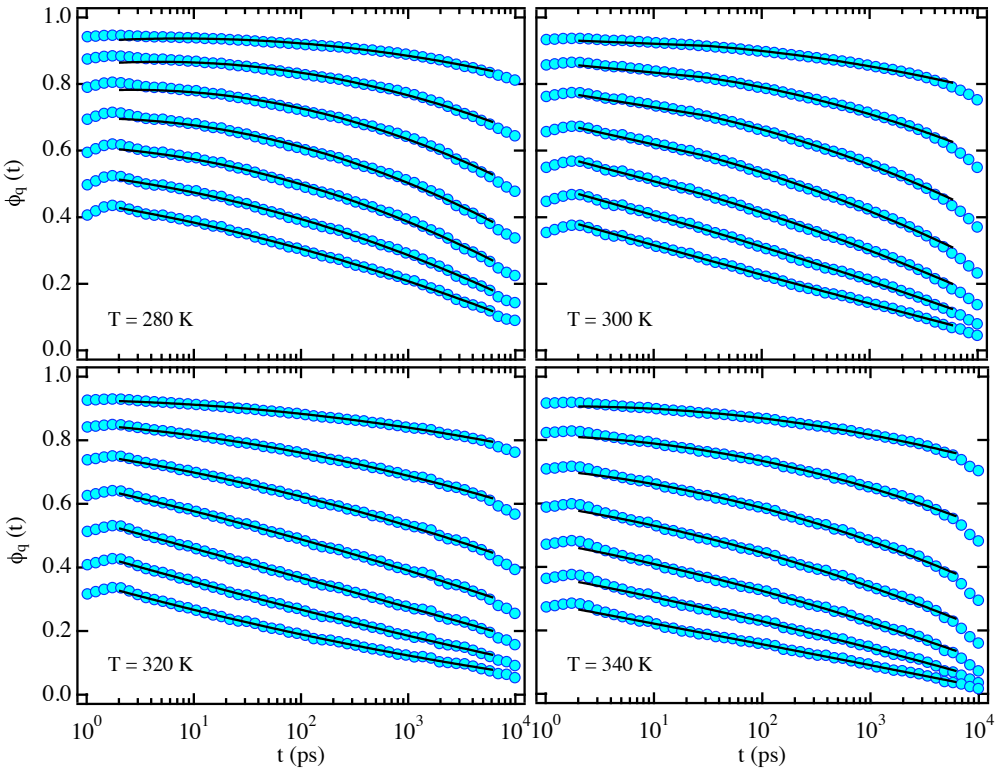

Figure 3.14: Protein $\phi_q(t)$: different temperatures - Protein intermediate scattering functions at 4 different temperatures (T = 280, 300, 320, 340 K) and 7 q-values: from 1.6 to 6.4 Å^{-1} (from top to bottom), with a 0.8 Å^{-1} interval. Continuous lines are the best fits according to Equation 3.3

- the q-values where $H_q'' = 0$ border a convex-to-concave crossover, as predicted by the theory. This is one of the main signatures of the higher-order MCT scenario. These q-values depend on the state point: as a general behavior, these values increase as temperature is decreased.

Below 280 K, instead, the q-value of the peak position of H_q' depends on the temperature, and the predictions of MCT break down. The predictions we listed are, in fact, valid only in the vicinity of the higher order singularity. It seems therefore that lowering the temperature at 280 K and below brings us further away from the hypothetical higher-order transition.

It is impressive that the asymptotic expansion of Equation 3.3, that should

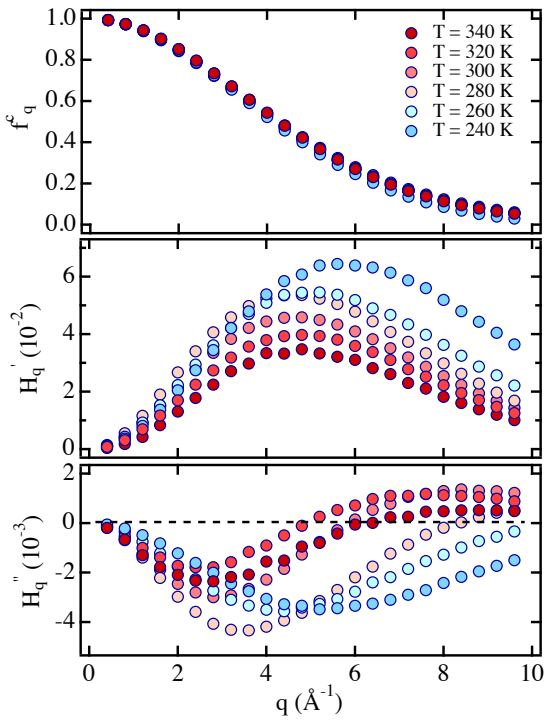

Figure 3.15: MCT parameters: f_q, H'_q, H''_q - Fitting parameters of Equation 3.3 as a function of q, for six different temperatures. *Upper panel*: f_q, Debye-Waller factor. All the curves collapse on top of each other, demonstrating that it does not depend on the state point. *Middle panel*: first coefficient, H'_q. Between 280 K and 340 K, the q-dependence of H'_q is the same for all the temperatures *Bottom panel*: H''_q, the dashed line at 0 intersects the curves at different q values depending on the temperature (border of a convex-to-concave crossover).

hold only very close to the transition, is valid over such a wide range of temperatures. MCT scaling laws are valid close to the critical MCT temperature T_c, which must be distinguished from the actual glass transition temperature T_g. The validity of the MCT scaling laws holds in a relative range $\epsilon = (T - T_c)/T_c$ between typically 0.01 and 0.1. For smaller values of ϵ hopping events restore ergodicity and the real glass transition arises at a lower temperature T_g. The difference between T_c and T_g is typically about a factor 1.2 for fragile liquids, which exhibit a Vogel-Fulcher-Tamann temperature dependence of the relaxation time below T_c or the power law behavior (135). So the MCT critical temperature is probably not far from the physiological temperature (see next section). In Figure 3.16 we show the Arrhenius plot of the β-relaxation time τ^β in Equation 3.3. We extracted this parameter from the fitting of $\phi_q(t)$ shown in Figure 3.16, fixing it so that f_q was independent on temperature. It turns out that this is possible for each temperature (in the range of validity of MCT), and this gives us a unique

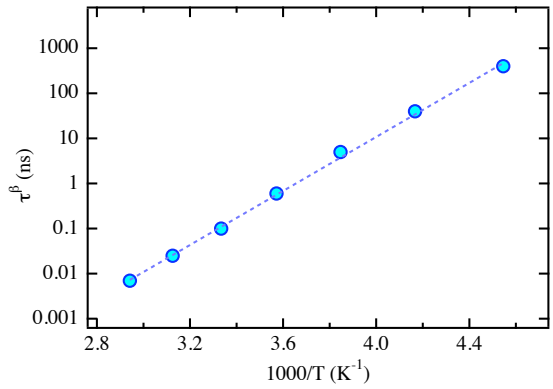

Figure 3.16: MCT parameters: τ^{β} - Arrhenius Plot of the β-relaxation time. The temperature dependence agrees with an Arrhenius behavior ($E_A = 13.7$ Kcal/mol), as usually found for the β peak of proteins and other glass-formers in dielectric spectroscopy.

value for $\tau^{\beta}(T)$. The Arrhenius behavior is evident in the whole temperature range, $220 - 340$ K, with a relatively high activation energy $E_A = 13.7$ Kcal/mol.

3.4 Long-time dynamics: Diffusion

3.4.1 An introduction to the protein-glass analogy

The long-time dynamics of native globular proteins has much in common with the ones of glass-forming liquids (5; 8). The reason for such a similarity has to be searched among the essential characteristics of these two types of material. They both consist of noncrystalline packing in which their constituents (either molecules in the case of glassy liquids or amino acid residues in the case of proteins) assemble (63). They also have a complex energy landscape (54), composed of a large number of alternative conformations at similar energies.

The analogy between a protein and a glass former can be seen from the following similarities: (1) at low temperatures proteins undergo the so-called *glass transition* (see Section 4.2.1), a sudden change of slope in their mean square displacement as a function of temperature, interpreted as the onset of anharmonic processes; (2) the low-energy inelastic spectra of proteins and their hydration water display a feature known as *boson peak*, typical of strong glass formers (87); (3) the protein denaturation can be seen as a sort of strong-to-fragile liquid transition (63), where the folding heavily decreases the number of liquid-like degrees of

freedom; (4) proteins have two types of equilibrium fluctuations, the cooperative α (involving large domains of the biomolecule) and the local β (involving side chains), typical of glass formers ((51; 53) and Section 1.3.2); (5) proteins exhibit both short- and intermediate-range orders, and the construction of a random elastic network using these structures leads naturally to the physics of a glassy material (49).

Proteins and glasses are complex systems, and one of the distinctive features of complex systems is a slow non-exponential relaxation of the density correlation functions $\phi_q(t)$ and of the single-particle correlation functions $\phi_q^S(t)$ observed in a wide range of time scales. The time dependence of the relaxation scenario usually follows these three steps: it begins with (a) a short-time Gaussian-like ballistic region, followed by (b) the β-relaxation region which is governed by either two power-law decays $\phi_q(t) \sim (t/\tau^\beta)^{-a}$ and $\phi_q(t) \sim (t/\tau^\beta)^b$ or a logarithmic decay $\phi_q(t) \sim A_q - B_q \ln(t/\tau^\beta)$, which then evolves into (c) an α-relaxation region that is governed by a stretched exponential decay (or Kohlrausch-Williams-Watts law), $\phi_q(t) \sim e^{-(t/\tau_q^\alpha)^\beta}$, as we saw at the beginning of this chapter, Figure 3.3.

Figure 3.17 shows the protein-glass analogy in a graphic way: while the left panel displays an all-atom representation of a lysozyme molecule, the right panel displays only the center of mass (CM) of the 129 amino acid residues of the protein. From this representation, it is possible to see how a single-molecule system like a globular native protein could resemble a many-body system like a dense short-ranged attractive colloidal solution. This is quantitatively taken into account with the liquid-like static structure factor S_q of the CM's. Since the partial specific volume of lysozyme is 0.757 cm^3/g (100) and the sum of the van der Waals volume of its atoms is 11.8 nm^3 (26), we can roughly estimate a volume fraction of $\phi = 0.66$ (close to the value $\phi = 0.61$ used in (126) to simulate a dense colloidal solution close to a higher order singularity). Besides all these similarities, proteins and glasses have also important differences: even though both systems are aperiodic, the organization of protein EL is far more sophisticated than the glass one.

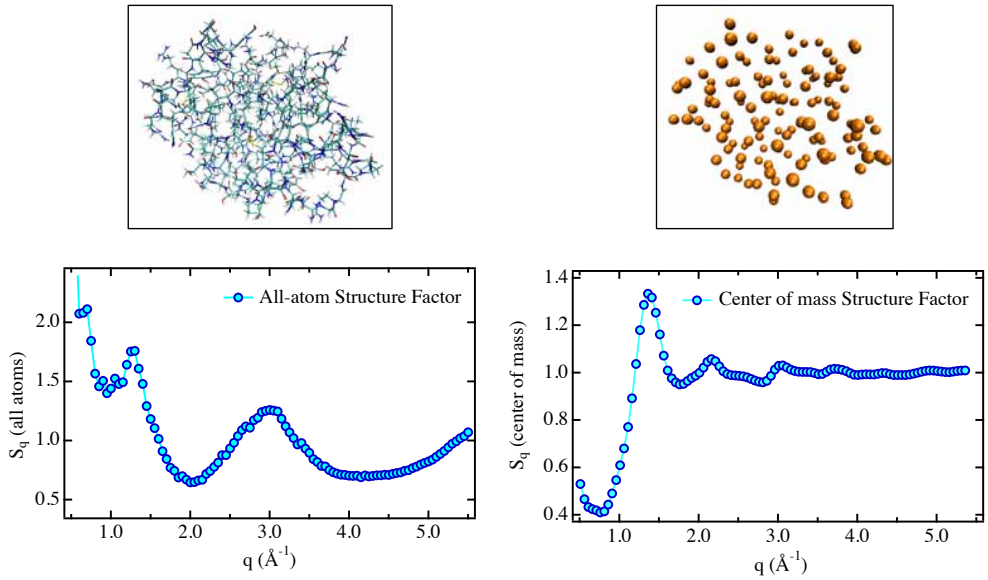

Figure 3.17: The protein-glass analogy - *Left*: All-atom representation of lysozyme, and its static structure factor S_q; *Right*: 129 amino acid centers of mass for lysozyme, and its S_q from MD simulations. S_q were calculated at T = 300 K, averaged over 10^3 configurations and 10^4 q-directions.

3.4.2 α relaxation: exponential decay

Enzymatic activity is known to require a precise balance between flexibility (to allow sufficient substrate binding) and stability (to retain their native structure). So one could ask: what is the long time behavior of the protein correlators? Do they decay to zero or reach a plateau? We were able to run very long simulations (up to 1 μs) and investigate the α-relaxation behavior of the protein intermediate scattering functions. This allowed us to extract a diffusion constant for protein powder at finite q-values in the temperature range 270 - 350 K. Quasi-Elastic Neutron Scattering allowed Bellissent-Funel and coworkers to extract the diffusion constant of the interior of C-phycocyanin (40). We fit the intermediate scattering functions with Equation 3.4, the results are plotted in Figure 3.18.

The complete decay of $\phi_q(t)$ to zero at the physiological temperature is further proof that the functioning proteins behave like a glassy liquid (7; 46) and not like

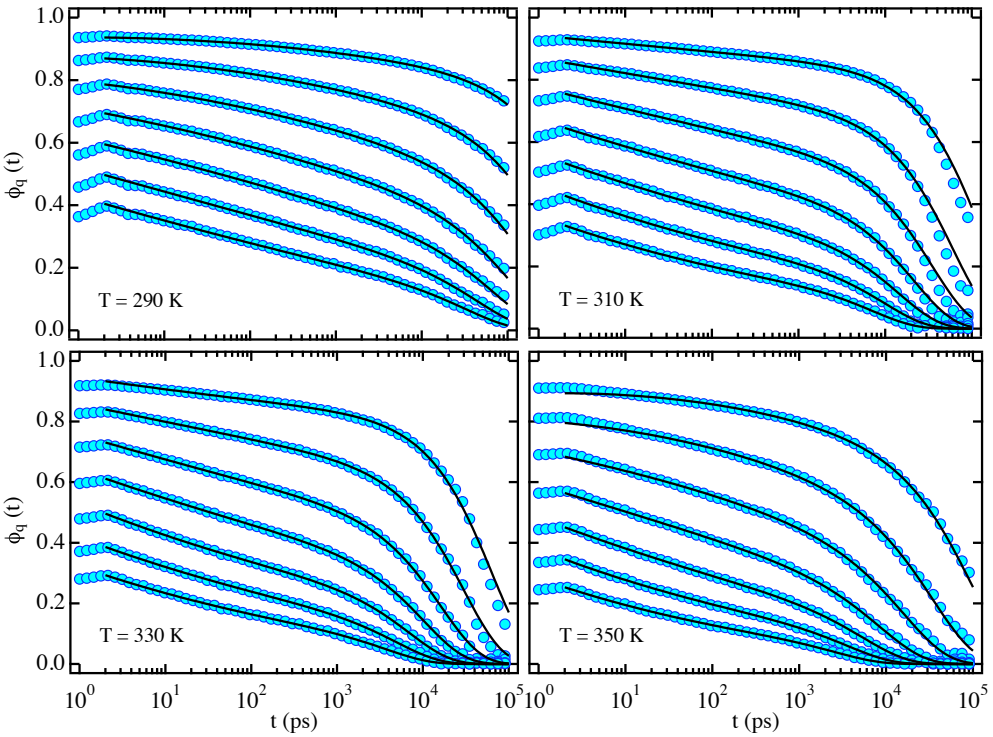

Figure 3.18: Long-time behavior of protein $\phi_q(t)$ - MD results for 4 different temperatures. q-values are, from top to bottom of each panel: 1.6, 2.4, 3.2, 4.0, 4.8, 5.6, 6.4 Å^{-1}. Continuous lines are best fits according to Equation 3.4

a solid, an idea developed back in the 1970s. The possibility of extracting a diffusion constant for protein powder is to be presented below.

3.4.3 Temperature dependence of α relaxation

The q and T-dependence of the protein α-relaxation time extracted from Equation 3.4 is shown in Figure 3.19.

The linear dependence allows us to extract the diffusion constant with the relation $1/\tau_q^\alpha = Dq^2$. It should be noted at this point that according to the theory of Volino and Dianoux (141), the diffusion in a finite system such as protein does not exist at $q = 0$. In this limit, the q-dependent α-relaxation time becomes independent of q instead of following the Dq^2 law. But this is true only

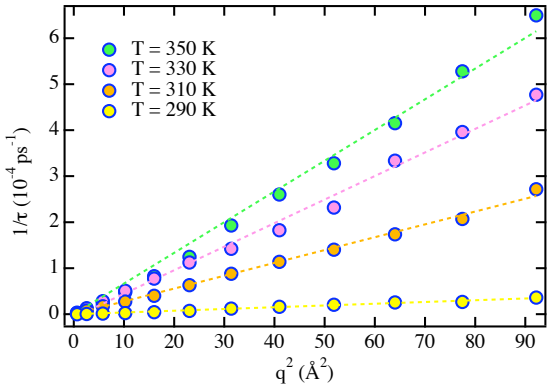

Figure 3.19: q-dependence of τ_q^α - Temperature dependence of the protein inverse α-relaxation time as a function of q^2 for 4 different temperatures ($T = 290, 310, 330$ and 350 K). Dashed lines are best linear fits to the numerical data for $q > 0.15$ Å^{-1}.

for $q < \pi/R$, which is ~ 0.2 Å^{-1}, where R is the diameter of the protein, and our lowest calculated $\phi_q(t)$ is for $q = 0.4$ Å^{-1}.

In Figure 3.20 we show the Arrhenius plot of the inverse of the diffusion constant at finite q: a fragile behavior is evident in this temperature range, 270 - 350 K. The results of this time-domain analysis agree with the frequency domain analysis extracted from dielectric relaxation spectra by Frauenfelder et al on myoglobin (53), where they found an Arrhenius behavior of the β-relaxation and a fragile one for the α-relaxation.

If we fit the curve to a VFT law (Figure 3.20) we get $T_0 = 248 \pm 5$ K. We can also extract an estimate of MCT T_c by fitting the Arrhenius plot of $1/D$ vs $1/T$ with the power law $1/D \sim |T - T_c|^{-\gamma}$. This gives us an estimated $T_c = 263 \pm 5$K. Comparing this plot to the one of a simple glass former, one realizes that the values of the protein amino acid CM diffusion constant are similar to the ones of a simple glass former near the critical temperature T_c. O-terphenyl, for example, is reported in literature to have a critical temperature $T_c = 285$ K and $\log D(T_c) \sim 13.0$ (when D is measured in s/m^2) (119), while salol has $T_c = 266$K and $\log D(T_c) \sim 12.5$ (145).

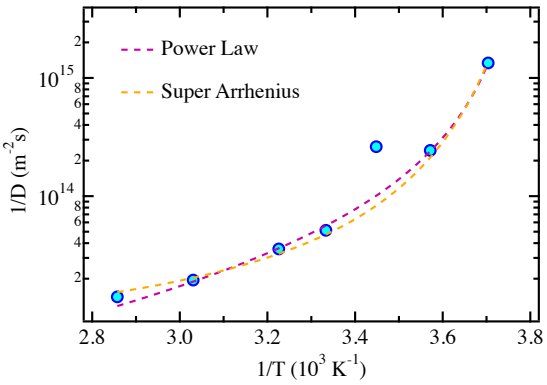

Figure 3.20: Arrhenius plot of the inverse diffusion constant - The temperature dependence follows a Super-Arrhenius behavior. The dashed line is the best fit with a VFT law, $1/D \sim 1/D_0 \exp(BT_0/(T-T_0))$ with $T_0 = 248$ K, or a MCT power law $1/D \sim |T-T_c|^{-\gamma}$ with $T_c = 263$ K, $\gamma = 1.8$.

3.5 Summary

In this chapter, we analyzed the dynamics of hydrated protein over the whole time range, from the fast phonons ($t < 1$ ps), to the exotic logarithmic decay (1 ps $< t <$ 1 ns), to the slow α relaxation ($t > 1$ ns).

First of all, we used IXS to observe a well-defined dispersion relation of intra-protein phonon-like excitations. We identify a significant temperature-dependence of the slowing-down and an increase in population of phonon-like collective motions in an intermediate q-range above the dynamic transition temperature T_l. We believe that these phonon-like modes are the result of the collective vibrational motions of the atoms in the α-helices and β-sheets. Below T_l the vibrational frequency is too high and the population of the modes is too low to be able to facilitate the biological function. That is the reason why proteins are not good enzymes below the dynamic transition temperature. A protein molecule is a 3D finite size system, which does not allow the long wavelength phonons to propagate, and this could be the reason why in our experiment the low-q phonons were not observed.

Second, we demonstrated that the β relaxation of globular protein single-particle dynamics follows a logarithmic decay, regardless of the proteins environment (powder, crystal or solution) or the particular biomacromolecule under consideration (lysozyme or ribonuclease). In particular, the intermediate scatter-

ing functions of the center-of-mass of the amino acid residues can be fitted from 1 ps to their complete decay with a function that consists of the product of two terms: a logarithmic expansion derived from the mode coupling theory (β relaxation) and a simple exponential function (α relaxation). The q-dependence of the parameters involved in the β relaxation agrees with the predictions of MCT scaling form in the temperature range 280 - 340 K, for the case of a proximity to a higher-order singularity. The temperature dependence of the β-relaxation time extracted from fitting the logarithmic decay appears to be Arrhenius over the whole temperature range investigated, 220 - 340 K.

Finally, we were able to extract the diffusion constant for the protein amino-acid residues: in the temperature range 270 - 350 K, the Arrhenius plot of lysozyme $1/D$ can be fitted either with a VFT law or with a power law (fragile behavior). We conjecture that $T_0 \sim 248$ K and $T_c \sim 263$ K for the hydrated lysozyme powder.

We would like to stress here that the agreement between the protein dynamics and the predictions of the idealized MCT does not provide evidence of the existence of a higher-order singularity in proteins. Only solving the MCT equations for this heteropolymeric system could provide an appropriate answer, and at present the MCT equations have only been solved for homopolymers (37). Nevertheless, mapping the protein dynamics onto the dynamics of a short-ranged attractive colloidal system reinforces the analogy between globular proteins and glass-forming liquids, and adds a piece to the puzzle of the interplay between the dynamics and the biological function of biomolecules. The next important question to be addressed is in fact why nature has chosen such a relaxational behavior for proteins. A possible answer could be that the logarithmic decay is the slowest possible time dependence of motion, and this could endow proteins with the appropriate resilience in response to the fluctuations of the external environment.

4

Water-Protein coupling

In wine there is wisdom,
in beer there is strength,
in water there is bacteria.
David Auerbach

4.1 Overview of protein hydration water dynamics

A characterization of protein hydration is essential for understanding (i) protein structure, (ii) protein folding and (iii) protein function. This requires elucidating the effects of both the solvent on the protein and the protein on the solvent. The importance of the role played by hydration water in protein science was realized after introduction in the literature of *hydrophobicity*, a concept related to protein stability for the first time by Kauzmann (79). From that moment on, a protein should have been defined as the system *peptide* + *water* (52) since the simple biomolecule is not able to perform its biological activity without at least one layer of water surrounding it. In particular the conformational flexibility of a protein (and therefore its functionality) is extremely sensitive to the characteristics of its hydrogen bonds with hydration water. This latter experimental fact is understandable considering that proteins evolved from their very beginning in an aqueous environment. While water has been considered as "life's solvent" (in a

passive sense) for a long time, only in the past 20 years has it become an active constituent of cell biochemistry and not just a uniform background. A representation of hydrated protein powder, a model that will be used in the simulations to be presented in Section 4.2.3, is sketched in Figure 4.1.

Hydration can be considered as a process, that of adding water incrementally to dry protein, until a level of hydration is reached beyond which further addition of water produces no change of the essential properties of the protein and only dilutes the biopolymer (121). The hydration shell can be defined as the water associated with the protein at the hydration end point, and it represents monolayer coverage of the protein surface. Water outside the monolayer is perturbed to a significantly smaller extent, typically not detected by measurements of properties such as heat capacity, volume or heat content. The threshold hydration level for protein functionality is $h = 0.2$, where h is the ratio between grams of water and grams of dry protein[1]. They showed that enzymatic activity closely parallels the development of surface motion, which is thus responsible for the functionality of the protein. While supercooling water is quite difficult in the bulk, it is relatively easy to achieve with adsorbed water on protein surface. Up to about $h = 0.4$, water is non-freezable: roughly two layers of water molecules adsorbed to the protein surface are not incorporated into ice crystals, when the aqueous protein solution freezes. The protein-water hydrogen bonds are generally stronger than water-water bonds, and they distort the network in such a way that crystallization is avoided.

Water molecules in protein solutions may be broadly classified into three categories: strongly bound, internal water molecules that occupy internal cavities and deep clefts; water molecules that interact with the protein surface; and bulk water. Internal waters, which can be identified crystallographically and are conserved in homologous proteins (121), are extensively hydrogen bonded and comprise an integral part of the protein structure. They have residence times ranging from $\sim$ 10 ns to ms, and their exchange with the bulk solvent requires local unfolding to occur. Surface water molecules are much less well defined structurally than

[1]This consideration is to some extent questionable, since in the absence of the solvent, the exchange and diffusion of substrate molecules are limited.

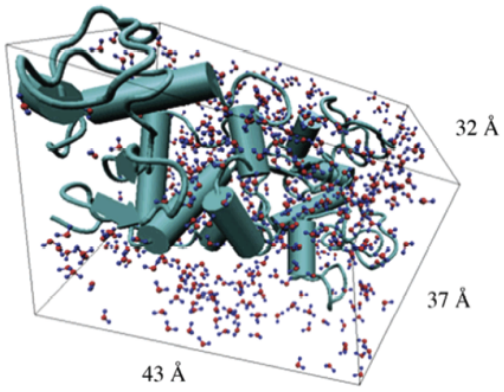

Figure 4.1: Perspective view of the simulation box - Snapshot from a MD simulation at $T = 250$ K and $P = 1$ atm of the hydrated lysozyme powder model, containing two protein molecules and 484 water molecules around them (hydration level $h = 0.3$). The box size is shown for each edge.

internal water molecules (in the sense that surface binding sites identified crystallographically are not highly conserved among different crystal forms of the same protein), and are much more mobile, with residence times on the order of tens of picoseconds. In addition to being important for protein stability, and in the energetics and specificity of ligand binding, surface waters also have a profound influence on the dynamics of a protein molecule as a whole.

Although the details of the connection between protein hydration and function have not yet been worked out, it is clear that surface water is required for the activation of fast conformational fluctuations (47; 60) that appear to be important in protein folding and function (12; 118). The observation of enzyme activity in partially hydrated powders (albeit lower activity than in solution) (121), where the amount of water present is far less than sufficient to completely cover the protein surface, suggests a crucial role for the water molecules in the first hydration shell. Consequently, it is of interest to characterize the dynamical properties of this so-called protein hydration water in detail, and to investigate their potential connection to functionally relevant protein motions. Numerous experimental and theoretical studies have demonstrated that the properties of protein hydration water are different from those of bulk water. X-ray and neutron diffraction experiments clearly indicate that the solvent structure in the vicinity of biomolecules differs from that of the bulk solvent (35; 138). Information about

the translational motion of water, derived from the rate of intermolecular spin relaxation (112; 133) indicated a slower motion on the surface of proteins, in agreement with long residence times in the first hydration shell (108). Chen et al. suggested that the water dynamics could also be described in terms of an α-relaxation model such as that applied to kinetic glass transitions in dense supercooled liquids, in analogy with their findings for water adsorbed in vycor glass (146). Settles and Doster (47) reached similar conclusions in their study of hydrated myoglobin, in which they determined the intermediate scattering function and the mean squared displacement of hydration water by inverting incoherent neutron-scattering data. Their results clearly demonstrated the anomalous character of the diffusion of water at the protein surface. More recently, molecular dynamics simulation studies of hydration water have been analyzed along these lines (19; 120), and have provided a detailed description of the spatial and temporal inhomogeneities that are at the roots of the anomalous behavior observed experimentally. Moreover, based on a MD simulation, Paciaroni et al. (109) predicted the presence of a low-frequency vibrational anomaly, the so-called boson peak, typical of glassy materials, which was subsequently confirmed by neutron scattering (110).

4.2 The low temperature dynamic crossover

4.2.1 An introduction to protein dynamic transition

Around $T_l = 220$ K, the protein has a transition that could be described as a *dynamic transition* (Section 1.3.3) or a so-called glass transition. The protein dynamic transition was introduced 20 years ago based on neutron scattering experiments with dry and hydrated myoglobin and lysozyme (46), and it was confirmed by mechanical relaxation experiments with hydrated protein films (104). This term comprises the two types of dynamic crossover, the *glass transition*, which is quite abrupt and the *percolation transition*, which is continuous. Both types lead to structural arrest on a macroscopic scale. The question, which concept applies to hydration water, is not yet resolved.

What is known is that below T_l, protein is in a glassy state and loses its conformational flexibility, showing hardly any biological functions (118). At and above T_l, this flexibility is restored and the protein is able to sample more conformational substates, thus becomes biologically active. This dynamic crossover in protein is traditionally detected by observing the changing of the slope of the mean square displacement $\langle x^2 \rangle$ of hydrogen atoms vs. T plot (39), and believed to be triggered by their strong coupling with their hydration water (23). IR data collected by Doster et al. (45) suggested that the transition in the hydration water could be described as the melting of amorphous ice and that this solvent network is composed of water clusters with relatively strong internal bonding. They used this information to address the problem of dynamic coupling of solvent motions with internal protein motions, suggesting that the cooperativity of the solvent network provides the coupling mechanism.

Since protein motions are *plasticized* by water molecules, one could suggest an analogy to polymer rubbers or elastomers (44). Stretching of rubbers induces structural relaxation processes, reducing their conformational entropy. The rubber elasticity vanishes, when the structural relaxation time crosses the experimental time window, which defines the rubber-glass transition. The protein elasticity in the native structure can be interpreted as the rubber plateau, which turns into a solid elastic state below the rubber-glass temperature. The plateau terminates at the protein-denaturation temperature, where the structure becomes liquid-like with reduced constraints of protein residues to translational diffusion. Experimental evidence suggests, that the liquid-glass transition of the solvation shell occurs simultaneously with the rubber-glass transition of the protein.

The plausible microscopic origin for the dynamic transition of a hydrated protein is thought to be due to the strong coupling of the dynamics of the hydration water and those of the side chains of the protein through their hydrogen bonds. In particular, it was shown by MD simulations that the slow structural relaxation of the protein, which is essential for the enzymatic function, is driven by the relaxation of the hydrogen bond network via solvent translational displacement (137; 140). In fact, this transition is also common to many biopolymers

and believed to be triggered by their strong coupling with mobility of their hydration water. We show experimentally and numerically that this feature can be described as a *dynamic crossover phenomenon*, i.e. a sudden switch in dynamical behavior of hydration water around biomolecules.

4.2.2 Theoretical framework

Incoherent neutron scattering offers many advantages for the study of hydrogen atom dynamics in a protein and its hydration water[1]. The main reason is that the scattering cross section of hydrogen is about 80 barns, and is much larger (at least 20 times) than that of other atoms in the system, composed also of oxygen, carbon, nitrogen and sulfur atoms. Furthermore, neutron scattering cross section of a hydrogen atom is mostly incoherent so that incoherent neutron spectra reflect, essentially, the self-dynamics of the hydrogen atoms in the protein or water. Combining this dominant cross section of hydrogen atoms with the use of spectrometers having different energy resolutions, we can study the molecular dynamics of water in a wide range of time-scale, encompassing ps to tens of ns.

Incoherent Elastic Scattering ($E = 0$). The density correlation function, $\phi_q(t)$, for an atom harmonically bound to a molecule can be written as

$$\phi_q(t) = \langle \exp[i\mathbf{q} \cdot (\mathbf{x}(t) - \mathbf{x}(0))] \rangle \tag{4.1}$$

where $\mathbf{x}(t)$ is the position of the atom at time t. It can be shown that in the Gaussian approximation, which is exact for the harmonically bound particle, one can write (29):

$$\phi_q(t) = f_q \exp(q^2 \langle x(0)x(t) \rangle) \tag{4.2}$$

where the first factor is called the Debye-Waller factor $f_q = S_q(E = 0) = \exp(-q^2\langle x^2 \rangle/3)$ which gives rise to the elastic scattering, and the second factor,

[1]The term *incoherent* refers to the scattering from the same nucleus at two successive times. One can therefore obtain information on the self-part of the density correlation function $\phi_q(t)$. There are no interference effects between the amplitudes scattered by different nuclei, which is instead *coherent* scattering

which involves the displacement-displacement time correlation function, gives rise to the inelastic scattering such as phonons.

We can therefore calculate $\langle x^2 \rangle$ from the Debye-Waller factor, by a linear fitting of the logarithm of $S_q(E = 0)$ vs. q^2 plot. To obtain the mean squared displacement, we performed fixed window scan (an elastic scattering measurement with a fixed resolution window of FWHM of $\pm 0.8 \mu$eV) (13) in the temperature range 40 - 290 K, covering completely the supposed crossover temperature T_L.

Incoherent Quasi-Elastic Scattering ($E \sim 0$). Quasielastic scattering is mainly interested in the low-frequency region ± 1 meV. The scattering originates from interactions of neutrons with particles diffusing or reorienting over the ps-ns time scale: such phenomena do not give rise to separate peaks in the spectrum, but they produce a broadening of the elastic line (that is associated with neutrons scattered without energy transfer).

In actual QENS experiment, we have to take into account only the signal coming from the hydrogen atoms in the hydration water, by taking the difference of the spectra of H_2O and D_2O hydrated samples. Denoting the fraction of the elastic scattering by p (coming both from the bound hydrogen atom in protein and too slow water molecules) we can analyze the experimental data according to the following model:

$$S_q(\omega) = pR_q(\omega) + (1 - p)FT\{\phi_q(t)R_q(t)\} \tag{4.3}$$

where $\phi_q(t)$ is the self-intermediate scattering function of hydrogen atoms which defines the quasielastic scattering, $R_q(\omega)$ is the experimental resolution function, and the symbol FT denotes the Fourier transform from time t to frequency ω.

4.2.3 The crossover from experiments and simulations

In this section, we shall review our neutron scattering experiments and molecular dynamics simulations as a function of temperature on protein hydration water (31; 32).

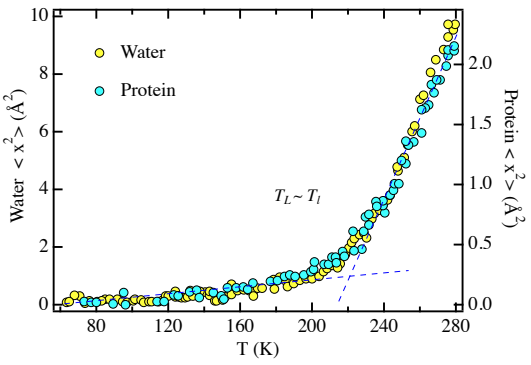

Figure 4.2: Protein and water $\langle x^2 \rangle$ - Hydration water $\langle x^2 \rangle$ is plotted using the scale on the left hand side and protein $\langle x^2 \rangle$ using the scale on the right hand side (the scale factor is 4.2). Lysozyme $\langle x^2 \rangle$ is taken from the elastic scan of D_2O hydrated sample. Note the coincidence of hydration water T_L with protein T_l.

Figure 4.2 shows the temperature dependence of the experimental $\langle x^2 \rangle$, both for lysozyme and its hydration water. In order to show the synchronization of the two MSDs, lysozyme $\langle x^2 \rangle$ is multiplied by a factor 4.2: the two curves superpose onto each other. So the crossover temperatures for both protein (T_l) and its hydration water (T_L), defined by a sudden change of slope of MSD from a low temperature behavior to a high temperature behavior, coincides within the experimental error bars (38).

Since $\int_{-\infty}^{+\infty} S_q(E)\, dE = 1$ at each q value, the peak height and the peak width of the incoherent quasi-elastic spectrum are related to each other. The peak height increases as temperature decreases, implying the narrowing of the peak width, which is a qualitative measure of the relaxation time (Figure 4.3). From this property we can already show the presence of a dynamic transition, without detailed analysis of the spectrum. In Figure 4.3 we present four examples taken from lysozyme hydration water case (for $q = 0.56$ and 1.11 Å^{-1}) of a quantitative RCM analysis (Section 2.1) by which we can extract the translational relaxation time $\langle \tau \rangle$ as a function of temperature.

From the fitting, we obtain three parameters: τ_0, β and γ and we are able to calculate the theoretical $\phi_q(t)$, which are plotted in Figure 4.4 for protein hydration water. It is important to note that using these three parameters, we can construct $\phi_q(t)$ over a broad range of time scale which was not covered in the original measurement within the resolution limit. The α-relaxation time of

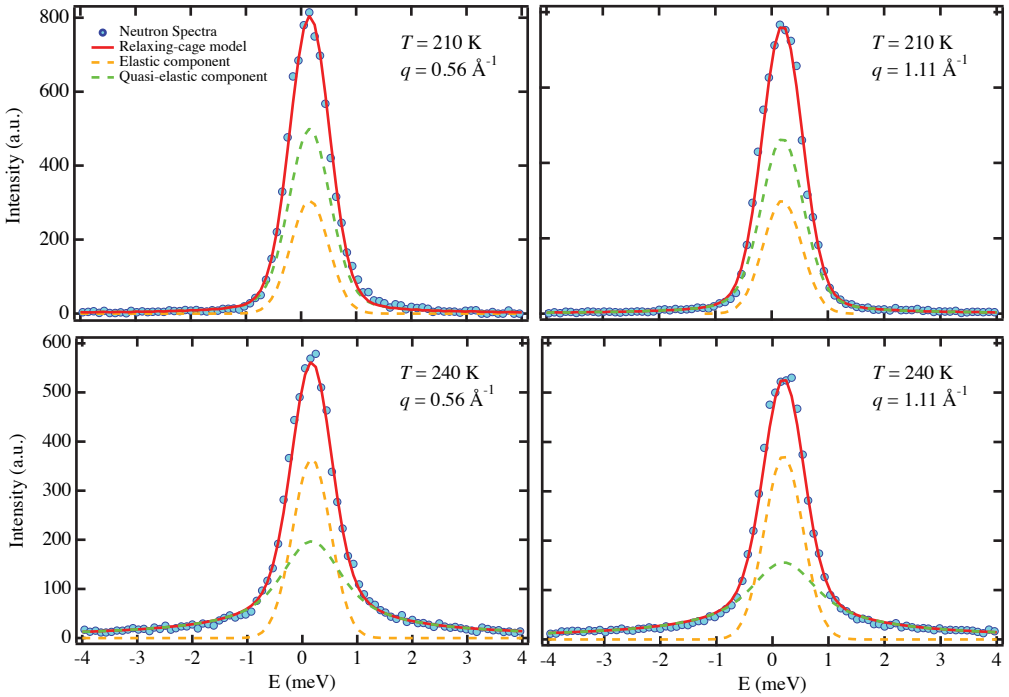

Figure 4.3: Protein hydration water QENS - An example of the RCM analysis for lysozyme hydration water at $T = 210$ K (below T_L) and 240 K (above T_L) respectively. Note for the higher temperature case, the quasi-elastic components are much broader and the peak height is much lower than the lower temperature case.

hydration water can now be extracted in two different ways. The first one is to use RCM model to calculate the $\phi_q(t)$ that fit the QENS spectra, and then graphically calculate τ_q^α. The second method is to use the fitted parameters of RCM to calculate the average translational relaxation time.

We shall stick to the second method, since it is more rigorous, and finally present the Arrhenius plot of $\langle\tau\rangle$ in Figure 4.5. As it is clear from the left panel, $\langle\tau\rangle$ switches from a Super-Arrhenius behavior at high temperature to an Arrhenius behavior at low temperature (see Section 1.3.3). In order to extract rigorously the dynamic transition temperature, we calculate the derivative of the Arrhenius plot (right panel). This shows a broad peak, with a maximum at $T_L \sim 225$ K, revealing a change in the dynamics of supercooled hydration water,

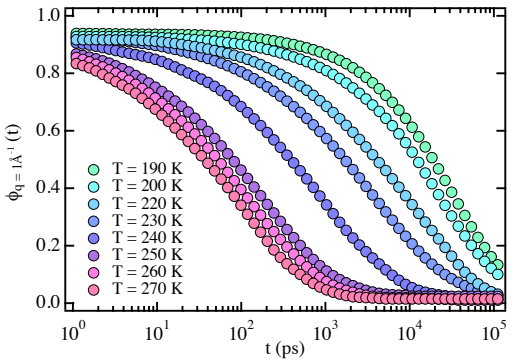

Figure 4.4: Protein hydration water $\phi_q(t)$ - An example of intermediate scattering functions $\phi_q(t)$ of hydrogen atoms of lysozyme hydration water extracted as a result of the RCM analysis for different temperatures.

in correspondence of an analogous transition in protein at T_l.

So far, we have shown experimentally that this low-temperature dynamic transition of protein (or more generally for many other biopolymers, as discussed in Section 2.2.2) at T_l is likely to be triggered by a dynamic crossover in the hydration water of these biopolymers at T_L. This is graphically demonstrated in Figure 4.6, where we plot both hydration water $\langle\tau\rangle$ and protein $\langle x^2\rangle$: they show a synchronized change at $T_L \sim T_l$.

Recently, an MD simulation (82) has been run for a model of hydration water in protein lysozyme and Dickerson dodecamer DNA. However, in this simulation the model used was not realistic enough for hydrated powder samples used in experiments to directly compare the temperature dependences of simulated quantities with the neutron scattering results. To better mimic the experimental system, we decided to perform MD simulations (85) on the *random powder model* developed and tested by Tarek and Tobias (136): this model has been shown to improve the agreement with experiments compared to the so-called protein/water cluster model used in (82), which is composed of just one protein surrounded by its hydration water (for more details, see Section B.3).

A perspective view of the simulation box is shown in Figure 4.1, where the two proteins and the hydration water surrounding them are displayed, together with the box dimensions. It should be noted that there are only a few water molecules sandwiched between the two proteins while there are more water molecules around other parts of protein surface. But on the average, $h = 0.3$ is supposed to be

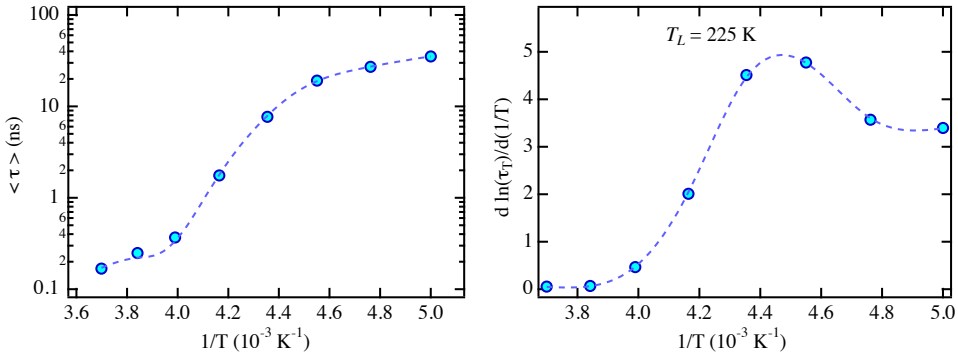

Figure 4.5: Protein hydration water $\langle\tau\rangle$: experiments - *Left*: Arrhenius plot of the average translational relaxation time $\langle\tau\rangle$ extracted from QENS spectra of lysozyme hydration water. *Right*: Derivative of the Arrhenius plot, showing a broad peak at $T_L \sim 225$ K.

only one monolayer of water covering each protein. The resulting density of the modeled hydrated powder protein is between 1.2 and 1.3 g/cm^3, depending on the temperature, in agreement with experimental data for lysozyme crystals (1.23 g/cm^3, (57)).

The RCM fits of the $\phi_q(t)$, both the time dependence and the q-dependence, are excellent allowing us to extract $\langle\tau\rangle$ as a function of temperature as shown in Figure 4.7. As in Figure 4.5, we report both the Arrhenius plot of the transport property (left panel) and its derivative (right panel). The peak is centered around $T_L \sim 230$ K, a value close to the experimental one. In summary, we demonstrated by MD simulations that the low temperature crossover phenomenon is due to the average translational motion of all the water molecules in the hydration layer, not to the long-range proton diffusion coupled to the motion of the so-called Bjerrum-type defects (134). Furthermore, by a simulation using a realistic powder model, one can quantitatively account for the temperature dependence of the neutron scattering data.

In Figure 4.8 we show the theoretical $\phi_q(t)$ for protein hydration water, obtained from the fitting with RCM of the calculated ones. Then, the dynamic response function, $\chi_T(t)$, is calculated with finite differences of the $\phi_q(t)$. The maximum of $\chi_T(t)$, $\chi_T^*(t)$, increases as temperature decreases, until it reaches

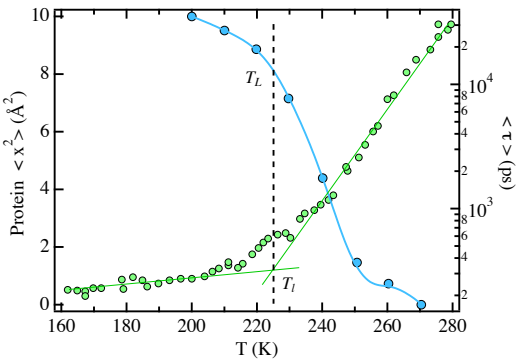

Figure 4.6: Coincidence of T_l and T_L - Superposition of the α-relaxation time of lysozyme hydration water (from quasi-elastic neutron scattering) and $\langle x^2 \rangle$ for lysozyme itself (from elastic neutron scattering). Both curves show a dynamic transition at the same temperature, i.e. $T_l \sim T_L$.

a maximum at $T = 225$ K, in agreement with the temperature extracted from experiments. Moreover, The crossover feature is clearly visible looking at the decay of $\phi_q(t)$ below and above T_L (see the arrow in Figure 4.8).

The success of the model described in the previous section stimulated us to run new simulations and extract new information from the trajectories. In particular, we were interested in the hydration level dependence of the dynamic crossover phenomenon: how does the relative amount of water that hydrates the protein powder affect its dynamics? To answer this question we increased the hydration level to $h = 0.45$ (726 water molecules) and $h = 0.6$ (968 water molecules).

In both cases, we started from a random distribution of the water molecules in a box with the two proteins. We equilibrated the systems in the NPT ($T = 280$ K, $P = 1$ bar) ensemble for several nanoseconds, until the edges of the box reached a constant length. Then we ran a 60 ns annealing simulation with a slow linear temperature ramp from 280 K to 190 K. Simulations at each temperature were then started from the equilibrated configuration of the annealing simulation. Each run lasted 50 more ns, and all the other details of the calculation are the same as in the $h = 0.3$ case.

Hydration $h = 0.3$ corresponds to the average coverage of the protein surface: when this parameter is increased, water is forced to keep its distance from the macromolecule. Merzel and Smith (99) showed that the first hydration layer (~ 2 Åfrom the protein surface) is about 15% more dense respect to bulk water, but

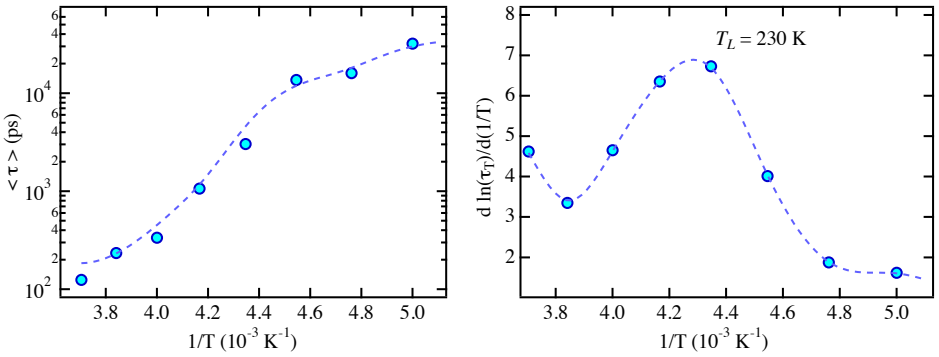

Figure 4.7: Protein hydration water $\langle\tau\rangle$: simulations - *Left*: Arrhenius plot of the average translational relaxation time $\langle\tau\rangle$ for water, extracted from MD trajectories of lysozyme hydrated powder model. *Right*: Derivative of the Arrhenius plot, showing a broad peak at $T_L \sim 230$ K.

that the normal density is recovered in the second hydration layer ($\sim$ 4.5 Å). Therefore, we expect that going from the $h = 0.3$ to the $h = 0.6$ case would shift water properties toward the bulk case.

Figure 4.9, where the Arrhenius plot of the average tau is plotted as a function of the hydration level, confirms the hypothesis that water-water interactions are less strong than protein-water interactions, so that the bulk water limit corresponds to minimum relaxation times. Three results are evident from this picture: as h increases,

- the average α-relaxation time $\langle\tau\rangle$ decreases
- the crossover temperature T_L remains almost constant
- the activation energy E_A of the Arrhenius part decreases

The first point confirms the hypothesis that the bulk water case is a limit case. In fact, our results show that a box of 512 TIP4P-Ew water molecules has a much faster average relaxation time, that switched from Super-Arrhenius to Arrhenius dynamic behavior at $T_L = 215$ K (see Section 2.2.3 and (148)). We can conclude that the protein-water interactions shift the temperature dependence of

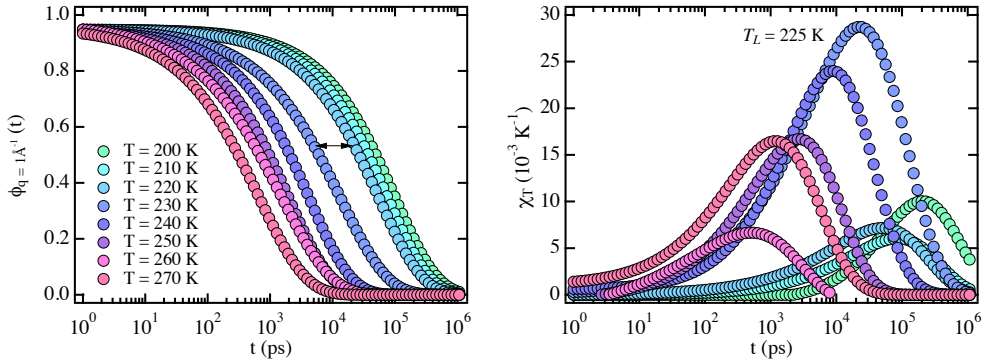

Figure 4.8: Numerical results for $h = 0.3$ - *Left*: Intermediate scattering functions $\phi_q(t)$ obtained from the fitting with RCM of the calculated ones. Notice the gap between the correlators bordering the dynamic transition in the translational dynamics. *Right*: Dynamic response function, $\chi_T(t)$, calculated with finite differences. The maximum at $T_L = 225$ K agrees with the crossover temperature extracted in Figure 4.7.

water dynamics to higher T, and still the essential characteristics and phenomena present in hydration water are qualitatively preserved.

4.3 The high temperature dynamic crossover

4.3.1 An introduction to protein denaturation

Denaturation is the process in which proteins lose their tertiary and secondary structure by application of some external stress or chemical or heat (e.g. when food is cooked, some of its proteins denature)[1]. Denatured proteins can exhibit a wide range of characteristics, from loss of solubility to aggregation (hydrophobic proteins come into contact to reduce the total area exposed to water). Since the structure of proteins determines their function, they can no longer work once they are denatured. This is in contrast to intrinsically unstructured proteins, which are unfolded in their native state, but still functionally active. Enzymes lose their

[1] A classic example of denaturing in proteins comes from egg whites, which are largely egg albumins in water. Cooking the thermally unstable whites (or adding acetone) turns them opaque, forming an interconnected solid mass. The skin which forms on curdled milk is another common example of denatured protein.

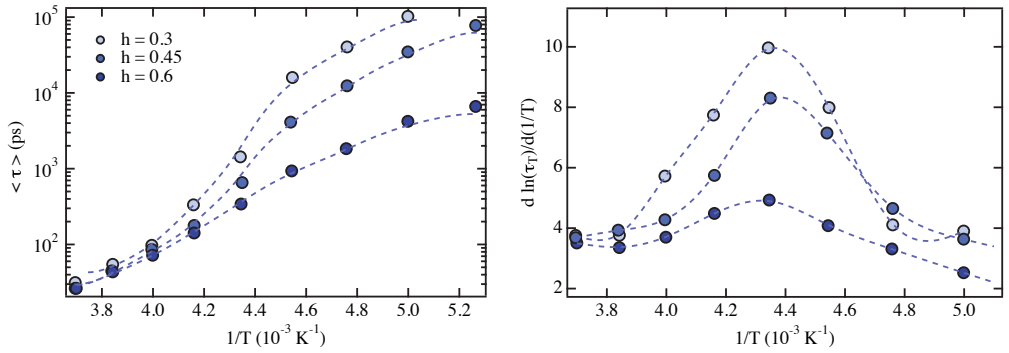

Figure 4.9: Hydration level dependence of $\langle\tau\rangle$ - The hydration level dependence of the dynamics of lysozyme hydration water. Note as the hydration level increases, the crossover temperature remains almost constant and the relaxation time $\langle\tau\rangle$ at T_L decreases.

activity, because the substrates can no longer bind to the denatured active site: the amino acid residues involved in stabilizing the transition states are no longer positioned to be able to do so.

Denaturation involves three of the four protein structures (the primary structure is held together by covalent peptide bonds and is not affected): in quaternary structure denaturation, protein subunits are dissociated and the spatial arrangement of protein subunits is disrupted; in tertiary structure denaturation i) covalent interactions between amino acid side chains (such as disulfide bridges between cysteine groups), ii) noncovalent dipole-dipole interactions between polar amino acid side chains (and the surrounding solvent), iii) Van der Waals (induced dipole) interactions between nonpolar amino acid side chains, are disrupted; in secondary structure denaturation, proteins lose all regular repeating patterns such as alpha-helices and beta-pleated sheets, and adopt a random coil configuration.

In many proteins denaturation is reversible (the proteins can regain their native state when the denaturing influence is removed)[1] and involves interme-

[1]This was important historically, as it led to the notion that all the information needed for proteins to assume their native state was encoded in the primary structure of the protein, and hence in the DNA that codes for the protein.

diate structures. In particular, lysozyme exhibits intermediate structures under chemical denaturation (65), pressure-induced denaturation (128), and thermal denaturation (122). Its unfolding process can therefore be considered as a three-state model $N \rightleftharpoons I \rightarrow U$. The first step is usually called *reversible denaturation* and can be seen as a kind of dynamic transition associated with the configurational entropy change (63), while the second step is the *irreversible denaturation* and it is due to an association of unfolded lysozyme units (128).

We suggest that this reversible denaturation is related to the dynamic crossover that protein hydration water undergoes at $T_D = 345 \pm 5$ K, showed by our neutron scattering experiments and molecular dynamics simulations. At this temperature, a sudden change in hydration water dynamics takes place, the inverse diffusion constant switches from a super-Arrhenius behavior at low temperatures to an Arrhenius behavior at high temperatures. We also extracted the migration distance d of the hydration water molecules from QENS and observed that d showed a pronounced increase above T_D. An NMR investigation of the long-time diffusion of the hydration water in lysozyme has confirmed the existence of both high and low temperature dynamic crossover phenomena (94).

The existence of this phenomenon can also be shown theoretically. In fact whenever the specific heat has a peak, the Arrhenius plot of the inverse of the diffusion constant has a slope change (see A.4). If we assume that the Adam-Gibbs equation is valid also at high temperatures for hydration water, the specific heat peak recently observed by calorimetry during lysozyme thermal denaturation by Salvetti et al. (122) suggests the existence of a high-temperature crossover phenomenon for the inverse of the diffusion constant. It was recently found that the contribution of the configurational disorder to entropy is dominant (95), then $S_{conf} \sim S$ and

$$S_{conf}(T) \sim S_{conf}(T_0) + \int_{T_0}^{T} \frac{C_p}{T}\, dT \tag{4.4}$$

As a numerical example, the Arrhenius plot of the resulting D_0/D as obtained by substitution in Equation A.17 of C_p reported in (122) is shown in Figure

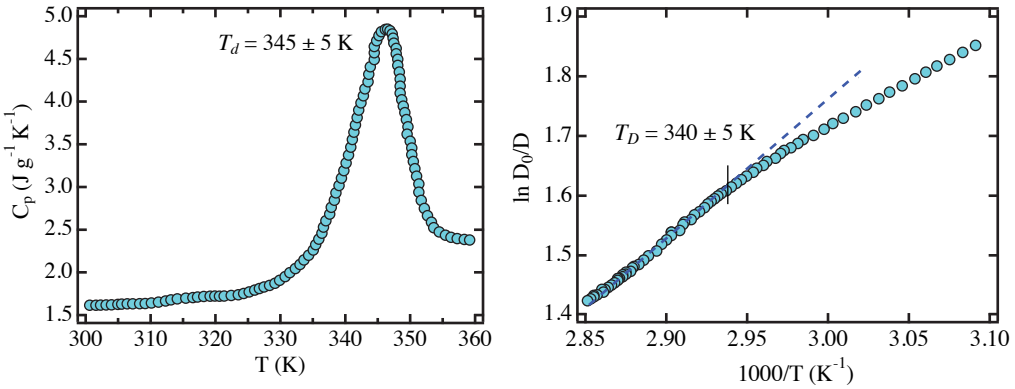

Figure 4.10: Adam-Gibbs theory for protein hydration water - *Left*: Specific heat measurement of lysozyme solution from (122). *Right*: Arrhenius plot of D_0/D calculated according to the Adam-Gibbs Equation A.17. D_0 is the prefactor in the Adam-Gibbs equation, $S_{conf}(T_0)$ is $S(T = 290\ \text{K})$. As a numerical example, we choose $S_{conf}(T_0) = 1\ \text{J/(gK)}$ and $A = 700\ \text{J/g}$. This equation predicts a change in the slope for the inverse of the diffusion constant at 340 ± 5 K.

4.10. The Arrhenius plot of D_0/D has a kink at $T = 340 \pm 5$ K, corresponding approximately to the maximum in the specific heat.

4.3.2 Theoretical framework

In this section, we build a model to extract the inverse diffusion constant $1/D$ and the migration distance d of the hydration water molecules from QENS spectra. QENS experiments essentially provide us with the incoherent dynamic structure factor $S_q(E)$ of the hydrogen atoms of the water molecules in the protein hydration layer. The measured neutron intensity $I_q(E)$ at each q is analyzed with the following model:

$$I_q(E) = A[p_q\delta(E) + (1 - p_q)S_q(E)] \otimes R_q(E) + B \tag{4.5}$$

where A is the normalization factor, p_q is the elastic scattering component, taking into account the scattering from particles that do not move a length comparable to $2\pi/q$ on the time scale corresponding to the spectrometer s elastic

energy resolution function. $R_q(E)$ is the q-dependent energy resolution function, and B is the nonlinear background. $S_q(E)$ is a convolution of the translational dynamic structure factor $S_q^T(E)$ and the rotational one $S_q^R(E)$, i.e., $S_q(E) = S_q^T(E) \otimes S_q^R(E)$. By using only the small q spectra ($q < 1$ Å^{-1}), the rotational contribution can be made negligibly small. Our computer simulation calculates the self-intermediate scattering function $\phi_q(t)$, which is the Fourier transform of the incoherent dynamic structure factor $S_q(E)$. It shows that the long time decay of $\phi_q(t)$ is a stretched exponential $\phi_q(t) \sim e^{-(t/\tau_q)^\beta}$. When the temperature is above the room temperature, the stretched exponent β is only slightly less than unity. So we can approximately use $\phi_q(t) \sim e^{-(t/\tau_q)}$, or equivalently in frequency domain $S_q(E)$ is approximated as a Lorentzian shape function (34; 127)

$$S_q(E) \sim S_q^T(E) = \frac{1}{\pi} \frac{\Gamma_q}{E^2 + \Gamma_q^2} \tag{4.6}$$

where $\Gamma_q = 1/\tau_q^\alpha$ is the half width at half maximum (HWHM). Its validity can also be confirmed by the good agreement between the experimental data and the fitted curve with the model for all temperatures and wave vector transfers. In the $q \to 0$ limit, it is well known that $\Gamma_q = Dq^2$. Thus for the finite but small q, we may take into account the next order correction to the q^2 dependence as follows:

$$\Gamma_q = Dq^2(1 - \xi^2 q^2 + ...) = \frac{Dq^2}{1 + \xi^2 q^2} \tag{4.7}$$

where D is the translational self-diffusion constant of water molecules. Equation 4.7 is indeed independent of any model in the low-q limit. With the objective to extract D from low-q spectra, Equation 4.7 is a very good approximation. In fact, the often used *jump diffusion model* is equivalent to putting $\xi^2 = D\tau_0$, where τ_0 is the average time duration that a water molecule spends oscillating in a cage formed by its nearest neighbors (34). On the other hand, in the so-called Singwi-Sjölander model of water, a motion of a typical water molecule is described as first trapping in a cage oscillating for a period τ_0 followed by a diffusion of a

duration τ_1. This pattern of motion repeats itself (127). The HWHM in this model is given by (in the short diffusion time τ_1 limit)

$$\Gamma_q = \frac{1}{\tau_0}\left[1 - \frac{f_q}{1 + Dq^2\tau_0}\right] \tag{4.8}$$

where the Debye-Waller factor is $f_q = \exp(-q^2\langle x^2\rangle/3)$. $\langle x^2\rangle$ is the mean square vibrational amplitude along the direction of q. It is $(0.5)^2$ Å^2 as determined previously by our computer simulation (30). Thus the Debye-Waller factor is approximately equal to unity for $q < 1$ Å^{-1}. Therefore, Equation 4.8 is also reduced to Equation 4.7 with $\xi^2 = D\tau_0$. One should notice that even though the physical pictures of these models are quite different, in the small q limit, they all give the same form of q dependence of the Lorentzian linewidth.

In the case of protein hydration water, the realistic picture of the motions of the water molecules is describable neither by the jump diffusion model nor by the Singwi-Sjölander model. In the dense liquid state near the room temperature, a water molecule is first trapped in a site for a time interval τ_0 on the order of 0.1 ps, oscillating in a cage formed by adjacent water molecules connected by hydrogen bonds. The hydrogen bonds are continuously breaking and reforming. After the time τ_0, the cage gradually relaxes and then the water molecule starts to move away from the trapped site for a time interval τ_1 until it gets trapped again in a new site. However, the cage relaxation time τ_1 is not necessarily much less than τ_0. It depends on the temperature of water and can be on the order of picosecond to nanosecond at low temperatures. In order to extract D, we can write Equation 4.7 as

$$\frac{1}{\Gamma_q} = \frac{1}{D}\left(\frac{1}{q^2} + \xi^2\right) \tag{4.9}$$

and plot $1/\Gamma_q$ versus $1/q^2$. The result is a linear equation with a slope $1/D$. On the other hand, after extracting D this way, we can then plot D/Γ versus $1/q^2$. The result is a set of parallel straight lines with a zero intercept ξ^2. In this way, ξ^2 is extracted with tolerable accuracy. One can thus calculate the characteristic migration distance between successive traps of water molecules using ξ^2 as $d = \sqrt{\langle l^2\rangle} = \sqrt{6\xi^2}$. It is the measure of the average distance that a water

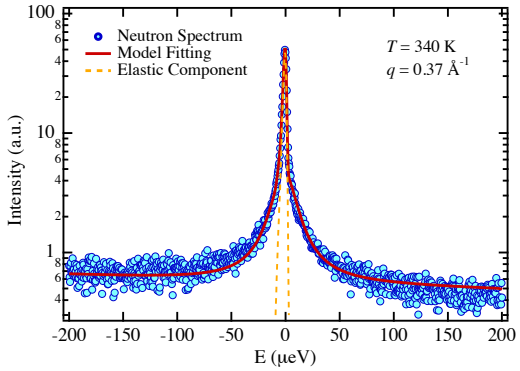

Figure 4.11: Analysis of a typical QENS spectrum of protein hydration water at high T - T = 340 K, q = 0.37 Å^{-1}. The hollow circles are the measured intensity as a function of energy transfer E. The solid line is the fitted curve using the model. The dashed line is the elastic scattering component.

molecule travels between two successive traps. While the self-diffusion constant D represents how fast a molecule diffuses, the migration distance d represents how far the center of mass of a typical molecule translates in the cage relaxation process before it gets trapped again.

4.3.3 The crossover from experiments and simulations

The model discussed above is used to analyze the measured QENS spectra of the protein hydration water for temperatures ranging from 290 to 380 K covering the denaturation process, occurring at T_d = 345 K (149). Using this model, the spectra measured at all temperatures and wave vector transfers can be fitted well in the whole energy transfer range of -200μeV$< E < +200\mu$eV. Figure 4.11 shows an example of the analysis of the spectrum at q = 0.37 Å^{-1}, T = 340 K. The analysis result indicates that the factor p_q takes a value of 0.54 (see Equation 4.5). This means that 46% of the spectral area is contributed from the hydration water that is free to diffuse in the time window of the spectrometer. The asymmetry of the spectra can be accounted for very well by allowing for an asymmetric shaped energy resolution function. The good agreement between the fitted curve and the measured intensity shows the validity of the model.

Figure 4.12 (right panel) shows the plot of $1/\Gamma_q$ versus $1/q^2$ extracted from spectra taken at all the temperatures. It displays clearly a series of straight lines. The slopes of these lines are the inverse diffusion constants, $1/D$. However, the

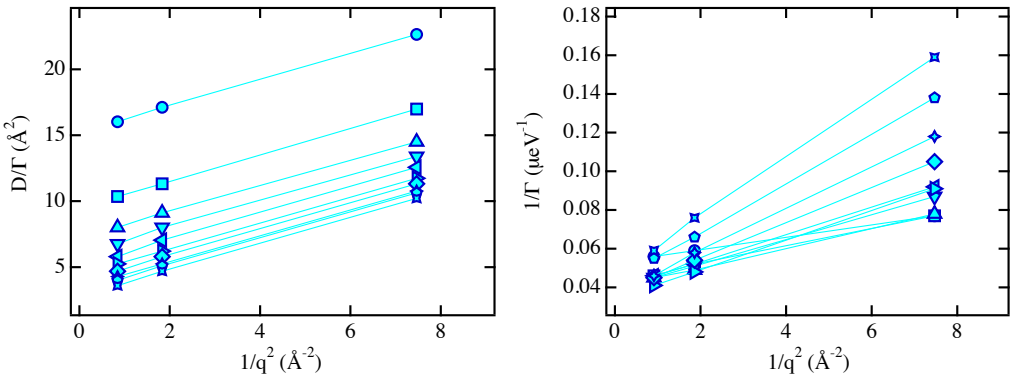

Figure 4.12: Fitting parameters - *Left panel*: D/Γ vs $1/q^2$ for measured temperatures from 290 to 380 K every 10 K at low $q = 0.37$, 0.73 , 1.07 Å^{-1}. The zero intercepts give ξ^2. *Right panel*: plot of $1/\Gamma$ vs $1/q^2$, the slopes of the straight lines give the inverse diffusion constant $1/D$.

uncertainties of the intercepts are too large to show any useful information. After extracting D this way, we can then instead plot D/Γ_q versus $1/q^2$ (Figure 4.12). They also exhibit a series of parallel straight lines, the zero intercepts of which give ξ^2. In this way, we bypassed the fitting of the original intercepts and got the new intercepts ξ^2 within tolerable uncertainties.

Figure 4.13 shows the Arrhenius plot of the extracted $\log(1/D)$ versus $1/T$ and d versus T from this model. Figure 4.13 (a) shows an evidence of an Arrhenius to super-Arrhenius dynamic crossover as the temperature is raised across $T_D = 345 \pm 5$ K. Below T_D, the inverse diffusion constant can be fitted with the VogelFucherTamman law as $1/D = 1/D_0 \exp(CT_0/(T - T_0)$ with $T_0 = 204 \pm 36$ K and $C = 0.94$. While above T_D, the inverse diffusion constant can be fitted with the Arrhenius law $1/D = 1/D_0 \exp(E_A/RT)$ with $E_A = 5.97 \pm 0.55$ kcal/mol. The exact value of T_D is then evaluated as the crossing point of the two laws. Figure 4.14 shows the extracted d that represents the migration distance of the water molecules between two successive trap sites. One can see that it is increasing slowly below T_D from 4.2 to 5.6 Å but rises sharply above T_D to 9.6 Å at 380 K.

The result is consistent with the previous results of $6 - 9$ Å at room tem-

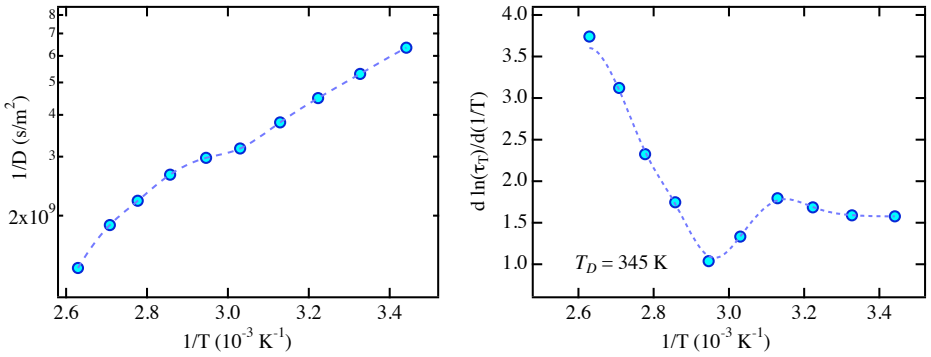

Figure 4.13: Transport property of hydration water - *Left panel*: Arrhenius plot of experimentally extracted $\log(1/D)$ vs $1000/T$ of the protein hydration water shows an evidence of a super-Arrhenius (nonlinear behavior) to Arrhenius (linear behavior) dynamic crossover as the temperature is raised through $T_D = 345 \pm 5$ K. *Right panel*: derivative of the Arrhenius plot, with a minimum coincident with T_d, protein denaturation

perature (13). The sharp changes in both the self-diffusion constant D and the migration distance d indicate a large scale enhanced movement of the water molecules above T_D when the lifetime of the hydrogen bonded network of the water molecules becomes shorter, and thus it is not able to maintain the shape of the protein. The following MD simulation results confirm this dynamic crossover and further show that the dynamic crossover in protein hydration water is probably connected to the first stage of the unfolding process of the protein. The protein backbone RMSD calculated from the trajectories shows a sudden increase between 330 and 340 K (Figure 4.15), signaling the beginning of the denaturation process.

While protein unfolding occurs on time scales of the order of milliseconds, a few nanoseconds are enough to capture at least its dynamic beginning. At the same temperature, the Arrhenius plot of $1/D$ (Figure 4.16) obtained from the MD simulation shows a change in its behavior at $T = 340 \pm 5$ K, reproducing well the neutron scattering data and qualitatively the Adam-Gibbs equation. In particular, the extracted activation energy $E_A = 5.25 \pm 0.5$ kcal/mol is in agreement with the experimental value, $E_A = 5.97 \pm 0.55$ kcal/mol. The underlying physical

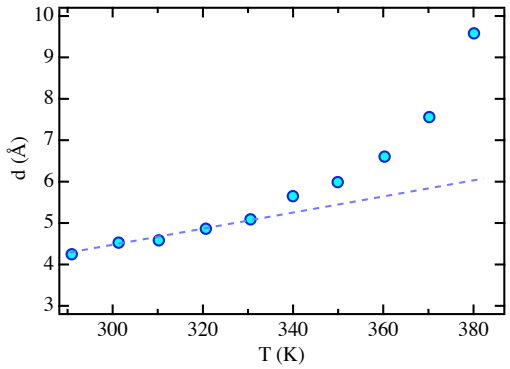

Figure 4.14: Migration distance - Plot of experimentally extracted average migration distance d of the hydration water. This quantity is slowly linearly increasing within experimental error bars below T_D, but rises sharply above T_D, indicating a longer migration of water molecules in between two successive trap sites.

mechanism for lysozyme reversible denaturation can be seen from examination of the following three physical quantities calculated from the MD simulations. Figure 4.17 (upper panel) displays the onset temperature of the reversible denaturation T_d: the protein hydrogen atoms MSD has a sharp increase as a function of temperature between 330 and 340 K in agreement with the onset temperature for reversible denaturation determined by calorimetry (122). Figure 4.17 (middle panel) shows that at the same temperature T_d, the inverse of the water-protein hydrogen bond relaxation time (relaxation rate) deviates from linearity, signaling the beginning of the breakdown of the hydrogen bond network around the protein.

The increase in the hydrogen bond relaxation rate is therefore the cause of the enhanced protein flexibility, as already pointed out for the low temperature protein dynamical transition (143). In that case, there is a correlation between the decrease in protein H-bond network relaxation time (due to the onset of water translational diffusion) and the sudden increase in the protein hydrogen atoms MSD at $T_L = 220$ K. The situation is qualitatively analogous for the high temperature case but with a quantitative difference: the solvent cage is not able to constrain the folded protein structure anymore and the macromolecule increases its ability of sampling the configurational space.

Due to the decrease in the hydrogen bond lifetime, its flexibility becomes large enough to start the unfolding process. Figure 4.17 (lower panel) shows that

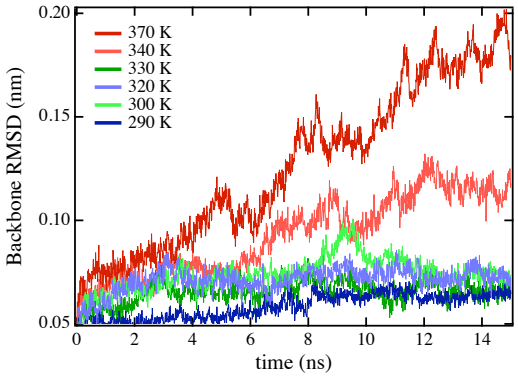

Figure 4.15: Backbone RMSD for different temperatures. - This quantity was calculated for the last 15 ns of the trajectories. No remarkable change is detected until 340 K when the protein increases its flexibility. The simulations are too short to follow the denaturation process, but they are able to capture its beginning.

as T further increases, the number of hydrogen bonds between water and the protein has a sharp change in its rate of decrease at $T_D = 340$ K from 0.3 to 1.2 H-bonds/K. That is to say, the dynamics of interfacial water and its interactions with the protein surface are critical for the stability of protein structure. As soon as the strength of H bonds at the interface between water and protein reaches a threshold value, the two-dimensional network around the protein that kept it folded collapses, allowing the macromolecule to increase its flexibility and to begin the denaturation process.

We believe that the crossover phenomenon is a characteristic of the whole water-protein system: the decreased interaction at the water-protein interface is the cause of both the crossover and the denaturation. On the one hand, water becomes more mobile (increased diffusion constant); on the other, protein is not constrained by the hydrogen bond network and can unfold.

4.4 Summary

In this chapter we examined the dynamics of the system composed of protein and its hydration water. We found that protein dynamics and stability are strongly dependent on their hydration shell, which implies a tight connection between water and the biological function of the biopolymers.

In particular, protein hydration water seems to have two important dynamic transitions in its translational dynamics temperature dependence (Section 1.3.3)

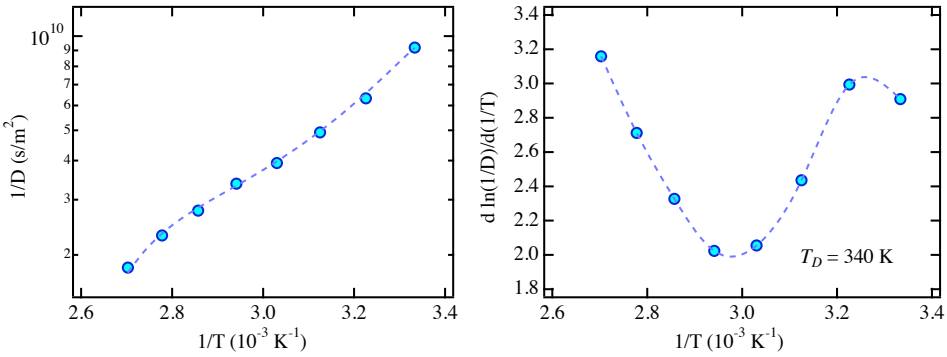

Figure 4.16: Arrhenius plot of the inverse diffusion constant at high T - *Left panel*: Arrhenius plot of the inverse diffusion constant for lysozyme hydration water, $1/D$ vs $1000/T$, calculated from MD simulations. The curve shows an Arrhenius (high T) to super-Arrhenius (low T) dynamic crossover similar to the one observed by quasielastic neutron scattering (see Figure 4.13). The diffusion constant has been calculated from the trajectories according to the Einstein relation with a linear fit of water MSD from 300 to 600 ps. *Right panel*: derivative of the Arrhenius plot, it shows a minimum at $T_D = 340$ K in agreement with experiments.

that border the ability of the protein to carry on its function. Starting from physiological temperature, one is encountered upon *cooling* in correspondence to the so-called protein glass transition (at $T_L = 225$ K, Section 4.2) and the other one upon *heating* in coincidence with the protein reversible denaturation (at $T_D = 340$ K, Section 4.3).

Protein is known to need a precise balance between *stability* and *flexibility* in order to work. While this is provided in the pretty wide temperature range 225 K $< T <$ 340 K, stability is too enhanced below 225 K, when the extended hydrogen bond network of hydration water becomes extremely structured, and flexibility is too enhanced above 340 K, when the network breaks down.

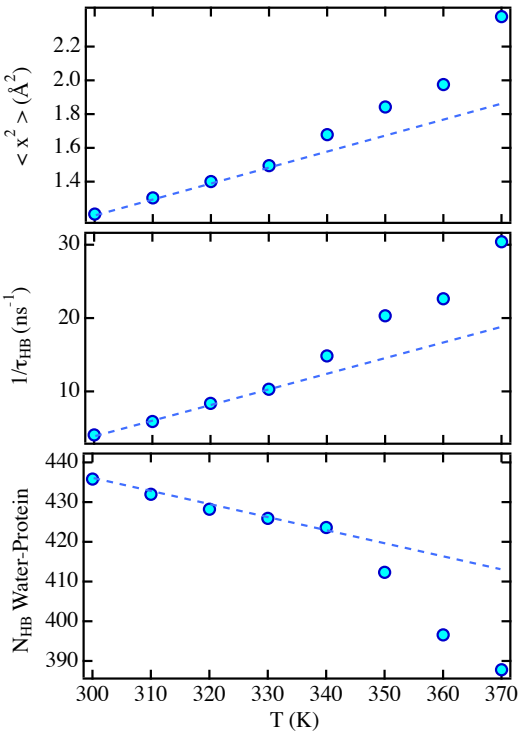

Figure 4.17: Water-Protein coupling - *Upper Panel*: Protein hydrogen atom mean square displacement $\langle x^2 \rangle$ calculated from MD simulations at 500 ps and averaged over the time origins for the last 10 ns of each simulation. *Middle Panel*: Relaxation rate (inverse of the hydrogen bond relaxation time) calculated from the $1/e$ value of the corresponding time correlation function. Only the hydrogen bonds between water molecules and protein were considered. *Lower Panel*: Number of hydrogen bonds between water molecules and protein as a function of temperature calculated averaging over the last 10 ns of the trajectories ($r = 3.5$ Å, $\theta = 30°$).

5

Conclusion

Please, be good enough to put your conclusions on one sheet of paper,
in the very beginning of your report
Winston Churchill

We investigate the rich dynamics of two complex liquid systems (Chapter 1): water and proteins. The importance of this study is implicit in the fundamental biological role of proteins: their function depends on their ability to sample the energy landscape, and if their dynamics is inhibited they are not able to work. Understanding their relaxations is therefore necessary to relate structure to function. Moreover, the strong coupling proteins have with the environment makes the biomolecules extremely sensitive to the dynamics of their biological solvent, water. We used the ideal tools for this investigations: molecular dynamics simulations and neutron scattering. The best experimental reference for the former is the latter, since both methods cover the same time and space domains (approximately 0.1 fs -100 ns, and 1 - 100 Å), and neutrons see the atomic nuclei (which are the basic objects in MD simulations). Once agreement between simulated and experimental spectra is found, the simulated trajectories can be analyzed in detail and information not accessible to experiments can be extracted from simulations. This approach is particularly useful for the study of complex molecular systems, such as biological macromolecules (80).

We approach this problem studying first the dynamics of pure water (Chapter 2). We observed a dynamic transition in deeply supercooled water, at $T_L = 225 \pm 5$ K. In order to reach this temperature avoiding crystallization, we confined water in a wide variety of systems (1-D confinement in cylindrical nanopores of MCM, 2-D confinement around biomolecules and 3-D confinement in interconnected networks of cured cement pastes). This phenomenon seems to be fairly independent on the dimensionality of the confinement, and is present in simulations of supercooled bulk water as well. In order to extract the dynamic transition temperature we i) took the derivative of the Arrhenius plot of the translational relaxation time of water molecules, ii) constructed experimentally the dynamic susceptibility $\chi_T(t)$. Both methods agree in evaluating $T_L \sim 225$ K. The dynamic crossover temperature T_L could be interpreted as a variant of the kinetic glass transition temperature T_c predicted by the idealized MCT (iMCT, Appendix A.1). iMCT breaks down below T_L, since the structural arrest transition is avoided by activated hopping processes below T_L. Indeed, by treating hopping as arising from the vibrational fluctuations in a quasi-arrested state, an extended version of the MCT (eMCT) shows that the ergodic to nonergodic transition is replaced by a smooth crossover (Appendix A.3). Furthermore, eMCT also demonstrates the growing of the dynamic length scales when approaching T_c. These two predictions were experimentally verified in this thesis. Below $T_c \sim T_L$, any structural relaxation requires a cooperative rearrangement of a large cluster of water molecules connected through hydrogen bonds. In conclusion, while T_g has just a conventional definition and T_c corresponds to an event that does not happen, T_L seems to be a better candidate to describe the slow dynamics of supercooled liquids.

Then we analyzed the dynamics of hydrated protein over the whole time range (Chapter 3), from the (i) fast phonons ($t < 1$ ps), to the (ii) exotic logarithmic decay (1 ps $< t <$ 1 ns), to the (iii) slow α relaxation ($t >$ 1 ns). (i) we observe (Section 3.2) a well-defined dispersion relation of intra-protein phonon-like excitations. We identify a significant temperature dependence of the slowing-down and an increase in population of phonon-like collective motions, in an intermediate q-range above the dynamic transition temperature T_l of the protein. We believe that these phonon-like modes are the result of the collective vibrational motions

of the atoms in the α-helices and β-sheets. Below T_l the vibrational frequency is too high and the population of the modes is too low to be able to facilitate the biological function. That is the reason why proteins are not good enzymes below the dynamic transition temperature. (ii) we demonstrated (Section 3.3) that the β relaxation of globular protein single-particle dynamics follows a logarithmic decay. Protein $\phi_q(t)$ can be fitted from 1 ps to their complete decay with a function consisted of the product of two terms: a logarithmic expansion derived from the mode-coupling theory (β relaxation) and a simple exponential function (α relaxation). The q-dependence of the parameters involved in the β relaxation agrees with the predictions of MCT scaling form in the temperature range 280 - 340 K, for the case of a proximity to a higher-order singularity (Appendix A.2). The temperature dependence of the β-relaxation time extracted from fitting the logarithmic decay appears to be Arrhenius over the whole temperature range investigated, 220 - 340 K. (iii) we were able to extract (Section 3.4) the diffusion constant for the protein amino-acid residues: in the temperature range 270 - 350 K, the Arrhenius plot of lysozyme powder diffusion constant can be fitted either with a VFT law or with a power law (fragile behavior). Mapping the protein dynamics onto the dynamics of a short-ranged attractive colloidal system reinforces the analogy between globular proteins and glass-forming liquids, and adds a piece to the puzzle of the interplay between the dynamics and the biological function of biomolecules.

Finally (Chapter 4) we examined the dynamics of the coupled system composed of protein and its hydration water. We found that protein dynamics and stability are strongly dependent on their hydration shell, which implies a tight connection between water and the biological function of the biopolymers. In particular, protein hydration water seems to have two important dynamic transitions in the temperature dependence of its translational dynamics (Section 1.3.3) that border the ability of the protein to carry on its function. Starting from physiological temperature, one is encountered upon *cooling* in correspondence to the so-called protein glass transition (at $T_L = 225$K, Section 4.2) and the other one upon *heating* in coincidence with the protein reversible denaturation (at $T_D = 340$ K, Section 4.3). Protein is known to need a precise balance between *stability* and

flexibility in order to work. While this is provided in the pretty wide temperature range 225 K $< T <$ 340 K, stability is too enhanced below 225 K, when the extended hydrogen bond network of hydration water becomes extremely structured, and flexibility is too enhanced above 340 K, when the network breaks down.

Appendix A

Liquid Theories

A.1 The ideal mode-coupling approach

The most successful approach to the glass transition is the *mode-coupling theory* (MCT), which dates back to the mid-1980s and has been developed since then mainly by Götze and coworkers (61; 125). MCT has been shown to be capable to interpret in a quantitative way, to a 0.2 level of accuracy, experimental data close to a supercooled liquid-glass transition. In the MCT the input static quantity is the wave vector q-dependent static structure factor S_q, which reflects the average structure on the scale of the intermolecular distance. But contrary to critical phenomena, close to the glass transition there is no static singularity leading to a diverging correlation length and to the Ornstein-Zernike anomaly of the structure factor. MCT predicts only a kinetic singularity in the evolution equations, which leads to an ergodic to non-ergodic transition characterized by the non-vanishing of the long time limit of the density correlation functions.

MCT assumes that coupled density fluctuations control the dynamics of the liquid, which leads to a dramatic slowing down of the relevant relaxation times in the supercooled regime. This mechanism of increasing the viscosity by nonlinear coupling of density fluctuations induces structural arrest, when a critical temperature T_c is reached. T_c specifies a true singularity, involving critical fluctuations in contrast to the calorimetric glass temperature or T_0 in the VFT law (Equation 1.11). Across the critical temperature T_c, the structure factor S_q changes

smoothly, while a discontinuous change results for the long-time value of the density correlation function from zero. The diffusion process in supercooled liquids can be visualized as a damped harmonic oscillator (DHO) equation for the density correlation function $\phi_q(t)$, with oscillator frequency ω_q^2. For Newtonian dynamics, the evolution equations read

$$\frac{\partial^2}{\partial^2 t}\phi_q(t) = -\omega_q^2\phi_q(t) - \int_0^t m_q(t-t')\frac{\partial}{\partial t'}\phi_q(t')\,dt' \tag{A.1}$$

with initial conditions $\phi_q(0) = 1$ and $\partial\phi_q(0)/\partial t = 0$. Here $\omega_q^2 \equiv q^2/(m\beta S_q)$ are characteristic frequencies, with $\beta = 1/k_B T$, where T is the temperature and k_B the Boltzmann constant. The kernels $m_q(t)$ are expressed in terms of correlators of the fluctuating forces.

The glass transition predicted by MCT is obtained solving the $t \to \infty$ limit of the equations for the normalized correlators $\phi_q(t)$, the so-called non-ergodicity factor f_q

$$f_q = \lim_{t\to+\infty} \phi_q(t) \tag{A.2}$$

The equations have the form

$$\lim_{t\to+\infty} m_q(t) = \frac{f_q}{1-f_q} \tag{A.3}$$

The solution to these equations admits not only the usual trivial solution $f_q = 0$ but also solutions with $f_q \neq 0$. The value of f_q at the transition point is denoted f_q^c. In MCT language, the transition is called a type B transition when f_q grows discontinuously on entering in the non-ergodic phase, and type A transition when f_q grows continuously from zero. A non-zero f_q implies that a complete relaxation of density fluctuations cannot not occur, which is equivalent to saying that the system cannot reach dynamic equilibrium.

The theory accounts also for so-called higher-order singularities related to bifurcation theory (named A_3 and A_4, see next section), whose realization requires a fine tuning of the interparticle potential parameters. The A_3 bifurcation is the end point of a type B transition. The existence of a singularity of purely kinetic

origin (i.e. not related to any thermodynamic singularity) is the most important prediction of the theory. The physical interpretation of the non-ergodicity transition is related to the well-known cage effect, the difficulty of a particle to move due to the crowd of the surrounding ones. Motion of the particle can only take place if a collective rearrangement of the particles forming the cage opens up a passage for the arrested particles.

One of the merits of MCT is to identify the universal features of the temporal decay of density correlators in terms of asymptotic power laws of approach to the ideal glass transition. In order to properly define the asymptotic laws, it is preliminarily necessary to define a parameter ϵ which quantifies, in terms of a control parameter x, the distance from the kinetic transition at x_c

$$\epsilon = \frac{x - x_c}{x_c} \tag{A.4}$$

It is usually related to the fractional distance from the transition expressed in terms of volume fraction ($x = \phi$) or temperature ($x = 1/T$). A convenient way of describing the universal characteristics of the decay is to introduce its relevant time scales and the behavior of the time correlators in the various time ranges, namely:

(i) The β-relaxation region corresponding to the decay toward a plateau f_q^c and the further decay below the plateau when $\epsilon < 0$, while there is ergodicity breaking for $\epsilon > 0$. In the vicinity of the plateau MCT proposes a general expression for the density correlators of the form

$$\phi_q(t) = f_q^c + h_q \sqrt{\epsilon} g_\pm \left(\frac{t}{\tau(\epsilon)} \right) \tag{A.5}$$

where the subscript in $g_\pm$ corresponds to the sign of ϵ, which goes under the name of factorization property, since the space and time dependencies separate, and scales with the characteristic time $\tau(\epsilon)$

$$\tau(\epsilon) = \tau_0 |\epsilon|^{-1/(2a)} \tag{A.6}$$

which in turn scales with an exponent related to the quantity a. The nonergodicity factor f_q^c, the critical amplitude h_q and the β-correlator $g_\pm$, are independent from ϵ. Given a particular system, $g_\pm$ is a function which can be determined knowing n and the interparticle potential, which determines the structure factor S_q. The leading behavior of the function $g_\pm$ above or below the non-ergodicity plateau is given by the power-law in time valid for $t/\tau(\epsilon) \ll 1$

$$g_+(t/\tau) \sim (t/\tau)^{-a} \tag{A.7}$$

with $0 < a \leq 1/2$, while for $t/\tau \gg 1$ the well-known von Schweidler law is valid, with

$$g_-(t/\tau) \sim -(t/\tau)^{b} \tag{A.8}$$

and $0 < b \leq 1$. It is possible to relate both exponents a and b through the following relation involving the Euler Γ function[1]

$$\lambda = \frac{(\Gamma(1-a))^2}{\Gamma(1-2a)} = \frac{(\Gamma(1+b))^2}{\Gamma(1+2b)} \tag{A.9}$$

(ii) The α-decay regime is the last stage of the decay, the cage break-up, and is characterized by a time scale τ^α which diverges on approaching the transition as a power law

$$\tau^\alpha \sim |\epsilon|^{-\gamma} \tag{A.10}$$

where the exponent γ is given by

$$\gamma = \frac{1}{2a} + \frac{1}{2b} \tag{A.11}$$

The time scale τ^α enters the so-called time-temperature superposition relation

$$\phi_q(t) = F_q\left(\frac{t}{\tau^\alpha}\right) \tag{A.12}$$

[1] In mathematics, the Gamma function (represented by the capital Greek letter Γ) is an extension of the factorial function to real and complex numbers. For a complex number z with positive real part, the Gamma function is defined by $\Gamma(z) = \int_0^\infty t^{z-1}e^{-t}\,dt$

where F_q is a master function of the scaled time t/τ^α which allows to draw a master plot of the density correlators. A good approximation of this function is very often given by the stretched exponential function

$$\phi_q(t) = A_q e^{-(t/\tau_q)^{\beta_q}} \tag{A.13}$$

A sketch of the typical shape of the density correlators, highlighting the different time regions described by MCT, is shown in Figure A.1.

Many aspects of the predictions of the ideal MCT have been tested in detail in various systems, both experimentally and using computer simulation, with good results. Many attempts have also been made to improve the ideal MCT and to account for activated hopping processes (Section A.3). Indeed, neglecting activated processes is probably a safe approximation only in the hard sphere case and when excluded volume is the driving force for caging. Activated processes may not be neglected when the attractive part of the interparticle potential plays a significant role in the caging process: ideal MCT predictions for the α-relaxation properly describe only the first three to four orders of magnitude in the slowing down of the dynamics. Depending on the material, the location of the MCT glass line can be very different from the location of the line at which arrest is observed on an experimental time scale (the calorimetric glass transition temperature). A well-recognized limitation of the idealized MCT is the predicted divergence of the α-relaxation time at the critical temperature T_c (also referred to as the *nonergodic transition*) which is not observed in experiments and computer simulations.

A.2 MCT higher-order singularities

In its ideal version (i.e., not including activated hopping events) MCT predicts a sharp transition from an ergodic liquid to a nonergodic arrested state (or *glass*) at a given value x_c of the relevant control parameter x (in practice the volume fraction ϕ or T). When crossing the transition point from the ergodic to the arrested state, the long-time limit of the density-density correlator for wave vector q jumps discontinuously from zero to a finite value f_q^c. In the MCT formalism, the standard liquid-glass transition is of the *fold type* (also denoted as A_2). The

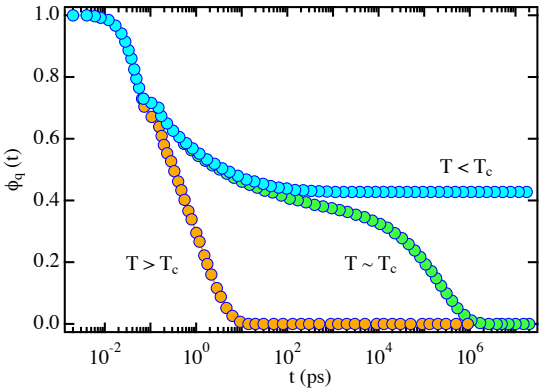

Figure A.1: Ergodic to Nonergodic transition - Three typical density correlators calculated according to the predictions of MCT above, at and below T_c. $\phi_q(t)$ does not decay to 0 below T_c, but to the Debye-Waller factor f_q: the system falls off of equilibrium and it becomes nonergodic

initial part of the α process (von Schweidler regime) is approximated by a power law expansion. But MCT also predicts higher-order transitions, denoted as A_{n+1} and characterized by $\lambda = 1$, which can emerge as the result from the interplay between $n \geq 2$ control parameters $\{x_1, x_2, ..., x_n\}$. Higher-order MCT transitions were initially derived for schematic models and later for short-ranged attractive colloids as a first realization in real systems. Close to a higher-order transition, or more generally to a fold transition with $\lambda \sim 1$, an anomalous relaxation scenario emerges. The mean squared displacement exhibits an intermediate sublinear regime with a decreasing exponent as the transition is approached. In the higher-order MCT scenario, $\phi_q(t)$ does not exhibit a defined plateau. Instead, in an intermediate time interval of several decades, it is approximated by a logarithmic expansion (62),

$$\phi_q(t) \sim f_q - H'_q ln(t/\tau) + H''_q ln^2(t/\tau) \tag{A.14}$$

where the prefactors H'_q and H''_q depend on q and on the distance of the state point $\mathbf{x}_n$ to the transition point $\mathbf{x}_n^c$. It is worthy of remark that a convex-to-concave crossover is present in the higher-order MCT scenario. It is indeed one of its main signatures and differentiates it from other theoretical frameworks for the logarithmic decay. The pure logarithmic decay is also present in the higher-order MCT scenario, which predicts lines in the control parameter space with $H''_q = 0$.

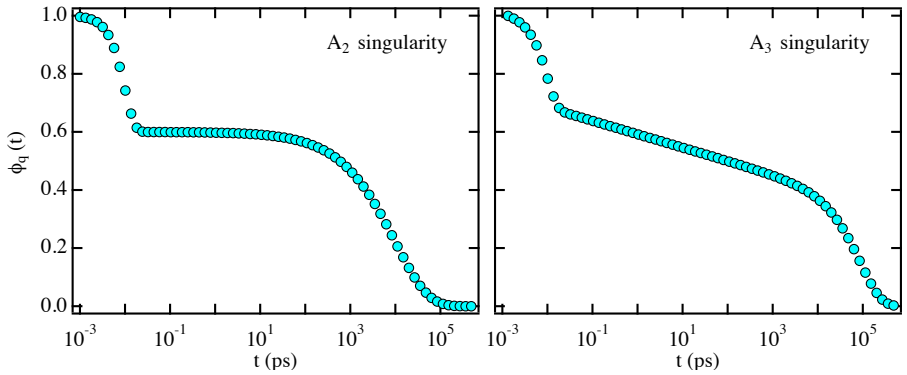

Figure A.2: Comparison between $\mathbf{A}_2$ and $\mathbf{A}_3$ correlators close to the transition - While the density correlators near T_c of a order-2 singularity display a well-defined plateau, the correlators close to a order-3 singularity show a logarithmic decay over several orders of magnitude in time, before decaying exponentially.

The coefficient H_q' factorizes as $H_q' = h_q B(\epsilon)$, where h_q only depends on q, and the q-independent term $B(\epsilon)$ depends on the state point. Hence, the values of H_q' obtained for different state points close to the transition point must be proportional.

Also MCT predictions for the higher-order scenario, the coefficient H_q'' is smaller than H_q', and does not obey scaling. The value of q for which $H_q'' = 0$ is dependent on the state point.

A.3 Extended mode-coupling theory

An extended version of MCT aims at incorporating activated hopping processes which smear out the sharp nonergodic transition and restore ergodicity for $T < T_c$, but its applicability has been restricted to schematic models. This is because of the presence of the subtraction term in the expression for the hopping kernel, which violates the positiveness of any correlation spectrum. Instead, the dynamical-theory approach (36) treats hopping as arising from vibrational fluctuations in the quasiarrested state where particles are trapped inside their cages, and the hopping rate is formulated in terms of the Debye-Waller factors characterizing the structure of the quasiarrested state. The resulting expression for

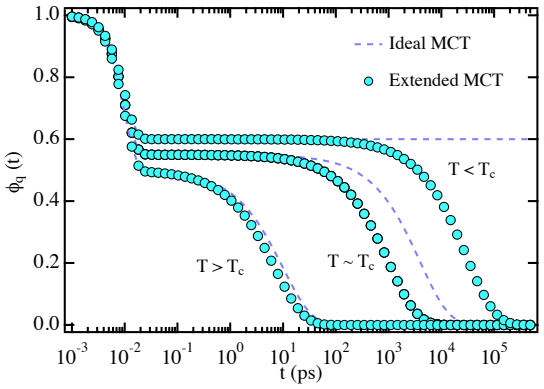

Figure A.3: Comparison between iMCT and eMCT: $\phi_q(t)$ - While the density correlators of ideal MCT (dashed lines) display a well-defined nonergodic transition, the correlators calculated with the extended version of MCT (circles) decay to 0 even for $T < T_c$. Hopping mechanisms restore ergodicity.

the hopping rate takes an activated form, and the barrier height for the hopping is self-generated in the sense that it is present only in those states where the dynamics exhibits a well defined plateau.

It is the factorization approximation that leads to the nonergodic transition at T_c. Therefore, one has to consider corrections, $m_q = m_q^{id} + \Delta m_q$, to go beyond the idealized MCT, which shall be quantified via the hopping kernel defined by $\delta_q = -1/m_q + 1/m_q^{id}$. The correction term reads $\Delta m_q = m_q^{id} m_q \delta_q$, and the memory kernel m_q can be expressed as

$$m_q = \frac{m_q^{id}}{1 - \delta_q m_q^{id}} \tag{A.15}$$

Dropping δ_q, this equation reduces to the one of the idealized MCT: approaching T_c from above, m_q^{id} becomes larger, and so does $\phi_q(t)$, leading to the nonergodic transition at $T = T_c$. In the presence of δ_q, on the other hand, the transition is cutoff. The long-time dynamics of $\phi_q(t)$ in this case is thus determined by δ_q. Thanks to the dynamical theory originally developed to describe diffusion-jump processes in crystals, one can adapt it to glass-forming liquids and treat hopping as arising from vibrational fluctuations (phonons) in the quasi-arrested state where particles are trapped inside their cages. The essential feature of the hopping process is that a jumping atom passes over a barrier formed by neighbors which block a direct passage to the new site. The criterion that

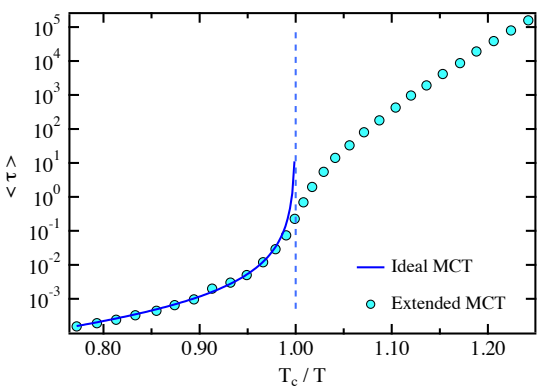

Figure A.4: Comparison between iMCT and eMCT: τ - While the relaxation time of ideal MCT (continuous line) displays a well-defined divergence at T_c, τ calculated with the extended version of MCT (circles) has a smooth crossover at T_c.

determines whether or not a given fluctuation is sufficient to cause a jump is therefore concerned with the relative displacements of the atom and the saddle point.

One arrives at the following expression for the hopping kernel:

$$\delta_q = i\omega_{hop} N_c [1 - \sin(qa)/(qa)]/f_q \tag{A.16}$$

where w_{hop} is the hopping rate, N_c is the coordination number and a is the average interparticle distance.

The density correlators calculated with the extended MCT are shown in Figure A.3, while the correspondent α-relaxation time (calculated graphically, taking the values at which the correlators $\phi_q(t) = 0.1$) is shown in Figure A.4 for a representative q-value. Hopping mechanisms therefore restore ergodicity, avoiding the criticality of iMCT. Figure A.4 is very similar to the relaxation times we extracted in this work (see for example Figures 2.10 and 2.13), so we can conclude that the extended version of the theory is able to reproduce correctly the experimental and numerical results.

A.4 The Adam-Gibbs theory

Adam-Gibbs theory (2) is one of the most widely accepted theories of glass-transition (130). As a matter of fact, the macroscopic equation of this theory

relating the temperature dependence of relaxation time with the configuration entropy is subject of great experimental and theoretical interest. It has been used to describe the relaxation of liquids approaching their glass transitions, and provides an explanation for the variation of diffusion constant D (even in anomalous cases, like SiO_2) and, by implication, the viscosity η. We use the prediction

$$\eta = \eta_0 \exp\left(\frac{A}{TS_{conf}}\right) \tag{A.17}$$

where A is a constant[1]. The configurational entropy of the liquid, $S_{conf} = S_{liquid} - S_{vib}$ is the entropy arising from the degeneracy of the basins the liquid can sample in the energy landscape picture (132). The vibrational component S_{vib} of the entropy is attributable to the thermal excitation the liquid experiences in the basin sampled.

Unfortunately, it is not possible to obtain S_{conf} without full knowledge of the vibrational entropy of the liquid, which is not experimentally accessible. For experimental tests of the Adam-Gibbs equation, the approximation $S_{vib} = S_{crystal}$ has been frequently employed; the approximation assumes that the shapes of the liquid and crystalline basins are identical, which one generally does not expect. Nonetheless, transport data, such as viscosity and dielectric relaxation time, have been linearized over many orders of magnitude using $S_{ex} = S_{liquid} - S_{crystal}$ in Equation A.17.

The excess entropy S_{ex} is related to the excess specific heat by the thermodynamic relation

$$S_{ex}(T) \sim S_{ex}(0) + \int_0^T \frac{C_p^{ex}}{T}\, dT \tag{A.18}$$

This relation requires the temperature dependence of any relaxation process to change sharply when the heat capacity peaks, as demonstrated for water in

[1] The Vogel-Fulcher-Tammann form $\eta = \eta_0 \exp(B/(T - T_0))$ for the temperature dependence of viscosity and characteristic times of liquids at low temperature can be obtained from Equation A.17 by assuming that $C_p^{ex} \sim T^{-1}$. Note that $T_0 < T_g$ is typically associated with an underlying *ideal* glass transition.

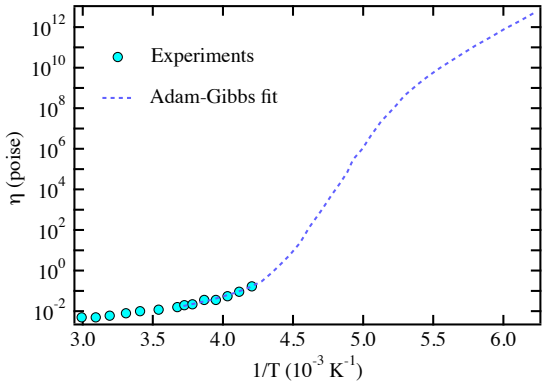

Figure A.5: Adam-Gibbs theory and water dynamic crossover - Fit of water viscosity η using Equation A.17, redrawn from (132). It shows behavior expected for a strong liquid for $T < 220$ K, i.e. Arrhenius behavior with an activation energy $E_A \sim T_g/3$ (in units of kJ/mol).

Figure A.5 (for the specific heat of water, see Figure 2.1). The slope of the Arrhenius plot is in fact predicted to be

$$\frac{d\ln(\eta/\eta_0)}{d(1/T)} = \frac{AC_p^{ex}}{S_{ex}(T)^3} \tag{A.19}$$

Therefore, a dynamic transition in the Arrhenius plot of the translational relaxation time can be explained either with the extended version of MCT or with the Adam-Gibbs equation.

Appendix B

Computer Experiments

B.1 Simulations in physics and chemistry

Simulations are best seen as *computer experiments* that serve as adjuncts to theory and experiments and provide otherwise inaccessible or, not easily accessible microscopic or macroscopic information that theorists and experimentalists can use (116). Experience has shown that even short simulations provide useful guidelines: a review of length and time scales for the most popular simulations are displayed in Figure B.1.

Simulations and experiments. Simulations can be useful in situations in which experiments are impractical (high T or P). Experimental practice rests on a long (occasionally blemished) tradition; computer simulation, because of its novelty, is still somewhat more haphazard, but methodologies are gradually evolving. The output of any simulation should be treated by the same statistical methods used in the analysis of experiments. In addition to estimating the reliability of the results (on the assumption that the measurements have been made correctly) there is also the issue of adequate sampling [1].

[1] In this context, it is of use quoting an episode of *Star Trek: The Next Generation*. The starship Enterprise is damaged and trapped in a debris field. Commander LaForge develops a plan to extricate the ship, but if it fails it would deplete all of the ship's energy resources. Captain Jean Luc Picard instructs Commander La Forge to run a simulation of his proposed plan. The simulation run indicates that his plan would be successful. However Captain Picard orders him: "Run it again". The result of the second run is the opposite, they would not escape

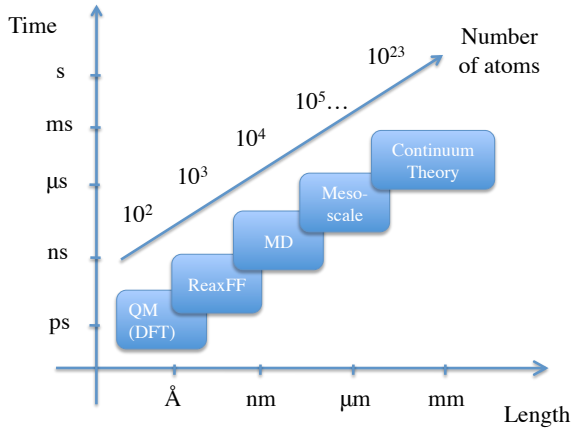

Figure B.1: Simulation techniques in physical chemistry - Systems at different time and length scales are modeled using different simulation techniques, derived from the appropriate governing equations. QM = Quantum Mechanics, DFT = Density Functional Theory, ReaxFF = Reactive Force Field, MD = Molecular Dynamics

Simulations and theory. The question arises as to how simulation is related to physical theory. In the real world, exact solutions are the notable exception. The N-body problem turns out to be insoluble for three or more bodies (117). Statistical mechanics provides a formal description, based on the partition function, of a system in equilibrium; however, with a few notable exceptions, there are no quantitative answers unless severe approximations are introduced, and even then it is necessary to assume large systems. Once out of equilibrium, theory has very little to say: only by means of simulation that progress is possible. Theory therefore relies heavily on approximation, both analytical and numerical, but this is often uncontrolled and so reliability may be difficult to establish. Thus it might be said that simulation rests on the basic theoretical foundations, but tries to avoid much of the approximation normally associated with theory, replacing it by a more elaborate numerical effort. They allow one to go beyond the inevitable simplifications characteristic of theoretical formulations e.g. mean-field approximations, so that the accuracy or acceptability of such approximations can be scrutinized systematically. Where theory and simulation differ is in regard to cost. Theory requires few resources beyond the cerebral and is therefore cheap;

the field. These conflicting results convinced the Captain to seek an alternate plan. The innate variability of the system results in corresponding variability in any system output.

simulation needs the hardware and, despite plummeting prices, a computer system for tackling problems at the forefront of any field can still prove costly.

Simulations and computer science. What distinguishes computer simulation in general from other forms of computation, is the manner in which the computer is used: instead of merely performing a calculation, the computer becomes the virtual laboratory in which a system is studied, a numerical experiment. The analogy can be carried even further; the results emerging from a simulation may be entirely unexpected, in that they may not be at all apparent from the original formulation of the model. A wide variety of modeling techniques have been developed over the years, and those relevant for work at the molecular level include, in addition to Molecular Dynamics, classical Monte Carlo, quantum based techniques involving path-integral and Monte Carlo methods, and MD combined with electron density-function theory, as well as discrete approaches such as cellular automata and the lattice-Boltzmann method.

B.2 Molecular dynamics simulations

The theoretical basis for MD embodies many of the important results produced by the great names of analytical mechanics - Euler, Hamilton, Lagrange, Newton. The simplest form of MD, that of structureless particles, involves little more than Newton's second law. Rigid molecules require the use of the Euler equations, perhaps expressed in terms of Hamiltons quaternions. Molecules with internal degrees of freedom, but that are also subject to structural constraints, might involve the Lagrange method for incorporating geometric constraints into the dynamical equations.

MD simulations solve Newtons equations of motion for a system of N interacting atoms (55):

$$m_i \frac{\partial^2 \mathbf{r}_i}{\partial^2 t} = \mathbf{F}_i \quad i = 1, ..., N \tag{B.1}$$

The forces are the negative derivatives of a potential function $V(\mathbf{r}_1, \mathbf{r}_2, ..., \mathbf{r}_N)$:

$$\mathbf{F}_i = -\frac{\partial V}{\partial \mathbf{r}_i} \tag{B.2}$$

The equations are solved simultaneously in small time steps. The system is followed for some time, taking care that the temperature and pressure remain at the required values, and the coordinates are written to an output file at regular intervals. The coordinates as a function of time represent a trajectory of the system. After initial changes, the system will usually reach an equilibrium state. By averaging over an equilibrium trajectory many macroscopic properties can be extracted from the output file. Given the modeling capability of MD and the variety of techniques that have emerged, what kinds of problem can be studied? Certain applications can be eliminated, owing to the classical nature of MD and to the hardware imposed limitations. Liquids represent the state of matter most frequently studied by MD methods. This is due to historical reasons, since both solids and gases have well-developed theoretical foundations, but there is no general theory of liquids. For solids, theory begins by assuming that the atomic constituents undergo small oscillations about fixed lattice positions; for gases, independent atoms are assumed and interactions are introduced as weak perturbations. In the case of liquids, however, the interactions are as important as in the solid state, but there is no underlying ordered structure to begin with. The following list includes an assortment of ways in which MD simulation is used:

- Fundamental studies: equilibration, tests of molecular chaos, kinetic theory, diffusion, transport properties, size dependence, tests of models and potential functions.

- Phase transitions: first- and second-order, phase coexistence, order parameters, critical phenomena.

- Collective behavior: decay of space and time correlation functions, coupling of translational and rotational motion, vibration, spectroscopic measurements, orientational order, dielectric properties.

- Complex fluids: structure and dynamics of glasses, molecular liquids, pure water and aqueous solutions, liquid crystals, ionic liquids, fluid interfaces, films and monolayers.

- Polymers: chains, rings and branched molecules, equilibrium conformation, relaxation and transport processes.

- Solids: defect formation and migration, fracture, grain boundaries, structural transformations, radiation damage, elastic and plastic mechanical properties, friction, shock waves, molecular crystals, epitaxial growth.

- Biomolecules: structure and dynamics of proteins, protein folding, micelles, membranes, docking of molecules.

- Fluid dynamics: laminar flow, boundary layers, rheology of non-Newtonian fluids, unstable flow.

B.3 Details of the computer experiments

This thesis is based on approximately 100 trajectories, run on 5 different model systems: bulk water, hydrated protein powder (lysozyme and ribonuclease), hydrated protein crystal and single protein in solution. In the bulk water case, the box was composed of 512 TIP4P-Ew water molecules (72). Both lysozyme (protein data bank file 1AKI.pdb, 129 amino acid residues and 1960 atoms) and ribonuclease (7RSA.pdb, 124 residues and 1856 atoms) are globular proteins. All simulations were done at pH = 7, so the amino acids Glu and Asp were taken to be deprotonated while Lys, Arg and His residues were protonated. Lysozyme and RNAse carry therefore a positive charge (+8e and +4e respectively). To achieve electroneutrality, we added an appropriate number of chloride ions. Simulations were performed with a parallel-compiled version of GROMACS 4.0 (70): Lennard-Jones interactions were truncated beyond 14 Å, while electrostatic interactions, calculated with the Particle Mesh Ewald method were truncated at 9 Å. All bonds were constrained at their equilibrium values using the LINear

Constraint Solver algorithm (LINCS, (69)). We now briefly describe the three systems.

Protein Powder. Tarek and Tobias (136) pointed out the poor agreement with experiments of the so-called *cluster model*, composed of a single protein covered by a shell (thin or thick) of water, which lacks the characteristic feature of the powder protein. They found that it produces serious errors and artifacts for any calculated properties. Therefore, we put in a box 2 OPLS-AA (78) lysozyme (or RNAse) molecules randomly oriented and 484 TIP4P-Ew water molecules (456 for RNAse, so that $h \sim 0.3$ for each protein). The final configuration is composed of 5872 atoms in the lysozyme case, and 5544 in the RNAse case. After an energy minimization of 5000 steps with the Steepest Descent algorithm, we equilibrated the system in a NPT ensemble (isobaric-isothermal) for 50 ns at several temperatures. We then performed 12 simulations in the NVT ensemble at different temperatures (from 220 K to 340 K, with 10 K of interval). Simulations were performed using a triclinic cell with periodic boundary conditions and each MD simulation length was 50 ns after the equilibration time. We also ran long trajectories of 1 μs for a few selected temperatures (from 250 to 350 K, with 20 K of interval).

Protein Crystal. We performed simulations on fully hydrated orthorhombic lysozyme crystals. In an orthorhombic crystal, four protein molecules related by the crystallographic symmetry P212121 are placed in the unit cell with $a = 59$ Å, $b = 68$ Å and $c = 30$ Å (73; 93). We repeated the unit cell once along the c direction, for a total of 8 proteins (1 x 1 x 2 lattice). We filled the empty spaces with water, removing the molecules at distance less than 1 Å from the protein surface. The final configuration was composed of 25512 atoms: 8 lysozyme molecules, 2442 water molecules ($h \sim 0.38$) and 64 Cl^- ions (see Figure B.2). After an energy minimization of 5000 steps with the Steepest Descent algorithm, we equilibrated the system in a NPT ensemble for 50 ns at 300 K. We then performed an MD simulations in the NVT ensemble at the same temperature for 50 ns.

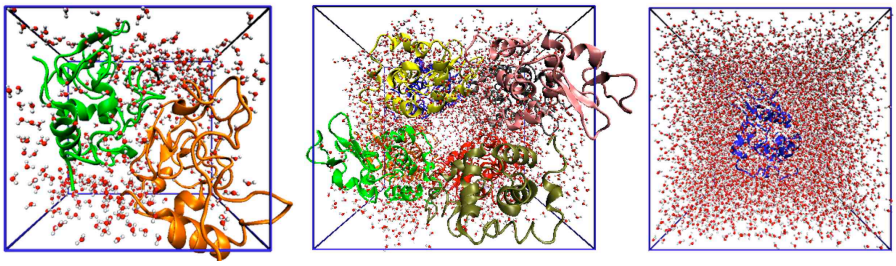

Figure B.2: Simulation boxes - Snapshots from MD simulations at $T = 300$ K for three different models for lysozyme. *Left Panel*: hydrated powder (2 lysozyme molecules, 484 water molecules); *Middle Panel*: hydrated crystal (8 lysozyme molecules, 2442 water molecules); *Right Panel*: protein solution (1 lysozyme molecule, 6448 water molecules)

Protein Solution. A single lysozyme molecule was placed in the center of a cubic box of side 59.3 Å. The box was filled with water, removing the molecules at distance less than 1 Å from the protein surface. The final configuration is composed of 27760 atoms: 1 lysozyme molecule, 6448 water molecules ($h \sim 8.0$) and 8 Cl^- ions (see Figure 2c). After an energy minimization of 5000 steps with the Steepest Descent algorithm, we equilibrated the system in a NPT ensemble (isobaric-isothermal) for 50 ns at 300 K. We then performed an MD simulation in the NVT ensemble at the same temperature for 50 ns.

For each run, we calculated the self-intermediate scattering functions ($\phi_q(t)$, or density autocorrelation functions, Section 1.2). These are defined as:

$$\phi_q(t) = \langle \exp[i\mathbf{q} \cdot (\mathbf{r}_i(t) - \mathbf{r}_i(0)] \rangle \tag{B.3}$$

where $\mathbf{q}$ is the wave vector, $\mathbf{r}_i$ is the position vector of particle i and the angle brackets denote an average over time origins and particles. Our choice for the particles was the center-of-mass (CM) of each amino acid residue: the results do not change qualitatively if one chooses all the atoms of the protein or just one type (hydrogens, carbons, oxygens), but the CM have the advantage of excluding rotations from the analysis. Moreover, we were only interested in the motions of the protein interior, not whole-molecule translations and rotations. While the

latter kinds of motion are small in the powder and the crystal model due to the close packing, they become more relevant for the solution case. To remove it, we subtracted the 6 whole-molecule degrees of freedom during the analysis of the trajectory for the protein solution case.

Appendix C

Published Papers

I herewith declare that I have produced this thesis without the prohibited assistance of third parties and without making use of aids other than those specified; notions taken over directly or indirectly from other sources have been identified as such. The main document has been compiled with LaTeX. All the figures reported here are original and produced with the following software: Igor, PowerPoint, Visual Molecular Dynamics, Cheetah3D, Adobe Illustrator, GraphClick. This thesis has not previously been presented in identical or similar form to any other Italian or foreign examination board.

The thesis work was conducted from January 1st, 2007 to December 31st, 2009 under the supervision of Prof. Piero Baglioni at the University of Florence, Department of Chemistry and CSGI. Within this period, the thesis work was conducted from July 1st, 2007 to December 31st, 2008 under the supervision of Prof. Sow-Hsin Chen at the Massachusetts Institute of Technology, Department of Nuclear Science and Engineering.

This thesis is loosely based on the following 14 co-published papers by the author.

C.1 Specific Anion Effects on the Optical Rotation of α-Amino Acids

Authors: Simona Rossi and Pierandrea Lo Nostro and Marco Lagi and Barry W Ninham and Piero Baglioni

Journal: Journal of Physical Chemistry B

Abstract: Changes in optical rotation of some alpha-amino acids are induced by electrolytes. Such effects on L- and D-enantiomers of a range of amino acids are explored for sodium salts with varying anion. The amino acids studied were alanine, aspartic acid, glutamic acid, glutamine, proline, threonine, and tryptophan. The anion's polarizability in solution accounts for the change in α only for the halides. Self-association of amino acids in solution and pH changes due to the presence of the electrolytes do not account for the observed variations in optical activity. Specific interactions of anions with the chiral amino acids (Hofmeister effects) and salt-induced perturbations of the amino acid hydration shell appear to be responsible for the effects, and conformational changes in the chiral solutes due to the presence of ionic species are discussed.

Pages: 10510–10519

Volume: 111

Year: 2007

Reference: Rossi, S.; Lo Nostro, P.; Lagi, M.; Ninham, B.W. and Baglioni, P. (2007) Specific Anion Effects on the Optical Rotation of α-Amino Acids *J. Phys. Chem. B* **111**, 10510–10519.

C.2 Organogels from a Vitamin C-based Surfactant

Authors: Pierandrea Lo Nostro and Roland Ramsch and Emiliano Fratini and Marco Lagi and Francesca Ridi and Emiliano Carretti and Moira Ambrosi and Barry W Ninham and Piero Baglioni

Journal: Journal of Physical Chemistry B

Abstract: A new double chained surfactant, 2-octyl-dodecanoyl-6-O-ascorbic. acid (8ASC10), with a L-ascorbic acid unit as the polar headgroup was synthesized for the first time. The behavior of the compound in the dry solid state has been characterized through DSC, XRD, and SAXS measurements. The surfactant forms stable viscous organogels in the presence of suitable organic solvents and also water-induced organogels upon addition of water to the organogel. These mixtures show shear-thinning properties and are birefringent. The behavior and properties of the organogels have been studied through rheology, DSC, and SAXS experiments. The organogels possess the same antioxidant properties of the original L-ascorbic acid ring and can be used to solubilize and protect valuable organic molecules.

Pages: 11714–11721

Volume: 111

Year: 2007

Reference: Lo Nostro, P.; Ramsch R.; Fratini, E.; Lagi, M.; Ridi, F.; Carretti, E.; Ambrosi, M; Ninham, B.W. and Baglioni, P. (2007) Organogels from a Vitamin C-based Surfactant *J. Phys. Chem. B* **111**, 11714–11721

C.3 The Low-Temperature Dynamic Crossover Phenomenon in Protein Hydration Water: Simulations vs Experiments

Authors: Marco Lagi and Xiangqiang Chu and Chansoo Kim and Francesco Mallamace and Piero Baglioni and Sow-Hsin Chen

Journal: Journal of Physical Chemistry B

Abstract: A Super-Arrhenius to Arrhenius dynamic crossover phenomenon has been observed in the translational α-relaxation time and in the inverse of the self-diffusion constant both experimentally and by simulations for lysozyme hydration water in the temperature range of $T_L = 223 \pm 2$ K. MD simulations are based on a realistic hydrated powder model, which uses the TIP4P-Ew rigid molecular model for the hydration water. The convergence of neutron scattering, nuclear magnetic resonance and molecular dynamics simulations supports the interpretation that this crossover is a result of the gradual evolution of the structure of hydration water from a high-density liquid to a low-density liquid form upon crossing of the Widom line above the possible liquid-liquid critical point of water.

Pages: 1571–1575

Volume: 112

Year: 2008

Reference: Lagi, M.; Chu, X.-C.; Kim, C.; Mallamace, F.; Baglioni, P. and Chen, S.-H. (2008) The Low-Temperature Dynamic Crossover Phenomenon in Protein Hydration Water: Simulations vs Experiments *J. Phys. Chem. B* **112**, 1571-1575

C.4 Collective headgroup conformational transition in twisted micellar superstructures

Authors: Francesca Baldelli Bombelli and Debora Berti and Silvia Milani and Marco Lagi and Pierluigi Barbaro and Goran Karlsson and Astrid Brandt and Piero Baglioni

Journal: Soft Matter

Abstract: We report on a comprehensive structural spectroscopic characterization of 1,2-dilauroyl-phosphatidyl-adenosine (DLPA) micelles in phosphate buffer. The experimental data, supplemented with MD simulations, indicate the presence of two possible states at room T, two different structures that depend on the thermal history of the sample. The twisted superstructures, produced by aging DLPA micelles through intermicellar assembly of locally cylindrical aggregates, collapse upon warming at 35°C, yielding aligned filaments and/or wormlike structures. The initial superstructures cannot be recovered by thermal inversion. The reason for this behaviour is that the thermal activation causes a redistribution of syn-anti conformations of adenosine headgroups, as indicated by spectroscopic results (NMR, CD, FTIR), which is then collectively frozen thanks to molecular constraints.

Pages: 1102–1113

Volume: 4

Year: 2008

Reference: Baldelli Bombelli, F.; Berti, D.; Milani, S.; Lagi, M.; Barbaro, P.; Karlsson, G.; Brandt, A. and Baglioni, P. (2008) Collective headgroup conformational transition in twisted micellar superstructures *Soft Matter* **4**, 1102–1113

C.5 DNA Closed Nanostructures: a Structural and Monte Carlo Simulation Study

Authors: Francesca Baldelli Bombelli and Filippo Gambinossi and Marco Lagi and Debora Berti and Gabriella Caminati and Tom Brown and Francesco Sciortino and Bengt Norden and Piero Baglioni

Journal: Journal of Physical Chemistry B

Abstract: DNA nanoconstructs are obtained in solution by using 6 unique 42-mer DNA oligonucleotides, whose sequences have been designed to form a pseudohexagonal structure. We show that hexagonally shaped nanostructures and their corresponding linear open constructs are formed by self-assembly of the specifically designed linear oligonucleotides. The dynamical characterization of the nanostructure is obtained by dynamic light scattering (DLS). A validation of the LS results is obtained through Monte Carlo (MC) simulations and atomic force microscopy (AFM). In particular, a mesoscale molecular model for DNA is exploited to perform MC simulations and to obtain information about the conformations as well as the conformational flexibility. The structural features obtained by MC and AFM are in good agreement with DLS.

Pages: 15283

Volume: 112

Year: 2008

Reference: Baldelli Bombelli, F.; Gambinossi, F.; Lagi, M.; Berti, D.; Caminati, G.; Brown, T.; Sciortino, F.; Norden, B. and Baglioni, P. (2008) DNA Closed Nanostructures: a Structural and Monte Carlo Simulation Study *J. Phys. Chem. B* **112**, 15283

C.6 Interconnected Networks: Structural and Dynamic Characterization of Aqueous Dispersions of diC$_8$PC

Authors: Pierandrea Lo Nostro and Sergio Murgia and Marco Lagi and Emiliano Fratini and Goran Karlsson and Matt Almgren and Maura Monduzzi and Barry W Ninham and Piero Baglioni

Journal: Journal of Physical Chemistry B

Abstract: Aqueous dispersions of the phospholipid dioctanoylphosphatidylcholine (diC8PC) phase-separate below a cloud-point temperature, depending on lipid concentration. The lower phase is viscous and rich in lipid. The structure and dynamics of this system were explored via cryo-transmission electron microscopy (cryo-TEM), small-angle X-ray scattering (SAXS), and NMR. The lower phase comprises a highly interconnected tridimensional network of worm-like micelles. A molecular mechanism for the phase separation is suggested.

Pages: 12625–12634

Volume: 112

Year: 2008

Reference: Lo Nostro, P.; Murgia, S.; Lagi, M.; Fratini, E.; Karlsson, G.; Almgren, M.; Monduzzi, M.; Ninham, B. and Baglioni, P. (2008) Interconnected Networks: Structural and Dynamic Characterization of Aqueous Dispersions of Dioctanoylphosphatidylcholine *J. Phys. Chem. B* **112**, 12625–12634.

C.7 Studies of phononlike low energy excitations of protein molecules by inelastic x-ray scattering

Authors: Dazhi Liu and Xiangqiang Chu and Marco Lagi and Yang Zhang and Emiliano Fratini and Piero Baglioni and Ahmed Alatas and Ayman Said and Ercan Alp and Sow-Hsin Chen

Journal: Physical Review Letters

Abstract: Molecular dynamics simulations and neutron scattering experiments have shown that many hydrated globular proteins exhibit a universal dynamic transition at $T_D = 220$ K, below which the biological activity of a protein sharply diminishes. We studied the phononlike low-energy excitations of two structurally very different proteins, lysozyme and bovine serum albumin, using inelastic x-ray scattering above and below T_D. We found that the excitation energies of the high-q phonons show a marked softening above T_D. This suggests that the large amplitude motions of wavelengths corresponding to this specific q range are intimately correlated with the increase of biological activities of the proteins.

Pages: 135501

Volume: 101

Year: 2008

Reference: Liu, D.; Chu, X.-Q.; Lagi, M.; Zhang, Y.; Fratini, E.; Baglioni, P.; Alatas, A.; Said, A.; Alp, E. and Chen, S.-H. (2008) Studies of phononlike low energy excitations of protein molecules by inelastic x-ray scattering *Phys. Rev. Lett.* **101**, 135501

C.8 Observation of dynamic crossover and dynamic heterogeneity in hydration water confined in aged cement paste

Authors: Yang Zhang and Marco Lagi and Francesca Ridi and Emiliano Fratini and Piero Baglioni and Sow-Hsin Chen

Journal: Journal of Physics: Condensed Matter

Abstract: High resolution quasi-elastic neutron scattering is used to investigate the slow dynamics of hydration water confined in calcium silicate hydrate gel in an aged cement paste at supercooled temperatures. A super-Arrhenius to Arrhenius dynamic crossover of the average translational relaxation time as a function of the inverse temperature is observed at $T_L = 231 \pm 5$ K, which coincides with a prominent peak in the differential scanning calorimetry cooling scan. The dynamic susceptibility χ_T(t) calculated using the experimentally determined temperature dependence of the self-intermediate scattering function shows direct evidence of the enhanced dynamic fluctuations and the associated growth in size of the dynamic heterogeneity in the confined water on approaching T_L.

Pages: 502101

Volume: 20

Year: 2008

Reference: Zhang, Y.; Lagi, M.; Ridi, F.; Fratini, E.; Baglioni, P. and Chen, S.-H. (2008) Observation of dynamic crossover and dynamic heterogeneity in hydration water confined in aged cement paste *J Phys-Condens Mat* **20**, 502101.

C.9 Observation of high-temperature dynamic crossover in protein hydration water and its relation to reversible denaturation of lysozyme

Authors: Yang Zhang and Marco Lagi and Dazhi Liu and Francesco Mallamace and Emiliano Fratini and Piero Baglioni and Eugene Mamontov and Sow-Hsin Chen

Journal: Journal of Chemical Physics

Abstract: The diffusive dynamics of hydration water in lysozyme is studied by high-resolution incoherent QENS and MD simulations in a temperature range of 290 - 380 K. Two lysozyme samples, the H_2O hydrated and the D_2O hydrated, are measured and the difference of the spectra are used to extract the dynamics of the hydration water. The Arrhenius plot of $1/D$ shows a dynamic crossover from a super-Arrhenius behavior at low temperatures to an Arrhenius behavior at high temperatures bordered at $T_D = 345 \pm 5$ K. We also observe a pronounced increase in the migration distance d of the hydration water molecules above T_D. This dynamic crossover temperature coincides with that of the reversible denaturation of lysozyme determined by specific heat measurements.

Pages: 135101

Volume: 130

Year: 2009

Reference: Zhang, Y.; Lagi, M.; Liu, D.; Mallamace, F.; Fratini, E.; Baglioni, P.; Mamontov, E. and Chen, S.-H. (2009) Observation of high-temperature dynamic crossover in protein hydration water and its relation to reversible denaturation of lysozyme *J. Chem. Phys.* **130**, 135101.

C.10 Dynamic Susceptibility of Supercooled Water and its relation to the Dynamic Crossover Phenomenon

Authors: Yang Zhang and Marco Lagi and Emiliano Fratini and Piero Baglioni and Eugene Mamontov and Sow-Hsin Chen

Journal: Physical Review E

Abstract: We study the dynamic susceptibility $\chi_T(q,t)$ of deeply supercooled water by means of quasielastic neutron scattering and molecular dynamics simulations. Both techniques show an increase in the peak height of $\chi_T(q,t)$ as the temperature is lowered toward the dynamic crossover temperature T_L. Below T_L, the peak height decreases steadily. We attribute this phenomenon to the change in slope of the Arrhenius plot of the translational relaxation time at T_L. In contrast, the peak height of the calculated four-point correlation function $\chi_4(q,t)$ directly related to the size of dynamic heterogeneity, increases toward and below T_L.

Pages: 040201

Volume: 79

Year: 2009

Reference: Zhang, Y.; Lagi, M.; Fratini, E.; Baglioni, P.; Mamontov, E. and Chen, S.-H. (2009) Dynamic Susceptibility of Supercooled Water and its relation to the Dynamic Crossover Phenomenon *Phys. Rev. E* **79**, 040201.

C.11 Absence of the Density Minimum of Supercooled Water in Hydrophobic Confinement

Authors: Yang Zhang and Kao-Hsian Liu and Marco Lagi and Dazhi Liu and Ken Littrell and Chung-Yuan Mou and Sow-Hsin Chen

Journal: Journal of Physical Chemistry B

Abstract: The surface effect on the peculiar dynamic and thermodynamic properties of supercooled water, such as the density, has been puzzling the scientic community for years. Recently, using the small angle neutron scattering method, we were able to measure the density of H_2O conned in the hydrophobic mesoporous material CMK-1-14 from room temperature down to the deeply supercooled temperature 130 K at ambient pressure. We found that the well-known density maximum of water is shifted 17 K lower and, more interestingly, that the previously observed density minimum in hydrophilic connement disappears. Furthermore, the deduced thermal expansion coefficient shows a much broader peak spanning from 240 to 180 K in comparison with the sharp peak at 230 K in hydrophilic confinement. These present results may help in the understanding of the effect of hydrophobic/hydrophilic interfaces on the properties of supercooled confined water.

Pages: 5007

Volume: 113

Year: 2009

Reference: Zhang, Y.; Liu, K.-H.; Lagi, M.; Liu, D.; Littrell, K.; Mou, C.-Y.; Chen, S.-H. (2009) Absence of the Density Minimum of Supercooled Water in Hydrophobic Confinement *J. Phys. Chem. B* **113**, 5007.

C.12 Neutron Scattering Studies of Dynamic Crossover Phenomena in a Coupled System of Biopolymer and Its Hydration Water

Authors: Sow-Hsin Chen and Francesco Mallamace and Xiangqiang Chu and Chansoo Kim and Marco Lagi and Antonio Faraone and Emiliano Fratini and Piero Baglioni

Journal: Journal of Physics: Conference Series

Abstract: We observed a Fragile-to-Strong Dynamic Crossover (FSC) phenomenon of the α-relaxation time and self-diffusion constant in hydration water of three biopolymers: lysozyme, B-DNA and RNA. The mean squared displacement of hydrogen atoms is measured by Elastic Neutron Scattering (ENS) experiments. The α-relaxation time is measured by QENS experiments and the self-diffusion constant by NMR experiments. We discuss the active role of the FSC of the hydration water in initiating the dynamic transition in the biopolymers. Finally, we show an MD simulation of a realistic hydrated powder model of lysozyme and demonstrate the agreement of the MD simulation with the experimental data.

Pages: 012006

Volume: 177

Year: 2009

Reference: Chen, S.-H.; Mallamace, F.; Chu, X.-Q.; Kim, C.; Lagi, M.; Faraone, A.; Fratini, E. and Baglioni, P. (2009) Neutron Scattering Studies of Dynamic Crossover Phenomena in a Coupled System of Biopolymer and Its Hydration Water *J Phys-Conf Series [JPCS]* **177**, 012006.

C.13 Logarithmic decay in single-particle relaxation of hydrated lysozyme powder

Authors: Marco Lagi and Piero Baglioni and Sow-Hsin Chen

Journal: Physical Review Letters

Abstract: We present the self-dynamics of protein amino acids of hydrated lysozyme powder around the physiological temperature by means of molecular dynamics simulations. The self-intermediate scattering functions of the amino acid residue center of mass display a logarithmic decay over 3 decades of time, from 2 ps to 2 ns, followed by an exponential α relaxation. This kind of slow dynamics resembles the relaxation scenario within the β-relaxation time range predicted by mode coupling theory in the vicinity of higher-order singularities. These results suggest a strong analogy between the single-particle dynamics of the protein and the dynamics of colloidal, polymeric, and molecular glass-forming liquids.

Pages: 108102

Volume: 103

Year: 2009

Reference: Lagi, M.; Baglioni, P. and Chen, S.-H. (2009) Logarithmic decay in single-particle relaxation of hydrated lysozyme powder *Phys. Rev. Lett.* **103**, 108102.

C.14 Evidence of dynamic crossover phenomena in water and other glass-forming liquids: experiments, MD simulations and theory

Authors: Sow-Hsin Chen and Yang Zhang and Marco Lagi and Song-Ho Chong and Piero Baglioni and Francesco Mallamace

Journal: Journal of Physics: Condensed Matter

Abstract: In a recent QENS experiment on water confined in cement paste, we find a dynamic crossover phenomenon at $T_L = 227 \pm 5$ K. Its DSC scan shows a peak at the same temperature. We also demonstrate with MD simulations that the dynamic crossover phenomenon is an intrinsic property of bulk water, and not due to the confinement. The extended version of the mode coupling theory (eMCT) shows that, instead of a structural arrest transition at T_c, a fragile-to-strong dynamic crossover phenomenon takes place, confirming both the experimental and the numerical results. We thus demonstrated with experiments, simulations and theory that a genuine change of dynamical behavior of both water and many glassy liquids happens at the crossover temperature T_L , which is 10-30% higher than the calorimetric glass transition temperature T_g.

Pages: 504102

Volume: 21

Year: 2009

Reference: Chen, S.-H.; Zhang, Y.; Lagi, M.; Chong, S.-H. and Mallamace, F. (2009) Evidence of Dynamic Crossover Phenomena in Water and Other Glass-Forming Liquids: Experiments, MD Simulations and Theory *J. Phys.: Cond. Matt.* **21**, 504102.

References

[1] E Abrahams. Nonexponential relaxation and hierarchically constrained dynamics in a protein. *Phys Rev E*, 71(5):051901, 2005. 49

[2] G Adam and J H Gibbs. On the temperature dependence of cooperative relaxation properties in glass-forming liquids. *J Chem Phys*, 43(1):139, 1965. 16, 103

[3] HC Andersen. Molecular dynamics studies of heterogeneous dynamics and dynamic crossover in supercooled atomic liquids. *P Natl Acad Sci Usa*, 102(19):6686–6691, 2005. 5

[4] PW Anderson. Through the glass lightly. *Science*, 267:1616, 1995. 12

[5] CA Angell. Formation of glasses from liquids and biopolymers. *Science*, 267(5206):1924–1935, 1995. 12, 57

[6] CA Angell. Insights into phases of liquid water from study of its unusual glass-forming properties. *Science*, 319(5863):582–587, 2008. 6, 20

[7] A Ansari. Langevin modes analysis of myoglobin. *J Chem Phys*, 110(3):1774–1780, 1999. 59

[8] A Ansari, J Berendzen, SF Bowne, H Frauenfelder, IET Iben, TB Sauke, E Shyamsunder, and RD Young. Protein states and protein quakes. *P Natl Acad Sci Usa*, 82(15):5000–5004, 1985. 39, 57

[9] A Arbe, AC Genix, J Colmenero, D Richter, and P Fouquet. Anomalous relaxation of self-assembled alkyl nanodomains in high-order poly(n-alkyl methacrylates). *Soft Matter*, 4(9):1792–1795, 2008. 49

[10] VA Avetisov, AK Bikulov, and VA Osipov. p-adic description of characteristic relaxation in complex systems. *J Phys A-Math Gen*, 36(15):4239–4246, 2003. 2

[11] P Ballesta, A Duri, and L Cipelletti. Unexpected drop of dynamical heterogeneities in colloidal suspensions approaching the jamming transition. *Nat Phys*, 4(7):550–554, 2008. 36

[12] LD Barron, L Hecht, and G Wilson. The lubricant of life: A proposal that solvent water promotes extremely fast conformational fluctuations in mobile heteropolypeptide structure. *Biochemistry*, 36:13143–13147, 1997. 67

[13] M Bee. Quasielastic neutron scattering. *Adam Hilger, Philadelphia, PA,*, 1988. 71, 86

[14] MC Bellissent-Funel, SH Chen, and JM Zanotti. Single-particle dynamics of water molecules in confined space. *Phys. Rev. E*, 51:4558, 1995. 24

[15] MJ Benham, JC Cook, JC Li, DK Ross, PL Hall, and B Sarkissian. Small-angle neutron scattering study of adsorbed water in porous vycor glass: Supercooling phase transition and interfacial structure. *Phys. Rev. B*, 39:633, 1989. 21

[16] R Bergman and J Swenson. Dynamics of supercooled water in confined geometry. *Nature*, 403:283, 2000. 21

[17] L Berthier, G Biroli, JP Bouchaud, L Cipelletti, DE Masri, D L'Hote, F Ladieu, and M Pierno. Direct experimental evidence of a growing length scale accompanying the glass transition. *Science*, 310(5755):1797–1800, 2005. 15

[18] L Berthier, G Biroli, JP Bouchaud, W Kob, K Miyazaki, and DR Reichman. Spontaneous and induced dynamic fluctuations in glass formers. i. general results and dependence on ensemble and dynamics. *J Chem Phys*, 126(18):184503, 2007. 16, 32

[19] AR Bizzarri and S Cannistraro. Anomalous and anisotropic diffusion of plastocyanin hydration water. *Europhys. Lett.*, 37:201–206, 1997. 68

[20] JP Boon and S Yip. Molecular hydrodynamics. *ed. McGraw Hill, New York*, page 417, 1980. 2, 4

[21] A Botti, F Bruni, A Isopo, MA Ricc, and AK Soper. Experimental determination of the site-site radial distribution functions of supercooled ultrapure bulk water. *J. Chem. Phys.*, 117:6196, 2002. 21

[22] JJ Brey and A Prados. Slow logarithmic relaxation in models with hierarchically constrained dynamics. *Phys Rev E*, 63(2):021108, 2001. 49

[23] G Caliskan, A Kisliuk, and AP Sokolov. Dynamic transition in lysozyme: role of a solvent. *Journal of Non-Crystalline Solids*, 307:868–873, 2002. 69

[24] H Cang, VN Novikov, and MD Fayer. Experimental observation of a nearly logarithmic decay of the orientational correlation function in supercooled liquids on the picosecond-to-nanosecond time scales. *Phys Rev Lett*, 90(19):197401, 2003. 49

[25] H Cang, VN Novikov, and MD Fayer. Logarithmic decay of the orientational correlation function in supercooled liquids on the ps to ns time scale. *J Chem Phys*, 118(6):2800–2807, 2003. 49

[26] TV Chalikian, M Totrov, R Abagyan, and KJ Breslauer. The hydration of globular proteins as derived from volume and compressibility measurements: Cross correlating thermodynamic and structural data. *J. Mol. Biol.*, 260:588, 1996. 58

[27] SH Chen. Quasi-elastic and inelastic neutron-scattering and molecular-dynamics of water at supercooled temperature. *NATO Adv. St. Inst. Hydr.-Bonded Liq.*, 329:289–332, 1991. 22

[28] SH Chen, WR Chen, and F Mallamace. The glass-to-glass transition and its end point in a copolymer micellar system. *Science*, 300(5619):619–622, 2003. 49

[29] SH Chen and M Kotlarchyk. Interactions of photons and neutrons with matter. *World Scientific Publishing Co.*, 2007. 70

[30] SH Chen, C Liao, F Sciortino, P Gallo, and P Tartaglia. Molecular-dynamics study of incoherent quasielastic neutron-scattering spectra of supercooled water. *Phys. Rev. E*, 24:6708, 1999. 24, 83

[31] SH Chen, L Liu, E Fratini, P Baglioni, A Faraone, and E Mamontov. Observation of fragile-to-strong dynamic crossover in protein hydration water. *P Natl Acad Sci Usa*, 103(24):9012–9016, 2006. 18, 22, 71

[32] SH Chen, F Mallamace, XQ Chu, C Kim, and M Lagi. Neutron scattering studies of dynamic crossover phenomena in a coupled system of biopolymer and its hydration water. *Journal of Physics: Conference Series*, 177:012006, 2009. 71

[33] SH Chen, F Mallamace, CY Mou, M Broccio, C Corsaro, A Faraone, and L Liu. The violation of the stokes-einstein relation in supercooled water. *P Natl Acad Sci Usa*, 103(35):12974–12978, 2006. 37

[34] SH Chen, J Teixeira, and R Nicklow. Incoherent quasi-elastic neutron-scattering from water in supercooled regime. *Phys. Rev. A*, 26:3477, 1982. 82

[35] X Cheng and BP Schoenborn. Hydration in protein crystals. a neutron diffraction analysis of carbonmonoxymyoglobin. *Acta Cryst.*, B46:195–208, 1990. 67

[36] SH Chong. Connections of activated hopping processes with the breakdown of the stokes-einstein relation and with aspects of dynamical heterogeneities. *Phys Rev E*, 78(4):041501, 2008. 101

[37] SH Chong and M Fuchs. Mode-coupling theory for structural and conformational dynamics of polymer melts. *Phys Rev Lett*, 88(18):185702, 2002. 63

[38] XQ Chu, A Faraone, C Kim, E Fratini, P Baglioni, JB Leao, and SH Chen. Proteins remain soft at lower temperatures under pressure. *J. Phys. Chem B*, 113:5001, 2009. 72

[39] RM Daniel, JC Smith, M Ferrand, S Hery, R Dunn, and JL Finney. Enzyme activity below the dynamical transition at 220 k. *Biophys. J.*, 75:2504–2507, 1998. 69

[40] S Dellerue, AJ Petrescu, JC Smith, and MC Bellissent-Funel. Radially softening diffusive motions in a globular protein. *Biophys J*, 81(3):1666–1676, 2001. 59

[41] LA Deschenes and DA Vanden Bout. Single-molecule studies of heterogeneous dynamics in polymer melts near the glass transition. *Science*, 292:255, 2001. 15

[42] F D'Orazio, S Bhattacharja, WP Halperin, K Eguchi, and T Mizusaki. Molecular diffusion and nuclear-magnetic-resonance relaxation of water in unsaturated porous silica glass. *Phys. Rev. B*, 42:9810, 1990. 21

[43] W Doster. The dynamical transition of proteins, concepts and misconceptions. *Eur Biophys J Biophy*, 37(5):591–602, 2008. 52

[44] W Doster. The protein-solvent glass transition. *BBA-Proteins and Proteomics*, 2009. 69

[45] W Doster, A Bachleitner, R Dunau, M Hiebl, and E Luscher. Thermal-properties of water in myoglobin crystals and solutions at subzero temperatures. *Biophys J.*, 50:213, 1986. 69

[46] W Doster, S Cusack, and W Petry. Dynamic instability of liquid-like motions in a globular protein observed by inelastic neutron-scattering. *Phys Rev Lett*, 65(8):1080–1083, 1990. 49, 59, 68

[47] W Doster and M Settles. The dynamical transition in proteins: The role of hydrogen bonds. in hydration processes in biology: Experimental and theoretical approaches. *ed. IOS Press, Amsterdam.*, pages 177–191, 1999. 67, 68

[48] MD Ediger. Spatially heterogeneous dynamics in supercooled liquids. *Annu Rev Phys Chem*, 51:99–128, 2000. 15

[49] P Etchegoin. Glassylike low-frequency dynamics of globular proteins. *Phys Rev E*, 58(1):845–848, 1998. 46, 58

[50] A Faraone, L Liu, CY Mou, CW Yen, and SH Chen. Fragile-to-strong liquid transition in deeply supercooled confined water. *J Chem Phys*, 121(22):10843–10846, 2004. 22, 25, 26

[51] PW Fenimore, H Frauenfelder, BH McMahon, and RD Young. Proteins are paradigms of stochastic complexity. *Physica A*, 351(1):1–13, 2005. 58

[52] F Franks. Protein stability: the value of 'old literature'. *Biophys Chem*, 96(2-3):117–127, 2002. 65

[53] H Frauenfelder, G Chen, J Berendzen, PW Fenimore, H Jansson, BH McMahon, IR Stroe, J Swenson, and RD Young. A unified model of protein dynamics. *P Natl Acad Sci Usa*, 106(13):5129–5134, 2009. 58, 61

[54] H Frauenfelder, P W Fenimore, and RD Young. Protein dynamics and function: Insights from the energy landscape and solvent slaving. *Iubmb Life*, 59(8-9):506–512, 2007. 40, 41, 42, 57

[55] D Frenkel and B Smit. Understanding molecular simulation: from algorithms to applications. *ed. Elsevier Science Technology Books*, page 638, 2002. 109

[56] P Gallo, F Sciortino, P Tartaglia, and SH Chen. Slow dynamics of water molecules in supercooled states. *Phys Rev Lett*, 76(15):2730–2733, 1996. 24

[57] JM Garciaruiz, A Moreno, A Parraga, and M Coll. Shaped protein single-crystals. *Acta Crystallogr. Sect. D-Biol. Crystallogr.*, 51:278–281, 1995. 75

[58] N Giovambattista, MG Mazza, S. V Buldyrev, FW Starr, and H. E Stanley. Dynamic heterogeneities in supercooled water. *J Phys Chem B*, 108(21):6655–6662, 2004. 16

[59] W Goetze and L Sjogren. Relaxation processes in supercooled liquids. *Reports on Progress in Physics*, 55:241, 1992. 20

[60] VI Goldanskii and YF Krupyanskii. Protein and protein-bound water dynamics studied by raleigh scattering of mossbauer radiation (rsmr). *Quart. Rev. Biophys.*, 22:39–92, 1989. 67

[61] W Götze. Complex dynamics of glass-forming liquids: A mode-coupling theory. *ed. Oxford University Press*, 2009. 95

[62] W Götze and M Sperl. Logarithmic relaxation in glass-forming systems. *Phys Rev E*, 66(1):011405, 2002. 100

[63] JL Green, J Fan, and CA Angell. The protein-class analogy - some insights from homopeptide comparisons. *J Phys Chem-Us*, 98(51):13780–13790, 1994. 57, 80

[64] WM Grundy and B Schmitt. The temperature-dependent near-infrared absorption spectrum of hexagonal h2o ice. *J Geophys Res*, 103:25809, 1998. 30

[65] M Hameed, B Ahmad, KM Fazili, K Andrabi, and RH Khan. Different molten globule-like folding intermediates of hen egg white lysozyme induced by high ph and tertiary butanol. *J. Biochem. (Tokyo)*, 573:141, 2007. 80

[66] JP Hansen and IR McDonald. Theory of simple liquids. *ed. Elsevier*, page 416, 2006. 3

[67] KA Henzler-Wildman and D Kern. Dynamic personalities of proteins. *Nature*, 450(7172):964–972, 2007. 39

[68] KA Henzler-Wildman, M Lei, V Thai, SJ Kerns, M Karplus, and D Kern. A hierarchy of timescales in protein dynamics is linked to enzyme catalysis. *Nature*, 450(7171):913–U27, 2007. 39, 40

[69] B Hess, H Bekker, HJC Berendsen, and JGEM Fraaije. Lincs: A linear constraint solver for molecular simulations. *J Comput Chem*, 18(12):1463–1472, 1997. 112

[70] B Hess, C Kutzner, D Van der Spoel, and E Lindahl. Gromacs 4: Algorithms for highly efficient, load-balanced, and scalable molecular simulation. *J Chem Theory Comput*, 4(3):435–447, 2008. 111

[71] K Hinsen, AJ Petrescu, S Dellerue, MC Bellissent-Funel, and GR Kneller. Liquid-like and solid-like motions in proteins. *J Mol Liq*, 98-9:381–398, 2002. 51

[72] HW Horn, WC Swope, JW Pitera, JD Madura, TJ Dick, GL Hura, and T Head-Gordon. Development of an improved four-site water model for biomolecular simulations: Tip4p-ew. *J Chem Phys*, 120(20):9665–9678, 2004. TIP4P-Ew water model. 34, 111

[73] Z Hu, J Jiang, and SI Sandler. Water in hydrated orthorhombic lysozyme crystal: Insight from atomistic simulations. *J Chem Phys*, 129(7):075105, 2008. 112

[74] K Ito, CT Moynihan, and CA Angell. Thermodynamic determination of fragility in liquids and a fragile-to-strong liquid transition in water. *Nature*, 398(6727):492–495, 1999. 20, 26

[75] HM Jaeger, CH Liu, and SR Nagel. Relaxation at the angle of repose. *Phys Rev Lett*, 62(1):40–43, 1989. 49

[76] HM Jennings. A model for the microstructure of calcium silicate hydrate in cement paste. *Cem Concr Res*, 30:101, 2000. 29

[77] HM Jennings and PD Tennis. Model for the developing microstructure in portland cement pastes. *J Am Ceram Soc*, 77:3161, 1994. 29

[78] WL Jorgensen and J Tirado-Rives. The opls [optimized potentials for liquid simulations] potential functions for proteins, energy minimizations for crystals of cyclic peptides and crambin. *J. Am. Chem. Soc.*, 110(6):1657–1666, 1988. 112

[79] W Kauzmann. Some factors in the interpretation of protein denaturation. *Adv. Protein Chem.*, 14:1, 1959. 65

[80] GR Kneller, K Hinsen, and MC Bellissent-Funel. Molecular dynamics simulation and neutron scattering from proteins. *LLB Sientific Report 2001-2002*, pages 144–145, 2002. 91

[81] R Kohlrausch. Theorie des elektrischen ruckstandes in der leidner flasche. *Poggendorff*, 91:56–82, 1854. 9

[82] P Kumar, Z Yan, LM Xu, MG Mazza, SV Buldyrev, SH Chen, S Sastry, and HE Stanley. Glass transition in biomolecules and the liquid-liquid critical point of water. *Phys Rev Lett*, 97(17):177802, 2006. 74

[83] V Kurkal-Siebert and J C Smith. Low-temperature protein dynamics: A simulation analysis of interprotein vibrations and the boson peak at 150 k. *J Am Chem Soc*, 128(7):2356–2364, 2006. 44

[84] M Lagi, P Baglioni, and SH Chen. Logarithmic decay in single-particle relaxation of hydrated lysozyme powder. *Phys Rev Lett*, 103(10):108102, 2009. 50

[85] M Lagi, XQ Chu, C Kim, F Mallamace, P Baglioni, and SH Chen. The low-temperature dynamic crossover phenomenon in protein hydration water: Simulations vs experiments. *J Phys Chem B*, 112(6):1571–1575, 2008. 53, 74

[86] SH Lee and PJ Rossky. A comparison of the structure and dynamics of liquid water at hydrophobic and hydrophilic surfacesa molecular dynamics simulation study. *J. Chem. Phys.*, 100:3334, 1994. 21

[87] H Leyser, W Doster, and M Diehl. Far-infrared emission by boson peak vibrations in a globular protein. *Phys. Rev. Lett*, 82:2987, 1999. 57

[88] CY Liao and SH Chen. Theory of the generalized dynamic structure factor of polyatomic molecular fluids measured by inelastic x-ray scattering. *Phys Rev E*, 64(2):021205, 2001. 45

[89] D Liu, XQ Chu, M Lagi, Y Zhang, E Fratini, P Baglioni, A Alatas, A Said, E Alp, and SH Chen. Studies of phononlike low-energy excitations of protein molecules by inelastic x-ray scattering. *Phys Rev Lett*, 101(13):135501, 2008. 44

[90] D Liu, Y Zhang, CC Chen, CY Mou, PH Poole, and SH Chen. Observation of the density minimum in deeply supercooled confined water. *P Natl Acad Sci Usa*, 104(23):9570–9574, 2007. 19

[91] L Liu, SH Chen, A Faraone, CW Yen, CY Mou, AI Kolesnikov, E Mamontov, and J Leao. Quasielastic and inelastic neutron scattering investigation of fragile-to-strong crossover in deeply supercooled water confined in nanoporous silica matrices. *J Phys-Condens Mat*, 18(36):S2261–S2284, 2006. 22

[92] Y Liu, SH Chen, D Berti, P Baglioni, A Alatas, H Sinn, E Alp, and A Said. Effects of counterion valency on the damping of phonons propagating along the axial direction of liquid-crystalline dna. *J. Chem. Phys.*, 123:214909, 2005. 47

[93] Kourosh Malek. Solute transport in orthorhombic lysozyme crystals: a molecular simulation study. *Biotechnol Lett*, 29(12):1865–1873, 2007. 112

[94] F Mallamace, SH Chen, M Broccio, C Corsaro, V Crupi, D Majolino, V Venuti, P Baglioni, E Fratini, C Vannucci, and HE Stanley. Role of the

solvent in the dynamical transitions of proteins: The case of the lysozyme-water system. *J Chem Phys*, 127(4):045104, 2007. 80

[95] F Mallamace, C Corsaro, M Broccio, C Branca, N Gonzalez-Segredo, J Spooren, SH Chen, and HE Stanley. Nmr evidence of a sharp change in a measure of local order in deeply supercooled confined water. *Proc. Natl. Acad. Sci. U.S.A.*, 105:12725, 2008. 80

[96] C Masciovecchio, F Bencivenga, and A Gessini. Water dynamics at the nanoscale. *Condensed Matter Physics*, 11(1):47–56, 2008. 8

[97] J Maxwell. On the dynamical theory of gases. *Philosophical transactions of the Royal Society of London*, 157:49–88, 1867. 2

[98] O. V Mazurin. Problems of compatibility of the values of glass transition temperatures published in the world literature. *Glass Phys Chem*, 33(1):22–36, 2007. 10, 11

[99] F Merzel and J C Smith. Is the first hydration shell of lysozyme of higher density than bulk water? *P Natl Acad Sci Usa*, 99(8):5378–5383, 2002. 76

[100] FJ Millero, GK Ward, and P Chetirkin. Partial specific volume, expansibility, compressibility, and heat capacity of aqueous lysozyme solutions. *J. Biol. Chem.*, 251:4001, 1976. 58

[101] G Monaco, A Cunsolo, G Ruocco, and F Sette. Viscoelastic behavior of water in the terahertz-frequency range: An inelastic x-ray scattering study. *Phys. Rev. E*, 60:5505, 1999. 45

[102] Angel J Moreno and J Colmenero. Is there a higher-order mode coupling transition in polymer blends? *J Chem Phys*, 124(18):184906, 2006. 49, 54

[103] Angel J Moreno and J Colmenero. Logarithmic relaxation in a kinetically constrained model. *J Chem Phys*, 125(1):016101, 2006. 49

[104] VN Morozov and S Gevorkian. Low temperature glass transition in proteins. *Biopol*, 24:1785–1799, 1985. 68

[105] Thomas Neusius, Isabella Daidone, Igor M Sokolov, and J C Smith. Subdiffusion in peptides originates from the fractal-like structure of configuration space. *Phys Rev Lett*, 100(18):188103, 2008. 52

[106] P Nordblad, P SvedLindh, L Lundgren, and L Sandlund. Time decay of the remanent magnetization in a cumn spin-glass. *Phys Rev B*, 33(1):645–648, 1986. 49

[107] VN Novikov and AP Sokolov. Universality of the dynamic crossover in glass-forming liquids: A "magic" relaxation time. *Phys Rev E*, 67(3):031507, 2003. 34

[108] G Otting. Nmr studies of water bound to biological molecules. *Prog. NMR Spect.*, 31:259–285, 1997. 68

[109] A Paciaroni, AR Bizzarri, and S Cannistraro. Molecular-dynamics simulation evidences of a boson peak in protein hydration water. *Phys. Rev. E.*, 57:6277–6280, 1998. 68

[110] A Paciaroni, AR Bizzarri, and S Cannistraro. Neutron scattering evidence of a boson peak in protein hydration water. *Phys. Rev. E.*, 60:2476–2479, 1999. 68

[111] RG Palmer, DL Stein, E Abrahams, and PW Anderson. Models of hierarchically constrained dynamics for glassy relaxation. *Phys Rev Lett*, 53(10):958–961, 1984. 10

[112] CF Polnaszek and RG Bryant. Nitroxide radical induced solvent proton relaxation: Measurements of localized translational diffusion. *J. Chem. Phys.*, 81:4038–4045, 1984. 68

[113] PH Poole, F Sciortino, U Essmann, and HE Stanley. Phase behaviour of metastable water. *Nature*, 360:324, 1992. 19

[114] PH Poole, F Sciortino, T Grande, HE Stanley, and CA Angell. Effect of hydrogen bonds on the thermodynamic behavior of liquid water. *Physical Review Letters*, 73:1632, 1994. 20

[115] AM Puertas, M Fuchs, and ME Cates. Comparative simulation study of colloidal gels and glasses. *Phys Rev Lett*, 88(9):098301, 2002. 49

[116] R Rajagopalan. Simulations of self-assembling systems. *Curr Opin Colloid Interf Sci*, 6(4):357–365, 2001. 107

[117] D Rapaport. The art of molecular dynamics simulation. *ed. Cambridge University Press*, 2004. 108

[118] BF Rasmussen, AM Stock, D Ringe, and GA Petsko. Crystalline ribonuclease a loses function below the dynamical transition at 220 k. *Nature*, 357:423–424, 1992. 67, 69

[119] R Richert and HJ Bassler. Dynamics of supercooled melts treated in terms of the random-walk concept. *J. Phys. Cond. Matt.*, 2:2273, 1990. 61

[120] A Rocchi, AR Bizzarri, and S Cannistraro. Water dynamical anomalies evidenced by molecular-dynamics simulations at the solvent-protein interface. *Phys. Rev. E.*, 57:3315–3325, 1998. 68

[121] JA Rupley and G Careri. Protein hydration and function. *Adv Protein Chem*, 41:37–172, 1991. 66, 67

[122] G Salvetti, E Tombari, L Mikheeva, and GP Johari. The endothermic effects during denaturation of lysozyme by temperature modulated calorimetry and an intermediate reaction equilibrium. *J. Phys. Chem. B*, 106:6081, 2002. 80, 81, 87

[123] F Sciortino, L Fabbian, SH Chen, and P Tartaglia. Supercooled water and the kinetic glass transition .2. collective dynamics. *Phys Rev E*, 56(5):5397–5404, 1997. 21

[124] F Sciortino, P Gallo, P Tartaglia, and SH Chen. Supercooled water and the kinetic glass transition. *Phys Rev E*, 54(6):6331–6343, 1996. 21

[125] F Sciortino and P Tartaglia. Glassy colloidal systems. *Adv Phys*, 54(6-7):471–524, 2005. 95

[126] F Sciortino, P Tartaglia, and E Zaccarelli. Evidence of a higher-order singularity in dense short-ranged attractive colloids. *Phys Rev Lett*, 91(26):268301, 2003. 49, 54, 58

[127] KS Singwi and A Sjolander. Diffusive motions in water and cold neutron scattering. *Phys. Rev.*, 119:863, 1960. 82, 83

[128] L Smeller, F Meersman, and K Heremans. Stable misfolded states of human serum albumin revealed by high-pressure infrared spectroscopic studies. *Biochim. Biophys. Acta*, 1764:497, 2006. 80

[129] KA Snyder and DP Bentz. Suspended hydration and loss of freezable water in cement pastes exposed to 90% relative humidity. *Cem. Concr. Res.*, 34:2045, 2004. 30

[130] H Solunov. The dynamic crossover temperature and the characteristic length of glass transition in accordance with the extended adam-gibbs theory. *Journal of Non-Crystalline Solids*, 352:4871–4876, 2006. 103

[131] RJ Speedy. Stability-limit conjecture - an interpretation of the properties of water. *Journal of Chemical Physics*, 86:982, 1982. 19

[132] FW Starr, CA Angell, and HE Stanley. Prediction of entropy and dynamic properties of water below the homogeneous nucleation temperature. *Physica A*, 323:51–66, 2003. 104, 105

[133] HJ Steinhoff, B Kramm, G Hess, C Owerdieck, and A Redhardt. Rotational and translational water diffusion in the hemoglobin hydration shell. *Biophys J*, 65:1486–1495, 1993. 68

[134] J Swenson, H Jansson, J Hedstrom, and R Bergman. Properties of hydration water and its role in protein dynamics. *J. Phys.-Condens. Matter*, 19:205109, 2007. 75

[135] P Taborek, RN Kleiman, and DJ Bishop. Power-law behavior in the viscosity of supercooled liquids. *Phys Rev B*, 34(3):1835–1840, 1986. 19, 56

[136] M Tarek and DJ Tobias. The dynamics of protein hydration water: A quantitative comparison of molecular dynamics simulations and neutron-scattering experiments. *Biophys J*, 79(6):3244–3257, 2000. 74, 112

[137] M Tarek and DJ Tobias. Role of protein-water hydrogen bond dynamics in the protein dynamical transition. *Phys. Rev. Lett.*, 88:138101, 2002. 69

[138] MM Teeter. Water-protein interactions: Theory and experiment. *Ann. Rev. Biophys. Chem.*, 20:577–600, 1991. 67

[139] C Toninelli, M Wyart, L Berthier, G Biroli, and JP Bouchaud. Dynamical susceptibility of glass formers: Contrasting the predictions of theoretical scenarios. *Phys Rev E*, 71(4):041505, 2005. 17, 35

[140] AL Tournier, JC Xu, and JC Smith. Translational hydration water dynamics drives the protein glass transition. *Biophys J.*, 85:1871, 2003. 69

[141] F Volino and A Dianoux. Neutron incoherent scattering law for diffusion in a potential of spherical symmetry: general formalism and application to diffusion inside a sphere. *Mol. Phys.*, 41:271, 1980. 60

[142] G Williams and DC Watts. Non-symmetrical dielectric relaxation behavior arising from a simple empirical decay function. *Transactions of the Faraday Society*, 66:80–85, 1970. 9

[143] K Wood, A Frolich, A Paciaroni, M Moulin, M. Hartlein, G Zaccai, DJ Tobias, and M Weik. Coincidence of dynamical transitions in a soluble protein and its hydration water: direct measurements by neutron scattering and md simulations. *J. Am. Chem. Soc.*, 130:4586, 2008. 87

[144] LM Xu, P Kumar, SV Buldyrev, SH Chen, PH Poole, F Sciortino, and HE Stanley. Relation between the widom line and the dynamic crossover in systems with a liquid-liquid phase transition. *P Natl Acad Sci Usa*, 102(46):16558–16562, 2005. 34

[145] Y Yang and KA Nelson. t_c of the mode-coupling theory evaluated from impulsive stimulated light-scattering on salol. *Phys. Rev. Lett.*, 74:4883, 1995. 61

[146] JM Zanotti, MC Bellissent-Funel, and SH Chen. Relaxational dynamics of supercooled water in porous glass. *Phys. Rev. E.*, 59:3084–3093, 1999. 68

[147] JM Zanotti, MC Bellissent-Funel, and SH Chen. Experimental evidence of a liquid-liquid transition in interfacial water. *Eur. Phys. Lett..*, 71:91, 2005. 21, 22

[148] Y Zhang, M Lagi, E Fratini, P Baglioni, E Mamontov, and SH Chen. Dynamic susceptibility of supercooled water and its relation to the dynamic crossover phenomenon. *Phys Rev E*, 79:040201, 2009. 14, 34, 77

[149] Y Zhang, M Lagi, Dazhi Liu, F Mallamace, and E Fratini. Observation of high-temperature dynamic crossover in protein hydration water and its relation to the reversible denaturation of lysozyme. *J Chem Phys*, 130:135101, 2009. 52, 84

[150] Y Zhang, M Lagi, F Ridi, E Fratini, P Baglioni, E Mamontov, and SH Chen. Observation of dynamic crossover and dynamic heterogeneity in hydration water confined in aged cement paste. *J Phys-Condens Mat*, 20(50):502101, 2008. 19, 22, 29, 36

[151] R Zwanzig. Time-correlation functions and transport coefficients in statistical mechanics. *Annual Review of Physical Chemistry*, 16:67–102, 1965. 3